Wrench Capabilities of Redundantly-Actuated Planar Parallel Manipulators

by

Alp Zibil
B. Eng., Dokuz Eylul University, 2002

A Thesis Submitted in Partial Fulfillment of the
Requirements for the Degree of

MASTER OF APPLIED SCIENCE

in the Department of Mechanical Engineering.

Wrench Capabilities of Redundantly-Actuated Planar Parallel Manipulators

by

Alp Zibil
B. Eng., Dokuz Eylul University, 2002

Supervisory Committee

Dr. Ron P. Podhorodeski (Department of Mechanical Engineering)

Co-supervisor

Dr. Scott B. Nokleby (Faculty of Engineering and Applied Science, University of Ontario Institute of Technology)

Co-supervisor

Dr. Bradley J. Buckham (Department of Mechanical Engineering)

Departmental Member

Dr. Pan Agathoklis (Department of Electrical and Computer Engineering)

Outside Member

David Lokhorst, M.A.Sc. (Tactex Controls Inc.)

Additional Member

Supervisory Committee

Co-supervisor: Dr. Ron P. Podhorodeski

Co-supervisor: Dr. Scott B. Nokleby

Departmental Member: Dr. Bradley J. Buckham

Outside Member: Dr. Pan Agathoklis

Additional Member: David Lokhorst, M.A.Sc.

Abstract

The wrench capability of a manipulator is defined as the maximum forces and moments that can be applied (or sustained) by the manipulator. Understanding these kinetostatic performances of a manipulator is crucial in design and control of manipulators. A novel analytical methodology for the determination of the force and moment capabilities of non-redundantly and redundantly actuated planar parallel manipulators is presented. This new methodology is compared to a previous methodology that used optimization and it is shown that the new methodology is computationally more efficient and yields more accurate results. Based on this methodology, five force and moment capability indices are proposed. The proposed indices are used to generate the wrench capabilities of nine different non-redundantly and redundantly-actuated planar parallel manipulator architectures.

Table of Contents

List of Figures

List of Tables

Acknowledgements

First, I would like to thank my supervisors Dr. Ronald P. Podhorodeski and Dr. Scott B. Nokleby for their guidance, support and exceptional patience during the completion of this thesis.

I would also like to thank to my friends and fellow RAM members Serdar Soylu and Dr. Flavio Firmani for their helpful discussions regarding my studies, and for their invaluable personal support. Flavio, if it wasn't for your curiosity, this project wouldn't have come this far.

Finally, I would like to thank my parents for their absolute confidence in me throughout my life.

Anneme, babama, ve kardeşime ...

Chapter 1

Introduction

1.1 Overview

An introduction will be given in this chapter. First, types of manipulators will be defined and redundancy in manipulators will be explained. Then, the concepts of force and wrench capabilities will be briefly defined. Following that, a literature review about force-moment capabilities will be given. The motivation behind the study and the contributions of the work will be stated. Finally, the organization of the thesis will be presented.

1.2 Robotic Manipulators

1.2.1 General Properties of Manipulators

A robotic manipulator is a mechanism which consists of links that are joined to one another for the purpose of performing a task. The end-effector, which is positioned by the links and the joints with respect to the base of the manipulator, holds the

necessary tool to perform the desired task.

The number of the independent variables required to position and orientate the end-effector is the degrees-of-freedom (DOF) of the manipulator. The joints of the manipulator create a relative motion between its links. There are two main joint types that permit 1-DOF motion: revolute (R), which allows a rotation between the links about an axis; and prismatic (P), which allows a translation along a direction. Joints with multiple DOF which are the combination of these two, such as cylindrical (C), universal (U), spherical (S), etc. also exist.

According to their mechanical architecture, manipulators can be classified into two[1] categories: serial and parallel.

1.2.2 Serial Manipulators

A serial manipulator consists of links that are serially connected to each other, forming an open chain structure between the base and the end-effector. The number of joints define the DOF of the manipulator. Due to the open chain structure, all of the joints must be actuated. Figure 1.1 shows the REIS Robot, a 6-DOF, all revolute jointed serial manipulator. Another example is the human arm which can be modeled as a 7-DOF, all revolute jointed serial manipulator, with the hand being the end-effector.

The advantages of serial manipulators are that they have relatively simpler architectures, and larger dexterous[2] workspaces. On the other hand, since the actuators have to carry the load of all the remaining links, fast motion and high accuracy are difficult to achieve [2].

[1] A third type, hybrid manipulators, can also be considered that are a combination of both serial and parallel manipulators.

[2] Dexterity is defined as the ability of reaching to a position with all possible orentations [1].

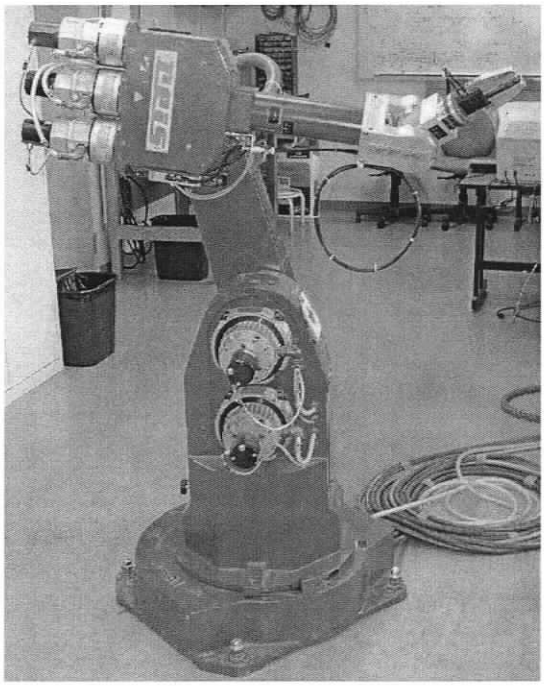

Figure 1.1: The REIS Robot

1.2.3 Parallel Manipulators

Parallel manipulators (PMs) are mechanisms comprised of two platforms, i.e., a base and an end-effector, that are connected by multiple branches, forming closed loop kinematic chains. Each independent chain is called a branch. Each branch must have at least as many DOF as the DOF of the task space in order to allow the end-effector to move in the task space.

A fully parallel manipulator is a PM which has as many branches as its DOF, consequently, having one actuated joint in each branch. Figure 1.2 shows a schematic diagram of a 6-DOF fully parallel PM which is called the Stewart-Gough Platform [3, 4]. This manipulator has six branches that are each comprised of a universal joint, a prismatic joint which is actuated, and a spherical joint (6-U$\underline{\text{P}}$S[3]).

[3]A parallel manipulator can be refered to by its number of branches, followed by the joint types

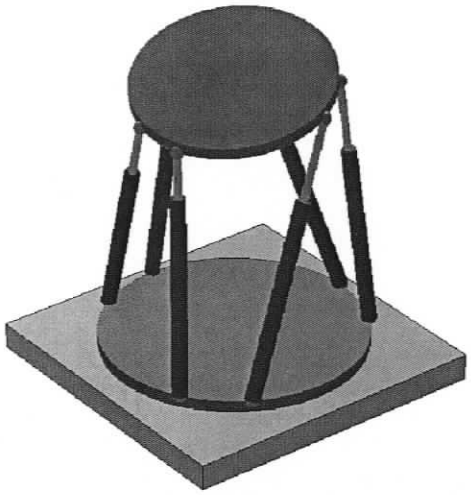

Figure 1.2: Model of a Stewart-Gough Platform

Due to their multiple branch structure, parallel manipulators have greater structural stiffness, higher position accuracy, and larger payload capacity than serial manipulators. These properties make PMs suitable in applications such as flight simulators, large telescopes, and machining. Some disadvantages of PMs include small workspace, poor dexterity, and greater complexity in terms of architecture and kinematic analysis. Another drawback of PMs is that they are prone to possess force unconstrained poses [5]. When all actuators are locked, a manipulator is expected to form a rigid structure. However, in a force unconstrained pose, due to the existence of unactuated joints in a branch, the manipulator instantaneously loses its rigidity and fails to sustain certain forces and moments.

In this thesis, planar parallel manipulators (PPMs) are considered. A PPM is a PM that has 3-DOF in a plane, i.e., translations along the x and y axes, and rotation about the z axis. An example of such a manipulator is the Reconfigurable Planar Parallel Manipulator (RPPM), built in the Robotics and Mechanisms Laboratory, at

that form the branch. An underlined joint type indicates an actuated joint.

the University of Victoria [6]. The RPPM is a 3-RRR manipulator with a reconfigurable actuation scheme. Figure 1.3 shows the 2-RRR-RRR configuration of the RPPM.

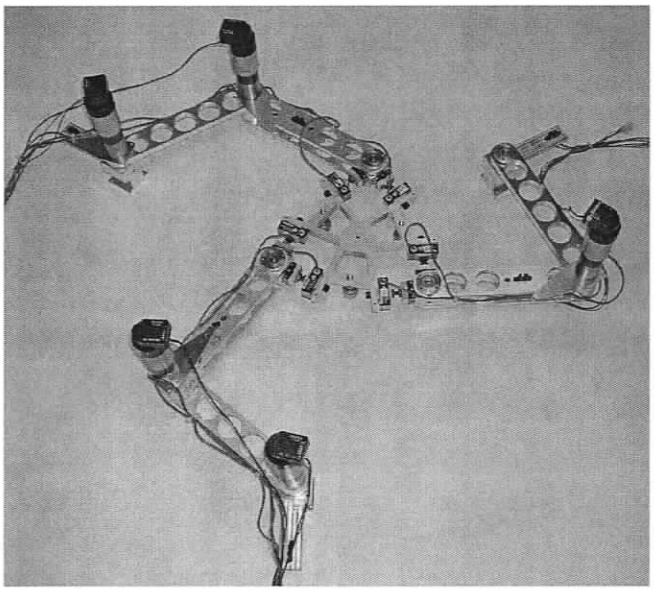

Figure 1.3: Reconfigurable Planar Prallel Manipulator

1.2.4 Redundancy in Parallel Manipulators

A manipulator is considered to be a redundant manipulator when the number of actuators (n) is larger than the DOF (m) of the task space. The degree of redundancy (DOR) is defined as the difference between n and m. Merlet [7] showed that redundancy improves manipulators in terms of reliability and load distribution. Redundancy in manipulators can be classified in two categories: kinematic and actuation redundancy [8].

Kinematic Redundancy

A kinematically redundant manipulator can have an infinite number of postures for a given pose of the end-effector. Serial redundant manipulators are considered in this category. Having more joints than the DOF of the task space, allows them to have a self motion while keeping the end-effector fixed. A human arm, for instance, which can be modeled as a 7-DOF serial manipulator, operates in 6-DOF[4] space, and thus, can have an infinite number of postures (1-DOR) while keeping its hand fixed.

For a PM, kinematic redundancy occurs when at least one of the branches has additional actuated joints. This type of redundancy can be used to enlarge the workspace and improve the dexterity of the manipulator, since the kinematically redundant branch(es) will provide more motion to the end-effector [5]. Kinematic redundancy can also be used to reduce or eliminate the force unconstrained poses by changing the posture of the kinematically redundant branch. However, kinematic redundancy cannot create internal forces in the manipulator, thus, the load capability cannot be optimized.

Actuation Redundancy

Actuation redundancy occurs when an infinite number of resultant forces of the branches can balance a given external force. Thus, there is an infinite number of solutions of joint torques for the static force problem. This creates internal forces in the manipulator that can be optimized. Also, force unconstrained poses can be reduced or eliminated [9, 10]. This type of redundancy can be implemented in two forms: *in-branch redundant* and *branch redundant* manipulators.

[4] A rigid body in 3-dimensional space has three translational and three rotational degrees of freedom, i.e., 6-DOF.

In-branch redundancy can be obtained by replacing one or more passive joints with actuated ones in a branch. Since the architecture is kept the same, there is no change in the workspace or dexterity. However, the additional actuators can increase the inertia of the moving links.

Branch redundancy can be obtained by adding one or more actuated branches to the system. When only the first joints are actuated, this addition does not significantly increase the inertia of the moving links. However, the workspace and the dexterity of the manipulator are reduced due to the added constraints associated with the additional branch.

In this thesis, non-redundant, in-branch redundant, and branch redundant PPM's will be considered.

1.3 Wrench Capabilities of Manipulators

1.3.1 Force Capabilities and Force Polygons

The force capability of a manipulator is the maximum force that can be applied (or sustained) at a given direction by the manipulator. This capability depends on the design, actuator hardware capabilities, and pose of the end-effector.

Force capabilities of planar manipulators are illustrated with force polygons. A force polygon shows the maximum forces that can be applied or sustained in all directions. Figure 1.4 shows a schematic diagram of a 3-$\underline{\text{R}}$RR manipulator, superimposed on its force polygon for its center pose. From Figure 1.4, the maximum force that can be applied or sustained along a given direction α, can be found by measuring the distance from the polygon center, to the point where the considered direction

crosses the polygon. Note that, since the polygon depicts the maximum forces, any

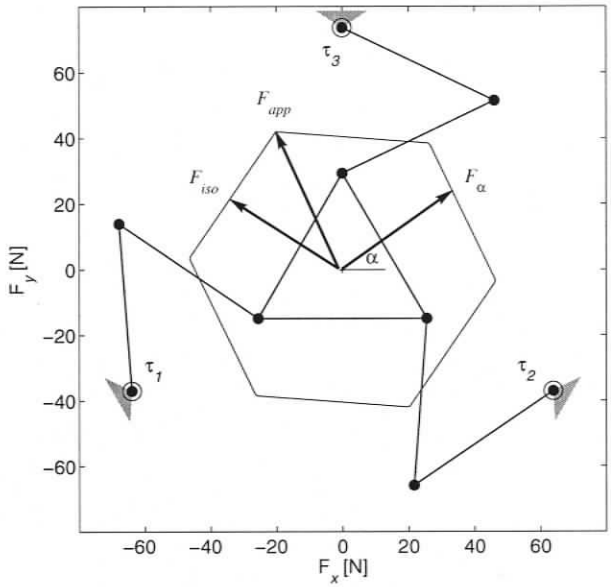

Figure 1.4: Force Polygon of a 3-RRR Manipulator

location within the boundaries of the polygon represents a force that is applicable by the manipulator.

The most significant information that can be extracted from a force polygon is the *maximum applicable force*, F_{app}, and the *maximum isotropic force*, F_{iso}, as shown in Figure 1.4. F_{app} is defined as the maximum applicable force of all directions in a given pose; and F_{iso} is defined as the maximum force that can be applied along all directions in a given pose. The magnitudes of these two forces are considered to be indices and are used to characterize the force polygon of a given pose.

1.3.2 Wrench Space and Wrench Polyhedrons

In addition to the force capabilities, moment capabilities of PPMs are presented in this work. Force and moment can be assembled in a vector which is known as a

wrench [11].

For a planar manipulator, the applicable force has two components in the x and y axes' directions, and the applicable moment has one component in the z axis direction. Therefore, a third dimension depicting the moment applied by the manipulator can be introduced into the force polygon. The resultant 3-dimensional space can be referred to as the wrench space, and it can be used to show the force-moment, i.e., wrench capabilities of a manipulator. The wrench capabilities are illustrated with a *wrench polyhedron*[5] in the wrench space. Figure 1.5 shows the wrench polyhedron of a 3-RRR manipulator.

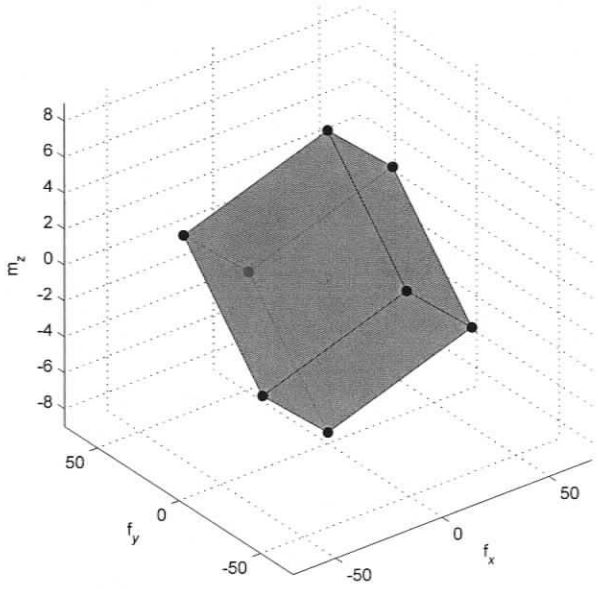

Figure 1.5: Wrench Polyhedron of the 3-RRR for Its Center Pose

[5] A polyhedron is a 3-dimensional region that is defined by a finite number of plane polygons, such that every side of each polygon belongs also to only one other polygon [12]. Polyhedrons are analogous to polygons in 2-dimensional space.

1.4 Literature Review

Early studies that dealt with kinetostatic capability indices were based on manipulability ellipsoids. Yoshikawa [13] proposed a quantitative measure for the manipulability of non-redundant and redundant manipulators, and introduced manipulability ellipsoids based on the singular values of the *Jacobian*[6] matrix. He used this measure to determine the "best posture" of a 4-DOF finger for a given grasping task [14]. Chiu [15] used the manipulability ellipsoid to determine the "preferred directions" for motion and force exertion of a given pose of the manipulators. Chiacchio et al. [16] extended the use of manipulability ellipsoids to co-operating robot systems. Melchiorri [17] showed that manipulability ellipsoids may lead to inaccurate results when used for co-operating robot systems. Doty et al. [18] further investigated manipulability ellipsoids and demonstrated some inconsistencies of the method caused by the fact that the task space wrench vector is not homogeneous in terms of its units, e.g., N for force and Nm for moment.

An alternative way to approach the force capabilities problem is using optimization. Zheng and Luh [19] optimized the force distribution in a manipulator system with two serial robots for different objectives. They also incorporated the torque capabilities of the actuators into their algorithms. Kumar and Waldron [20] used the pseudo-inverse solution of the inverse force problem for redundantly-actuated closed-loop kinematic chains, which essentially coincides with minimizing the $2-norm$ of the torque vector. They showed that this solution yields no internal force in the system. Tao and Luh [21] used the manipulability measure as their objective function in closed-loop kinematic chains. Buttolo and Hannaford [22] used linear programming

[6] Jacobian matrix is a matrix that maps the time derivative of the joint space coordinates to the time derivative of the task space coordinates.

to minimize the $\infty - norm$ of the torque vector, and they showed that their results yields higher force capabilities compared to the pseudo-inverse solution. Beiner [23] constructed a constrained optimization problem for minimizing the $2 - norm$ of the torque vector, and derived a closed-form solution for a 2-DOF redundantly-actuated parallel manipulator. Nokleby et al. [24] optimized a high norm of the torque vector using a scaling factor to incorporate the actuator torque capabilities into the problem and generated the force capabilities of a 3-RRR PPM. Nokleby [25] presented more results for different orientations of this manipulator using the same methodology. This methodology, i.e., *scaling factor* methodology, will be explained in detail in this thesis in order to give a comparison with the new methodology that was developed in this work.

Another index that was used for the force capabilities in the literature is the *force polytope*[7] of the manipulators. Kokkinis and Paden [26] first introduced the concept of using polytopes to represent the feasible forces in the task space. They showed that force polytopes are much more realistic and accurate compared to using manipulability ellipsoids for the same purpose. Bicchi et al. [27] formulated velocity polytopes of manipulators by using "slack variables" to represent the variation in the joint velocities between their positive and negative limits[8]. Lee [28] further investigated the relation between force ellipsoids and force polytopes, and proposed a method to construct the polytope by defining its vertices. Finotello et al. [29] proposed a more efficient method to generate the force polytopes by partitioning the task space wrench into its force and moment polytopes. Hwang et al.[30] showed

[7] A polytope is a finite convex region of n-dimensional space enclosed by a finite number of hyperplanes [12]. Polygons, and polyhedrons are 2 and 3-dimensional polytopes, respectively.

[8] Force and velocity spaces show duality in manipulators since they are associated with the same Jacobian matrix when mapping between their respective task spaces and the joint spaces.

that the computation time that is required to determine the bounding vertices of the polytope increases exponentially with the DOR of the manipulator. They proposed a recursive algorithm that successively removes the internal points when they are detected, thus they significantly reduced the computation time. Kurt et al. [31] proposed a method to find the largest ellipse that can be inscribed in the force polygon by using scaling and rotation operations on the ellipse. Even though this method does not require the explicit computation of the force polygon and thus, is computationally efficient, the results are not accurate.

1.5 Motivation and Contributions

In robotics research, investigating the static characteristics of robotic manipulators is one of the main objectives. Thorough understanding of the kinetostatic performances of a manipulator is crucial in designing and controlling manipulators. By being able to graphically visualize the exact force and moment capabilities, comparisons between different design parameters, such as actuator selection and link lengths can be explored.

Previously proposed methods to determine the force and moment capabilities of manipulators have been shown to have problems and implementation difficulties. Force ellipsoids have been shown to be inaccurate and posses fundamental problems. Optimization methods are slow and do not yield accurate solutions as will be shown later on in this thesis. Force polytopes, on the other hand, are exact indices of force capabilities but they suffer from being computationally inefficient.

In this thesis, a new analytical methodology to find the wrench capabilities of PPMs that is based on the force polytopes will be presented. The proposed in-

dices to measure the force and moment capabilities are combined under five studies. Although these indices correspond to the geometrical properties of the force polytopes, the calculation does not require the computationally expensive generation of the whole polytope. Instead, these five studies extract the relevant information from the polytope in order to find the proposed force and moment indices.

The first and the third studies were first published in [32], and all studies were compiled in [33]. A 3-RRR PPM was used as an example in these papers. Further analyses that employed this methodology were presented in [34, 35, 36] where 3-RRR, 3-RPR, and 3-PRR architectures; 3-RRR and 4-RRR architectures; and 4-RRR, 4-RPR and 4-PRR architectures were considered and compared, respectively. Garg et al. [37] also implemented this methodology for redundantly-actuated spatial PMs.

1.6 Thesis Outline

The second chapter will present the screw theory which is used as a mathematical tool for the geometric properties of the PPMs throughout the thesis.

In chapter three, the scaling factor methodology for the force capabilities will be explained and the limitations of the methodology will be discussed.

The new explicit methodology and five studies for the force-moment capability indices will be explained in detail in chapter four. Some examples will be shown in order to make a comparison between the scaling factor and the explicit methodology.

Chapter five will present the wrench capability analyses for nine PPM architectures using the explicit methodology.

Finally, a conclusion and recommendation for future work will be given in chapter six.

Chapter 2

Screw Theory

2.1 Overview

Screw theory provides a convenient basis to model joints of a manipulator and allows one to analyze the statics and instantaneous kinematics. This chapter will present the basics of screw theory as a tool used throughout the rest of the work.

The use of the screw concept in mechanics dates back to the late 18th century with the screw axis studies of Mozzi in 1763 [38]. Poinsot was the first who established the theory of a system of forces acting on a rigid body with screws in 1806 [39]. Chasles used screws to represent infinitesimal displacement of rigid bodies in 1832 [40]. It was almost half a century later that a firm physical base of the mathematics of screw theory was established, and the terminology used today was introduced by Ball in 1876 [41].

2.2 Screw Quantities

2.2.1 Screw Coordinates

Analytical representation of a screw requires knowledge of line coordinates. A line in 3-dimensional space is specified by four independent parameters. For instance, the direction of a line can be expressed by a unit vector which is two independent quantities. Then, a minimum distance between the origin of the reference frame and the line can be assigned as a third parameter, which will constrain the loci of the line onto a circle. A fourth parameter then can be used to fix the position of the line on this circle.

Plücker line coordinates [42] are used in the representation of screw quantities. A unit vector (direction), $\hat{\boldsymbol{l}}$ of the line, and the moment, $\boldsymbol{l}_o$, of this vector about the origin of the reference frame define the line in 3-dimensional space; where $\boldsymbol{l}_o$ is defined as:

$$\boldsymbol{l}_o = \boldsymbol{r}_{o\to l} \times \hat{\boldsymbol{l}} \tag{2.1}$$

where $\boldsymbol{r}_{o\to l}$ is a vector from the origin of the reference frame to a point on the line. Since $\hat{\boldsymbol{l}}$ is a unit vector, it holds two independent parameters, and since vector $\boldsymbol{r}_{o\to l}$ can point anywhere on the line, the total number of independent parameters is four. These can be analytically expressed as follows;

$$\begin{aligned} \left\|\hat{\boldsymbol{l}}\right\| = l_1^2 + l_2^2 + l_3^2 &= 1 \\ \boldsymbol{l}_o \cdot \hat{\boldsymbol{l}} &= 0 \end{aligned} \tag{2.2}$$

A screw ($\boldsymbol{S}$) is a line in space having an associated pitch and a magnitude. A

screw quantity can be represented as:

$$\boldsymbol{S} = \begin{Bmatrix} \boldsymbol{s}_p \\ \boldsymbol{s}_o \end{Bmatrix} = \lambda \begin{Bmatrix} \hat{\boldsymbol{l}} \\ \boldsymbol{l}_o + p\hat{\boldsymbol{l}} \end{Bmatrix} \tag{2.3}$$

where $\boldsymbol{s}_p$ is a 3×1 vector called the primary screw coordinates, $\boldsymbol{s}_o$ is a 3×1 vector called the secondary screw coordinates, λ is the associated magnitude of the screw, $\hat{\boldsymbol{l}}$ and $\boldsymbol{l}_o$ are the Plücker line coordinates, and p is the pitch of the screw. The pitch is defined as "the rectilinear distance through which the nut is translated parallel to the axis of the screw, while the nut is rotated through the angular unit of circular measure" [11], and can be found from:

$$p = \frac{\boldsymbol{s}_p \cdot \boldsymbol{s}_o}{\boldsymbol{s}_p \cdot \boldsymbol{s}_p} \tag{2.4}$$

2.2.2 Twists and Wrenches

Screw quantities can be used to represent instantaneous displacements of a rigid body. The 3×1 angular velocity vector ($\boldsymbol{\omega}$) and the 3×1 translational velocity vector ($\boldsymbol{v}$) construct what is called a "twist" ($\boldsymbol{V}$) of a rigid body as a screw quantity:

$$\boldsymbol{V} = \begin{Bmatrix} \boldsymbol{\omega} \\ \boldsymbol{v} \end{Bmatrix} = \alpha \begin{Bmatrix} \hat{\boldsymbol{l}} \\ \boldsymbol{l}_o + p\hat{\boldsymbol{l}} \end{Bmatrix} \tag{2.5}$$

where $\hat{\boldsymbol{l}}$ is the unit vector of the angular velocity and, α is the magnitude of the angular velocity, which is called the amplitude of the twist. The translational velocity $\boldsymbol{v}$ has two components. The first one, $\boldsymbol{l}_o$, is contributed by the moment of the angular velocity, and it is perpendicular to the angular velocity axis. The second one, $p\hat{\boldsymbol{l}}$, is along the angular velocity axis. The pitch of the screw p is the ratio between the

angular velocity and the translational velocity along the angular velocity direction. Hence, a pure rotational twist about the screw axis can be specified by setting the pitch to zero, while a pure translational twist can be achieved with an infinite pitch.

Similarly, the system of forces acting on a rigid body, called a wrench ($\boldsymbol{F}$), is represented by a 3×1 resultant force vector ($\boldsymbol{f}$), and a 3×1 moment vector ($\boldsymbol{m}$), and can be assembled as a screw quantity:

$$\boldsymbol{F} = \begin{Bmatrix} \boldsymbol{f} \\ \boldsymbol{m} \end{Bmatrix} = f \begin{Bmatrix} \hat{\boldsymbol{l}} \\ \boldsymbol{l}_o + p\hat{\boldsymbol{l}} \end{Bmatrix} \tag{2.6}$$

where $\hat{\boldsymbol{l}}$ is the unit vector of the resultant wrench, and f is the magnitude of this wrench, which is called the wrench intensity. The pitch is the ratio between the force and the moment's component along the force direction. A pure force is a zero pitch wrench, and a pure moment is an infinite pitch wrench.

2.2.3 Properties of Screw Quantities

Unit Screws

A general screw quantity ($\boldsymbol{S}$) can be broken into unit screw coordinates ($\$$) and a magnitude (λ):

$$\boldsymbol{S} = \begin{Bmatrix} \boldsymbol{s}_p \\ \boldsymbol{s}_o \end{Bmatrix} = \lambda \$ = \lambda \begin{Bmatrix} \$_p \\ \$_o \end{Bmatrix} \tag{2.7}$$

where $\$_p$ is the primary unit screw coordinates, and $\$_o$ is the secondary unit screw coordinates. A screw is called a unit or normalized screw ($\$$) when the primary vector is a unit vector ($\|\boldsymbol{s}_p\| = 1$). In case of an infinite pitch screw, the screw quantity is normalized with respect to the secondary vector and $\boldsymbol{s}_p$ becomes a zero

vector:

$$\boldsymbol{S} = \begin{Bmatrix} \mathbf{0}_{3\times1} \\ \boldsymbol{s}_o \end{Bmatrix} = \lambda \begin{Bmatrix} \mathbf{0}_{3\times1} \\ \boldsymbol{s}_o \end{Bmatrix} \tag{2.8}$$

For an infinite pitch screw quantity to be a unit screw, the secondary vector has to be a unit vector ($\|\boldsymbol{s}_o\| = 1$).

Screw Transformations

Screw quantities are written with respect to a reference frame. A transformation matrix $[\mathbf{T}]$ is therefore required if the screw quantity is desired to be written with respect to another reference frame:

$${}^{B}\boldsymbol{S} = {}^{B}_{A}[\mathbf{T}]\,{}^{A}\boldsymbol{S} \tag{2.9}$$

where ${}^{A}\boldsymbol{S}$ and ${}^{B}\boldsymbol{S}$ are screw quantities written in terms of reference frames A and B, respectively. Transformation matrix ${}^{B}_{A}[\mathbf{T}]$ can be constructed as follows:

$${}^{B}_{A}[\mathbf{T}] = \begin{bmatrix} {}^{B}_{A}[\mathbf{R}] & \mathbf{0}_{3\times3} \\ {}^{B}\tilde{\mathbf{p}}_{O_B\rightarrow O_A}\,{}^{B}_{A}[\mathbf{R}] & {}^{B}_{A}[\mathbf{R}] \end{bmatrix} \tag{2.10}$$

where ${}^{B}_{A}[\mathbf{R}]$ is a 3×3 rotation matrix describing the orientation of the reference frame A, in terms of the reference frame B; and ${}^{B}\tilde{\mathbf{p}}_{O_B\rightarrow O_A}$ is a 3×3 cross-product skew-symmetric matrix of the vector ${}^{B}\boldsymbol{p}_{O_B\rightarrow O_A}$, which is from the origin of the reference frame B, to the origin of the reference frame A, and written in terms of the reference

frame B. If $\boldsymbol{p} = \{p_x, p_y, p_z\}^{\mathrm{T}}$, then the skew symmetric matrix is defined as follows:

$$\tilde{\mathbf{p}} = \begin{bmatrix} 0 & -p_z & p_y \\ p_z & 0 & -p_x \\ -p_y & p_x & 0 \end{bmatrix} \tag{2.11}$$

Reciprocal Product and Reciprocity

The reciprocal product of a wrench screw quantity and a twist screw quantity gives the power generated by the wrench applied to the twist, and can be calculated as:

$$\boldsymbol{F} \circledast \boldsymbol{V} = \boldsymbol{f} \cdot \boldsymbol{v} + \boldsymbol{m} \cdot \boldsymbol{\omega} \tag{2.12}$$

where $\circledast$ is the reciprocal product operator and $\boldsymbol{F} = \{\boldsymbol{f}^{\mathrm{T}}, \boldsymbol{m}^{\mathrm{T}}\}^{\mathrm{T}}$, and $\boldsymbol{V} = \{\boldsymbol{\omega}^{\mathrm{T}}, \boldsymbol{v}^{\mathrm{T}}\}^{\mathrm{T}}$. The reciprocal product operation can also be expressed as follows:

$$\boldsymbol{F} \circledast \boldsymbol{V} = \boldsymbol{V} \circledast \boldsymbol{F} = \boldsymbol{F}^{\mathrm{T}} \boldsymbol{\Delta} \boldsymbol{V} = \boldsymbol{V}^{\mathrm{T}} \boldsymbol{\Delta} \boldsymbol{F} \tag{2.13}$$

where $\boldsymbol{\Delta}$ denotes an operator that swaps the primary and the secondary screw coordinates:

$$\boldsymbol{\Delta} = \begin{bmatrix} \mathbf{0}_{3\times3} & \mathbf{I}_{3\times3} \\ \mathbf{I}_{3\times3} & \mathbf{0}_{3\times3} \end{bmatrix} \tag{2.14}$$

Reciprocity of two screw quantities can be explained by considering a rigid body subjected to a twist and a wrench. If the wrench acting on the body cannot contribute to the rate of work being done on the body moving with the twist, the wrench and the twist are said to be reciprocal to each other [42]. If we consider a revolute joint of a manipulator, a force with a line of action passing through the joint axis will not have

an effect on the rotation of the joint, and therefore is reciprocal to the joint screw. Also, a force couple is reciprocal to a revolute joint screw when it is perpendicular to the joint axis. In case of a prismatic joint, a force's line of action has to be perpendicular to the joint axis in order to be reciprocal to it. A pure force couple however, is always reciprocal to a prismatic joint since it can never have an effect on translation.

Analytically, when two screw quantities are reciprocal to each other, the reciprocal product of the two screws is zero.

2.3 Modelling of Manipulators With Screws

2.3.1 Screw Coordinates of Joints

A robotic manipulator's joints cause motion at the end-effector. The motion of rigid bodies has been previously seen to be able to be described as twist screw quantities. Therefore, the effect of a joint on the end-effector can be modeled as a twist quantity. Unit screws are used to model a joint in order to distinguish the motion from its magnitude. The unit screw plus a magnitude, which together forms a twist, can be used to describe a moving joint as:

$$\boldsymbol{V} = \dot{q}\boldsymbol{\$}$$

where $\dot{q}$ is the displacement rate (rotational for revolute and translational for prismatic) of the joint.

A revolute joint causes only a rotational motion between the two links it is attached to. Lacking a translational motion yields a zero pitch screw quantity. The primary

screw coordinates will be equal to the unit vector of the axis of rotation. The secondary screw coordinates will be the moment of the primary coordinates about a point ($\boldsymbol{p}$) where the linear velocity will be described. Therefore, the unit screw coordinates of a revolute joint are described as:

$$\$_{revolute} = \begin{Bmatrix} \$_p \\ \$_o \end{Bmatrix} = \begin{Bmatrix} \hat{\boldsymbol{z}} \\ \boldsymbol{r}_{\boldsymbol{p}\rightarrow\hat{\boldsymbol{z}}} \times \hat{\boldsymbol{z}} \end{Bmatrix} \tag{2.15}$$

where $\hat{\boldsymbol{z}}$ is the axis of rotation of the joint and $\boldsymbol{r}_{\boldsymbol{p}\rightarrow\hat{\boldsymbol{z}}}$ is a vector from the point $\boldsymbol{p}$ to a point on $\hat{\boldsymbol{z}}$.

In the case of a prismatic joint, an infinite pitch unit screw is used since a prismatic joint can only produce a translational motion. As mentioned before, infinite pitch screws are normalized with respect to the secondary coordinates, and the primary coordinates become a zero vector. The secondary vector is the unit vector of the direction of the prismatic joint. Therefore, the unit screw coordinates of a prismatic joint are described as:

$$\$_{prismatic} = \begin{Bmatrix} \$_p \\ \$_o \end{Bmatrix} = \begin{Bmatrix} \mathbf{0}_{3\times1} \\ \hat{\boldsymbol{z}} \end{Bmatrix} \tag{2.16}$$

where $\hat{\boldsymbol{z}}$ is the direction of the prismatic joint.

In a planar manipulator, $\$_o$ will always be $\{\$_{o_x}, \$_{o_y}, 0\}^{\mathrm{T}}$; $\$_p$ will be $\{0, 0, 1\}^{\mathrm{T}}$ for a revolute joint and $\{0, 0, 0\}^{\mathrm{T}}$ for a prismatic joint. Eliminating the zero elements will yield a more compact representation of the screw coordinates for planar manipulators. The compact form of a revolute joint is denoted as $\$_{revolute} = \{1; \$_{o_x}, \$_{o_y}\}^{\mathrm{T}}$, and for a prismatic case it is denoted as $\$_{prismatic} = \{0; \$_{o_x}, \$_{o_y}\}^{\mathrm{T}}$.

2.3.2 Associated Reciprocal Screw Coordinates of Joints

A robotic manipulator's joints cause force and moment at the end-effector. Therefore, the effect caused by one of the manipulator's joints acting on the end-effector can be modeled as a wrench screw quantity. The total wrench that can be applied to the end-effector of the manipulator is the sum of the individual wrenches that can be applied by each joint. Hence, the wrench of the joint being considered can be distinguished from the total wrench, by finding a wrench that the remaining joints are not capable of producing. In other words, one wants to find a wrench that does not produce any twists at the remaining joints. These conditions are the reciprocity conditions of two screw quantities. It should be noted that this approach only resolves the direction of the wrench, i.e., the unit wrench. The wrench intensity of the wrench is found through conservation of power in the Wrench Intensity sub-section.

Unit Wrench

The unit wrench that is caused by a particular joint, is termed as the *Associated Reciprocal Screw* (ARS) of the joint. An ARS is reciprocal to all other joint screws in the branch under consideration, and it is denoted as $\$'$. Mathematically, it means that the reciprocal products are zero, and can be found by solving the following equation set:

$$\$_j \circledast \$'_k = 0, \quad \text{for all } j \neq k \tag{2.17}$$

where $\$'_k$ is the ARS coordinates of joint k, and $\$_j$ is the screw coordinates of joint j (i.e., every joint other than k^{th} joint). Geometrically, ARS coordinates of a joint is a unit screw that is perpendicular to the rest of the joints in its branch and it intersects them. The ARS coordinates of the manipulators analyzed in this work are computed

geometrically in Appendix A.

Wrench Intensity

The wrench created by the k^{th} joint, $\boldsymbol{F}_k$, can then be shown as:

$$\boldsymbol{F}_k = w_k \boldsymbol{\$}'_k \tag{2.18}$$

where w_k is the wrench intensity applied by joint k. This magnitude is related to the torque in the case of a revolute joint or to the force in the case of a prismatic joint. Let τ_k be the torque or the force of joint k, depending on the joint type. The wrench intensity in equation (2.18) can be replaced by:

$$w_k = u_k^* \tau_k \tag{2.19}$$

where u_k^* is a scalar which translates the joint's torque or force to its wrench intensity. Therefore, u_k^* has to be determined in order to express the wrench. Conservation of power can be used in the determination of u_k^*. Let the wrench applied by joint k be $\boldsymbol{F}$, and the twist created by this joint be $\boldsymbol{V}$. The power generated by this joint will be $\boldsymbol{F} \circledast \boldsymbol{V}$. In case of a revolute joint the power is equal to the torque of the actuator (τ) times the angular velocity of the joint ($\dot{q}$):

$$\tau \dot{q} = \boldsymbol{F} \circledast \boldsymbol{V} \tag{2.20}$$

Noting that $\boldsymbol{V} = \dot{q}\boldsymbol{\$}$:

$$\tau \dot{q} = w \boldsymbol{\$}' \circledast \dot{q} \boldsymbol{\$} \tag{2.21}$$

Since equation (2.21) is true for all $\dot{q}$:

$$\tau = w\$' \circledast \$ \tag{2.22}$$

If equation (2.19) is substituted into equation (2.22), the w^* of a revolute joint is seen to be:

$$w^*_{revolute} = \frac{1}{\$' \circledast \$} \tag{2.23}$$

Similarly, in the case of a prismatic joint, the power generated is equal to the force of the actuator (f) times the linear velocity of the joint ($\dot{x}$):

$$f\dot{x} = \boldsymbol{F} \circledast \boldsymbol{V} \tag{2.24}$$

Noting that $\boldsymbol{V} = \dot{x}\$$:

$$f\dot{x} = w\$' \circledast \dot{x}\$ \tag{2.25}$$

Since equation (2.25) is true for all $\dot{x}$:

$$f = w\$' \circledast \$ \tag{2.26}$$

If equation (2.19) is substituted into equation (2.26), w^* of a prismatic joint is seen to be:

$$w^*_{prismatic} = \frac{1}{\$' \circledast \$} \tag{2.27}$$

which is identical to the w^* of a revolute joint.

As in screw coordinates, it is possible to write ARS coordinates ($\$'$) and wrenches ($\boldsymbol{F}$) in a compact form as well. For a planar manipulator, $\$'_p$ will be in the

form $\left\{\$'_{p_x}, \$'_{p_y}, 0\right\}^{\mathrm{T}}$, and $\$'_o$ will be in the form $\{0, 0, \$'_{o_z}\}^{\mathrm{T}}$. Therefore, ARS coordinates of a planar manipulator's joints can be written in the compact form as $\$' = \left\{\$'_{p_x}, \$'_{p_y}; \$'_{o_z}\right\}^{\mathrm{T}}$.

In the same manner, $\boldsymbol{f}$ of the wrench will be in the form $\{f_x, f_y, 0\}^{\mathrm{T}}$, and $\boldsymbol{m}$ of the wrench will be in the form $\{0, 0, m_z\}^{\mathrm{T}}$. Therefore, the wrench of a planar manipulator can be written in the compact form as $\boldsymbol{F} = \{f_x, f_y; m_z\}^{\mathrm{T}}$.

2.3.3 Velocity Solution of Manipulators

Serial Manipulators

The forward velocity problem of a manipulator is defined as calculating the end-effector velocity, given the joint rates of the manipulator. For a n-joint serial manipulator, the velocity of the end-effector ($\boldsymbol{V}$) is the summation of all the twists about each joint:

$$\boldsymbol{V} = \begin{Bmatrix} \boldsymbol{\omega} \\ \boldsymbol{v} \end{Bmatrix} = \sum_{j=1}^{n} \dot{q}_j \, \$_j \tag{2.28}$$

This expression can be written in a matrix form as follows:

$$\boldsymbol{V} = [\$]\dot{\boldsymbol{q}} \tag{2.29}$$

where, $[\$] = [\$_1 \ \$_2 \ \cdots \ \$_n]$ is the screw coordinate matrix, with the screw coordinates of all joints, and $\dot{\boldsymbol{q}}$ is a $n \times 1$ vector that contains the joint rates. Note that the screw matrix $[\$]$ is commonly known as the *Jacobian Matrix*.

In the inverse velocity problem, the velocity of the end-effector is known and the

joint rates are to be found. This can be solved by inverting the screw matrix:

$$\dot{\boldsymbol{q}} = [\$]^{-1}\boldsymbol{V} \tag{2.30}$$

Note that the inversion of the screw matrix is not possible when it is non-square (i.e., a redundant or an underactuated manipulator) or when it is singular (i.e., a velocity degenerate[1] manipulator pose).

Parallel Manipulators

Similar to serial manipulators, the velocity of the end-effector of a parallel manipulator is the summation of all the twists of all joints in one branch. Assume a parallel manipulator with b branches, n_i joints in the i^{th} branch, and m_i joints that are actuated in the i^{th} branch. Then the twist of the end-effector ($\boldsymbol{V}$) can be expressed in terms of all $i = 1 \ldots b$ as:

$$\boldsymbol{V} = \sum_{j=1}^{n_i} \dot{q}_{j_i} \boldsymbol{\$}_{j_i} \tag{2.31}$$

where $\dot{q}_{j_i}$ is the joint rate of the j^{th} joint of the i^{th} branch, and $\boldsymbol{\$}_{j_i}$ is the screw coordinates of the j^{th} joint of the i^{th} branch.

In the parallel case however, joint rates of all joints in a branch are not known, i.e., only the actuated joint rates are known. Let k be the actuated joints of the branches, and $\boldsymbol{\$}'_{k_i}$ be the unit wrench (i.e., ARS) of the actuated joint k in the i^{th} branch. The ARS's of the actuated joints of branches will be reciprocal to the other

[1] A velocity degenerate pose is a pose when the manipulator instantaneously loses one ore more DOF.

joints' screw coordinates:

$$\$_{j_i} \circledast \$'_{k_i} = 0, \quad \text{for } j = 1 \dots n_i,\ j \neq k \tag{2.32}$$

Considering equation (2.32), taking the reciprocal product of equation (2.31) with $\$'_{k_i}$, cancels out the unknown joint twists:

$$\boldsymbol{V} \circledast \$'_{k_i} = \sum_{j=1}^{n_i} \dot{q}_{j_i} \$_{j_i} \circledast \$'_{k_i} \tag{2.33}$$

yielding:

$$\boldsymbol{V} \circledast \$'_{k_i} = \dot{q}_{k_i} \$_{k_i} \circledast \$'_{k_i} \quad \text{for } k = 1 \dots m_i \tag{2.34}$$

Recalling equations (2.23) and (2.27), the joint rate of an actuated joint yields:

$$\dot{q}_{k_i} = u^*_{k_i} \boldsymbol{V} \circledast \$'_{k_i} \tag{2.35}$$

Defining the transmission matrix as $[\mathbf{W}^*] = diagonal\{\cdots\ u^*_{k_i} \cdots\}$, and the ARS matrix of all actuated joints as $[\$'] = [\cdots\ \$'_{k_i} \cdots]$, equation (2.35) can be written in matrix form obtaining the inverse velocity solution:

$$\dot{\boldsymbol{q}} = [\mathbf{W}^*][\$']^{\mathrm{T}} \boldsymbol{\Delta V} \tag{2.36}$$

where $\dot{\boldsymbol{q}} = \{\cdots\ \dot{q}_{k_i} \cdots\}^{\mathrm{T}}$, $k = 1 \dots m_i$, and $i = 1 \dots b$.

As for the forward velocity problem of a non-redundantly-actuated manipulator,

equation (2.36) can be solved for the end-effector velocity:

$$\boldsymbol{V} = \boldsymbol{\Delta} \left([\mathbf{W}^*][\$']^{\mathrm{T}} \right)^{-1} \dot{\boldsymbol{q}} \tag{2.37}$$

Note that equation (2.37) is not solvable when the resulting matrix to be inverted is singular (i.e., a velocity degeneracy in at least one of the branches in the case of $[\mathbf{W}^*]$ being singular and/or a force unconstrained pose of the manipulator in the case of $[\$']$ being singular).

2.3.4 Force Solution of Manipulators

The forward force problem of manipulators is defined as calculating the wrench applied by the end-effector, given the actuators forces or torques. The solution is the same for both serial and parallel manipulators; the applied wrench can be found by summing all wrenches caused by the actuated joints:

$$\boldsymbol{F} = \begin{Bmatrix} \boldsymbol{f} \\ \boldsymbol{m} \end{Bmatrix} = \sum_{i=1}^{b} \sum_{k=1}^{m_i} w_{k_i} \boldsymbol{\$}'_{k_i} \tag{2.38}$$

In matrix form, equation (2.38) can be written as:

$$\boldsymbol{F} = [\$']\boldsymbol{w} \tag{2.39}$$

where $\boldsymbol{w}$ is a vector of wrench intensities. The transmission matrix introduced in Section 2.3.2, can be used to relate the output wrench to the actuator forces or torques, (i.e., τ_{k_i}):

$$\boldsymbol{F} = [\$'][\mathbf{W}^*]\boldsymbol{\tau} \tag{2.40}$$

where $\boldsymbol{\tau} = \{\cdots \ \tau_{k_i} \cdots\}^{\mathrm{T}}$ is the vector of actuator magnitudes.

The inverse force problem for a non-redundantly-actuated manipulator can be solved by taking the inverse of equation (2.40):

$$\boldsymbol{\tau} = ([\$'][\mathbf{W}^*])^{-1} \boldsymbol{F} \tag{2.41}$$

Note that equation (2.41) is not solvable when the resulting matrix to be inverted is singular (i.e., a force unconstrained pose of the manipulator in the case of $[\$']$ being singular and/or a velocity degeneracy in at least one of the branches in the case of $[\mathbf{W}^*]$ being singular).

Chapter 3

Force Capability Analysis with the Scaling Factor Methodology

3.1 Overview

In many robotics applications a desired task is defined by its force requirements. Thus, it is useful to determine the possible forces that a manipulator can exert or sustain. The force capability of a manipulator is defined as the maximum wrench that can be applied (or sustained) by the manipulator for a given pose, based on its actuators' torque/force limits. Considering the potential applicable force for all possible directions, a force capability plot can be drawn for a given pose of the manipulator.

This chapter will cover the scaling factor methodology, developed by Nokleby et al. [24], used in the force capability analysis of PPM's. First, the methodology for non-redundantly-actuated manipulators will be described. Following this, two solutions for the redundantly-actuated manipulators will be presented: a pseudo-

inverse solution, and an optimization based solution.

3.2 Forward Force Solution

In order to create a force capability plot for a given pose of a manipulator, the forward force solution is used. As described in Section 2.3.4, in the forward force solution, the output wrench (i.e., $\boldsymbol{F}$) of the manipulator is calculated from:

$$\boldsymbol{F} = [\$'][\mathbf{W}^*]\boldsymbol{\tau} \tag{3.1}$$

By finding a maximum applicable output wrench for all possible directions, the force capability plot can be drawn. Since the forward force solution requires knowledge of the joint torques/forces (i.e., $\boldsymbol{\tau}$ vector), a $\boldsymbol{\tau}$ vector that yields the maximum wrench along the desired direction has to be found for all directions. This will be achieved by solving the inverse force solution.

3.3 Inverse Force Solution

The wrench that is applied by the manipulator is a screw quantity and can be written in terms of its magnitude (f) and its unit coordinates($\$_F$):

$$\boldsymbol{F} = f\,\$_F = f \begin{bmatrix} \cos\alpha \\ \sin\alpha \\ m' \end{bmatrix} \tag{3.2}$$

where the unit screw $\$_F$ is called the unit wrench which represents the direction α of the applied wrench and the ratio $m' = m/f$. Therefore, in order to find the maximum wrench along a desired direction, one needs to find the maximum f that is within the torque/force limits of the manipulator's actuators. This magnitude will be determined by a relative comparison process between the actuator values and actuator limits.

The inverse force solution will be solved by considering the unit wrench to obtain a $\boldsymbol{\tau}$ vector (i.e., $\boldsymbol{\tau}_{\$}$). Using the unit wrench in the inverse force solution will reveal the ratio between individual joint torques/forces while ensuring that the resultant $\boldsymbol{\tau}_{\$}$ vector yields a wrench in the desired direction. According to this ratio, the magnitudes of the torques/forces will be scaled up in order to gain the highest output wrench magnitude (f).

The inverse force solution differs for a non-redundant and redundant manipulator, and therefore they will be explained separately.

3.3.1 Non-Redundantly-Actuated

In a non-redundantly-actuated manipulator the number of actuators is equal to the DOF of the manipulator. A PPM has three DOFs (two translational, and one rotational). Therefore, the number of rows in an ARS matrix ($[\$']$) is three[1] and it is equal to the number of the columns since there has to be three actuators. Hence, given that $[\$']$ is a square matrix, the inverse force solution of equation (2.41) can be rewritten for $\boldsymbol{\tau}_{\$}$ and $\$_F$:

$$\boldsymbol{\tau}_{\$} = ([\$'][\mathbf{W}^*])^{-1} \$_F \tag{3.3}$$

[1]Note that the number of elements in the compact form of the joint screws and ARS's for a PPM is also three as mentioned in Sections 2.3.1 and 2.3.2.

and the inverse of the $[\$'][\mathbf{W}^*]$ is possible. Note that $[\mathbf{W}^*]$ is a square matrix with its dimensions being equal to the number of actuators. From this point forward, the matrix product of the matrix $[\$']$ and the matrix $[\mathbf{W}^*]$ will be denoted as $[\$'\mathbf{W}]$ for the simplicity in the notation.

It is assumed that the maximum possible torques/forces (i.e., actuator capabilities, $\tau_{k_i\,\max}$) for all actuated joints are known. A term called the *scaling factor* (sf_{k_i}) is introduced for all actuated joints as the absolute value of the ratio between the limit $\tau_{k_i\,\max}$ and the actual value $\boldsymbol{\tau}_{\$k_i}$:

$$sf_{k_i} = \left| \frac{\tau_{k_i\,\max}}{\tau_{\$k_i}} \right| \tag{3.4}$$

where sf_{k_i} is the scaling factor of the k^{th} actuator of the i^{th} branch. The actuator with the smallest scaling factor ($sf_{\min}$) is the relatively-weakest actuator, and all actuators can be safely scaled up with this factor ensuring that they all are within their limits, i.e.:

$$sf_{\min} = \min_{k_i} (sf_{k_i}) \tag{3.5}$$

Scaled unit torque/force vector ($sf_{\min}\boldsymbol{\tau}_{\$}$) can now be used in the forward force solution of equation (3.1):

$$\boldsymbol{F} = [\$'\mathbf{W}] sf_{\min}\boldsymbol{\tau}_{\$} \tag{3.6}$$

Since $[\$'\mathbf{W}]\boldsymbol{\tau}_{\$}$ is equal to the unit wrench ($\boldsymbol{\$}_F$), the maximum possible magnitude of the applied wrench in equation (3.2) is:

$$f = sf_{\min} \tag{3.7}$$

To generate the force capability plot, the unit wrench $\$_F$ in equation (3.2) is varied through all possible directions and the magnitude f is calculated from the inverse force solution for each direction. The resultant applied force $\boldsymbol{F}$ is then drawn on the plot according to its direction.

It should be noted that when solving for the maximum applicable force for a given direction, it is also required to specify a moment value as well as the direction since the unit wrench screw $\$_F$ needs to be set. This moment component can be varied in order to explore force capabilities under a certain moment, or force capabilities along with moment capabilities.

3.3.2 Redundantly-Actuated

In a redundantly-actuated manipulator the number of the actuators is greater than the DOF of the manipulator and the difference between the number of actuators and the DOF defines the degree-of-redundancy (DOR) of the manipulator. Therefore, a PPM with four or more actuators is considered a redundant manipulator.

The ARS matrix ($[\$']$) of a redundantly-actuated manipulator is not a square matrix. Since only square matrices are invertible, the Moore-Penrose pseudo-inverse can be used in the inverse force solution (equation (3.3)):

$$\boldsymbol{\tau}_{\$} = [\$'\mathbf{W}]^{+} \$_F \tag{3.8}$$

where $[\$'\mathbf{W}]^{+}$ denotes the pseudo-inverse of $[\$'\mathbf{W}]$ and is defined as:

$$[\$'\mathbf{W}]^{+} = [\$'\mathbf{W}]^{\mathrm{T}} \left([\$'\mathbf{W}][\$'\mathbf{W}]^{\mathrm{T}} \right)^{-1} \tag{3.9}$$

The same methodology of scaling factor can be applied to determine the force capabilities of redundantly-actuated manipulators by using the pseudo-inverse in lieu of the inverse of [$'W].

It should be noted that in a redundantly-actuated manipulator there are infinitely many solutions of τ to the inverse force problem. The pseudo-inverse solution yields a τ that has the smallest magnitude, i.e., a minimization of the 2-norm of the actuated joint torques/forces vector [43].

3.4 Optimization-Based Solution

Although being a minimization, the pseudo-inverse solution is not necessarily the optimum solution to the maximum force capability problem. To obtain the maximum force capabilities of the redundantly-actuated manipulator with the scaling factor methodology, further optimization is required.

3.4.1 The Objective Function

The objective of the optimization is to maximize the magnitude f of the output wrench. It has been shown that this magnitude is equal to the smallest scaling factor (equation (3.7)). Therefore the minimum of the scaling factors of all the actuated joints has to be maximized. Essentially, that means minimizing the torques/forces by taking the actuator capabilities into account. This can be formulated as a minimization problem by introducing a vector called the normalized torque/force vector ($\hat{\tau}_{\$}$) which is defined as:

$$\hat{\tau}_{\$} = \left\{ \cdots \quad \frac{\tau_{\$k_i}}{\tau_{k_i \max}} \quad \cdots \right\}^{\mathrm{T}} \tag{3.10}$$

The objective function to be minimized can now be defined as the maximum absolute value of the normalized torque vector:

$$f_{obj} = \max\left(|\hat{\boldsymbol{\tau}}_{\$}|\right) \tag{3.11}$$

There is a high possibility that f_{obj} will be a non-differentiable function because of the max operator. Since it is more reliable to optimize a differentiable function as opposed to a non-differentiable one, the objective function is approximated by using a high p-norm of $\hat{\boldsymbol{\tau}}_{\$}$:

$$f_{obj} = \|\hat{\boldsymbol{\tau}}_{\$}\|_p \tag{3.12}$$

where the p-norm [44] of a vector is defined as:

$$\|\boldsymbol{x}\|_p = \left(\sum_{i=1}^{n} |\boldsymbol{x}_i|^p\right)^{\frac{1}{p}}, p \geq 1 \tag{3.13}$$

The effects of this approximation will be discussed later in this chapter.

3.4.2 Design Parameters

To accommodate the design parameters in the objective function the inverse force solution is broken up into its homogeneous and particular solution:

$$\$_F = [\$'\mathbf{W}]\left(\boldsymbol{\tau}_{\$_{\text{particular}}} + \boldsymbol{\tau}_{\$_{\text{homogeneous}}}\right) \tag{3.14}$$

where the particular solution satisfies:

$$\$_F = [\$'\mathbf{W}]\boldsymbol{\tau}_{\$_{\text{particular}}} \tag{3.15}$$

and the homogeneous solution satisfies:

$$\mathbf{0} = [\$'\mathbf{W}]\boldsymbol{\tau}_{\$_{\text{homogeneous}}} \tag{3.16}$$

A $\boldsymbol{\tau}_{\$_{\text{homogeneous}}}$ can be found by using Singular Value Decomposition (SVD) on the $[\$'\mathbf{W}]$ matrix. SVD on the $[\$'\mathbf{W}]$ matrix of size $m \times n$ and rank r yields the matrices $[\mathbf{U}]_{m\times m}$, $[\mathbf{S}]_{m\times n}$, and $[\mathbf{V}]_{n\times n}$ which satisfy:

$$[\$'\mathbf{W}] = [\mathbf{U}]\,[\mathbf{S}]\,[\mathbf{V}]^{\mathrm{T}} \tag{3.17}$$

where $[\mathbf{S}]$ is a diagonal matrix of the square roots of the non-zero eigenvalues of $[\$'\mathbf{W}][\$'\mathbf{W}]^{\mathrm{T}}$ and $[\$'\mathbf{W}]^{\mathrm{T}}[\$'\mathbf{W}]$. The $[\mathbf{U}]$ and $[\mathbf{V}]$ matrices are orthogonal matrices that provide bases for the four fundamental spaces of $[\$'\mathbf{W}]$ [45]. The last $n - r$ columns (the DOR of the manipulator) of $[\mathbf{V}]$ can be extracted to be $[\mathbf{V}']$ which spans the null space of $[\$'\mathbf{W}]$. Therefore the homogeneous solution is:

$$\boldsymbol{\tau}_{\$_{\text{homogeneous}}} = [\mathbf{V}']\,v \tag{3.18}$$

where v is any $(n - r)\times 1$ vector which is mapped into the torque/force null space through $[\mathbf{V}']$ for the given $[\$'\mathbf{W}]$, and therefore satisfies equation (3.16). Physically, the resultant $\boldsymbol{\tau}_{\$_{\text{homogeneous}}}$ is a set of actuator torques/forces that does not contribute to the wrench being applied by the manipulator. Instead, it causes an internal self-cancelling force within the end-effector. This ensures that the unit wrench $\$_F$ will not be altered for any choice of vector v. Hence the vector v is chosen to be the design parameter of the optimization problem.

For the particular part of the inverse force problem, the pseudo-inverse solution

is chosen for $\boldsymbol{\tau}_{\$_{\text{particular}}}$ since it satisfies equation (3.15).

With the particular and homogeneous parts defined, the $\boldsymbol{\tau}_{\$}$ to be used in the objective function becomes:

$$\boldsymbol{\tau}_{\$} = [\$'\mathbf{W}]^{+} \$_F + [\mathbf{V}']\, v \tag{3.19}$$

which finalizes the set up of the optimization problem.

The solution of the optimization problem is done using the unconstrained minimization function (`fminunc`) of the Optimization Toolbox in MatLab® [46]. This function uses the Broyden-Fletcher-Goldfarb-Shanno Quasi-Newton method for updating the approximation of the Hessian matrix, and a mixed quadratic and cubic polynomial interpolation & extrapolation method as its line search algorithm.

The optimized torque/force vector is used in lieu of equation (3.3), and the same methodology of scaling factors as for non-redundantly-actuated manipulators can be applied in order to calculate the maximum force capabilities.

3.4.3 Some Remarks on the Optimization-Based Solution

It has been mentioned before that, the pseudo-inverse solution is a power 2-norm minimization. However this minimization is different than the one presented in the optimization section. Note that in pseudo-inverse solution, the vector that is minimized is the actual force/torque vector ($\boldsymbol{\tau}_{\$}$). Hence it does not take the actuator capabilities into account. It minimizes the torque/force magnitudes, i.e., the power that is consumed at a given instant. However, in the optimization case, the vector to be minimized is the normalized torque/force vector ($\hat{\boldsymbol{\tau}}_{\$}$) which includes the actuator capability information. Therefore, unless all the scaling factors are the same, the

pseudo-inverse solution and the optimization solution with power 2-norm does not yield the same solution.

It has been mentioned that the homogeneous part of the torque/force vector in the inverse force solution results in no output wrench. Such a torque/force set creates what is called an internal force. Kumar and Waldron [20] showed that the pseudo-inverse solution yields no internal forces in the manipulator. Therefore, the optimization starts with no internal forces and searches for the $\boldsymbol{\tau}_{\$}$ by introducing internal forces. In other words, the optimization solution exploits the use of internal forces in order to achieve the maximum force capability.

3.5 Comparison Between the Pseudo-Inverse Solution and the Optimization-Based Solution

In order to compare the pseudo-inverse and the optimization-based solution, a set of analyses have been made. Force capability plots have been generated for a non-redundantly-actuated, a redundantly-actuated with pseudo-inverse solution and a redundantly-actuated with optimization-based solution cases.

The manipulator considered in these analyses is a three-branch, three-revolute joints per branch (3 RRR) PPM. The dimensions and the actuator capabilities are modeled after the RPPM [6]. The base and the platform of the RPPM are equilateral triangles. The edge lengths of the base triangle are 0.5 m. The link lengths and the edge lengths of the platform triangle are all 0.2 m. The platform is positioned at the centre of the workspace, i.e., the centre of the base triangle, and the orientation is zero. The actuation scheme of the manipulator is 3-$\underline{\text{R}}$RR for the non-redundant

case and 3-RRR for the redundant case. The maximum torque capabilities of the actuators are assumed to be ± 4.2 Nm for the base joints, and ± 2.1 Nm for the elbow joints. Applied moments are set to zero, i.e., the manipulator applies pure force, and the direction of the force is changed every degree. A schematic diagram of these manipulators are shown in Figure 3.1.

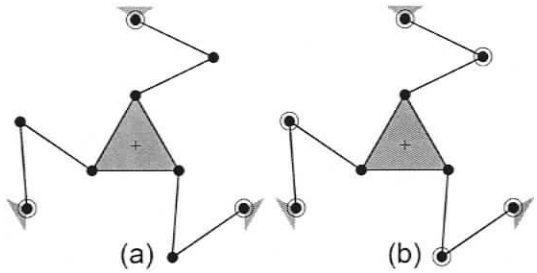

Figure 3.1: Schematic diagrams of a) 3-RRR and b) 3-RRR

Figure 3.2 shows the force capability plot when the manipulator is non-redundantly-actuated. The individual lines show the force capabilities constrained by their corresponding actuators capabilities, τ_{j_b}, where the subscripts denotes the actuator of joint j of branch b. The inner hexagon formed by the lines is the force capability polygon of the manipulator. The selection of the smallest scaling factor in equation (3.5) corresponds to finding the closest actuator line crossing the direction α, meaning that this actuator will perform at its maximum capability while the remaining actuators will perform below their capabilities. The distance between the centre of the polygon and the first crossed line yields the scaling factor, and thus, the magnitude of the maximum applicable force along that direction. Note that, at the vertices of the polygon there are two actuators limiting the force capability at the same time, i.e., performing at their maxima, whereas for all other directions there is only one actuator limiting the force capabilities. For this case, the maximum applicable force

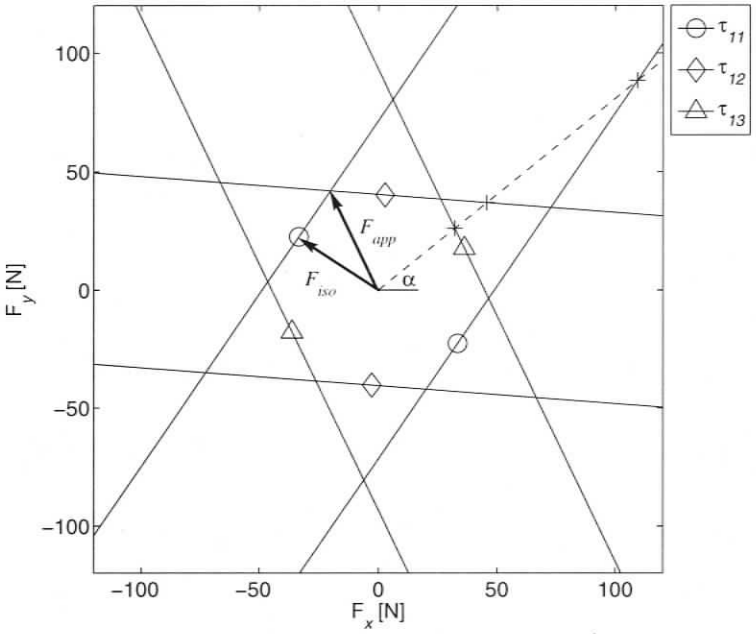

Figure 3.2: Force Polygon (Non-redundant Case)

F_{app} is found to be 46.44 N at 116°, and the maximum isotropic force F_{iso} is found to be 40.22 N at 146°.

Figure 3.3 shows the force capability plot of the 3-RRR actuation scheme with the pseudo-inverse solution. The maximum applicable force 49.26 N is slightly higher than the non-redundantly case since there are more actuators in the system, and it occurs at 250°. It's also seen that the inner most hexagon formed by the lines is larger as well. However, there is still only one actuator that limits the polygon for the directions pointing the edges of the force polygon. These limit lines are formed by the elbow joint actuators which signifies that the base joint actuators perform below their capabilities, i.e., they are underused.

Finally, Figure 3.4 shows the force capability plot of the 3-RRR actuation scheme with the optimization-based solution. The choice of the power of the p-norm will be

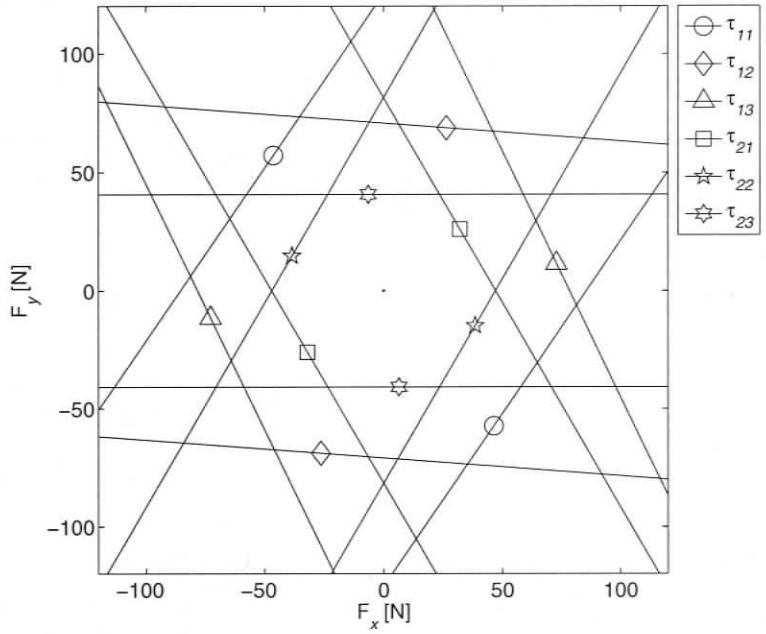

Figure 3.3: Force Ploygon (Redundant Case with Pseudo-inverse Solution)

discussed later in this chapter. For this analysis, p is set to 100 as shown suitable in the work of Nokleby et al. [24]. The maximum applicable force achieved with this solution is 90.58 N, and it occurs at 283°. Note that the constraints of the individual actuators are bent lines as opposed to straight lines as in the previous analyses. This shows that the optimization pushes the actuator forces towards their maximum capabilities and makes the most use out of them. For a given force direction, there are four out of the six actuator lines that are either limits or very close to limiting the edges of the force polygon, whereas at the vertices there are five actuator lines intersecting.

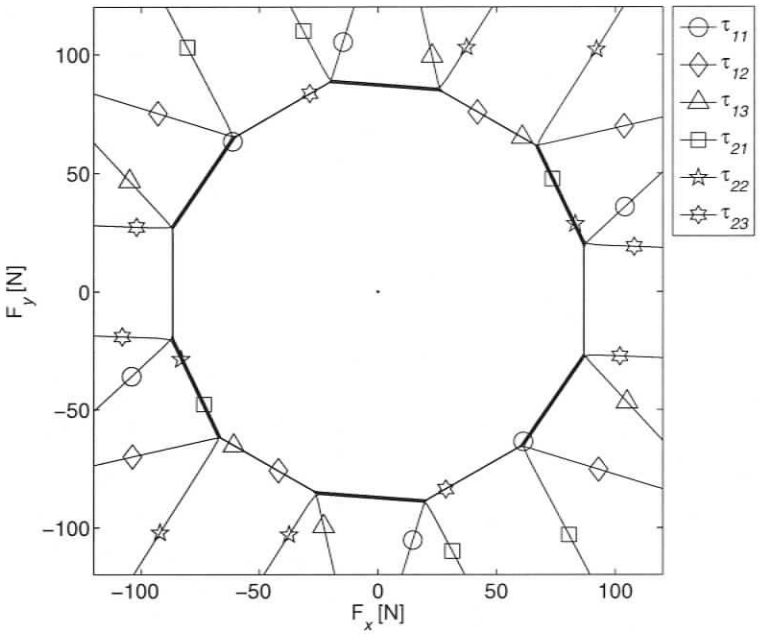

Figure 3.4: Force Ploygon (Redundant Case with Optimization-based Solution)

3.6 Limitations of the Scaling Factor Methodology

3.6.1 Uncontrollable Moment

In both the non-redundantly and redundantly-actuated cases, the unit wrench is specified in equation (3.3) in order to set the force direction. The first two elements of the unit wrench specify the direction, and the last element specifies the moment. The final output wrench is obtained by multiplying the unit wrench by the derived scaling factor. As a consequence, the moment value in the unit wrench is altered by the scaling factor around the force polygon, and it is not constant. This prevents the user from explicitly specifying a desired moment for the analysis except in the case where the moment is set to zero. In the previous works [24, 25], this problem is approximated by exhaustively computing many different moments, and inter/extrapolating

to fill in the missing results in the force capability plots of a fixed moment value. Thus the results are not exact and the process is computationally intensive.

3.6.2 The Effect of the p-Norm

As mentioned before, the p-norm function is used in lieu of the max operator to avoid a non-differentiable objective function. The higher the even power of p of the p-norm function, a better approximation to the max operator results. Theoretically, an infinite power of p in the p-norm is equivalent to the max operator.

On the other hand, a lower power p-norm function is smoother than a higher one, and hence makes it easier for the optimization routine to converge. Moreover, a smoother surface in the search variables' space means less local minima for the optimization routine to be caught in.

The following two examples are given in order to show the effect of the p-norm. The manipulator system is the same as in Section 3.5. Figures 3.5 and 3.6 show the actuated torques along with the resulting wrench direction for the two cases where p-norm uses $p = 10$ and $p = 10^6$, respectively. When the p-norm has $p = 10$, the elbow joints are far from their maxima, whereas when $p = 10^6$ they are at their maxima but the quality of the plot is decreased. The maximum wrench obtained with the p-norm with $p = 10$ was 65.74 N and with the p-norm with $p = 10^6$ was 68.26 N.

3.6.3 Optimization Problems

The optimization algorithm requires an initial starting point. Once the first maximum force for a desired direction is found, it can be considered as the starting point for the next iteration. Nevertheless, if the starting point of the first iteration yields

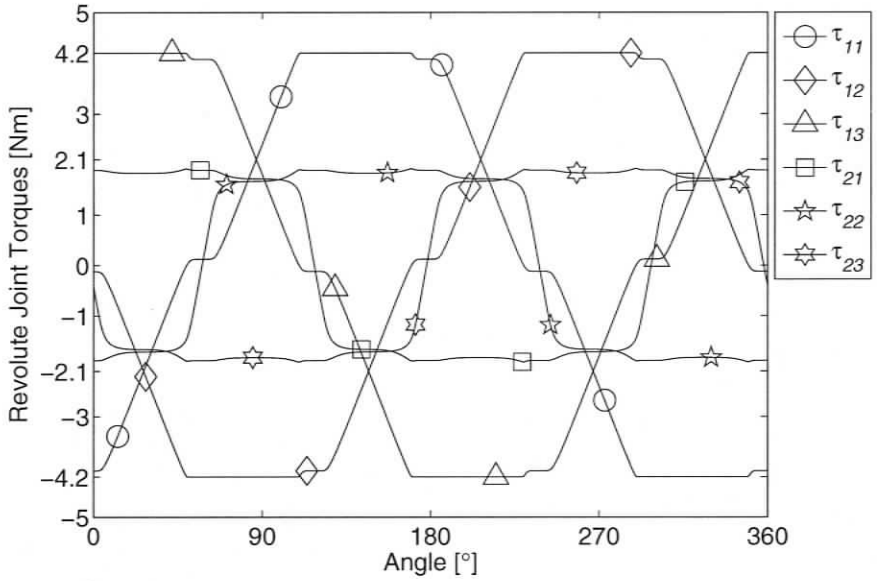

Figure 3.5: Actuator Torques, with p-norm=10

a local minimum, the path taken by the other iterations would be incorrect, i.e., it will most likely hit the same local minimum. This prevents the use of a high p-norm value since it is more likely to have more local minima. The more local minima encountered the less accurate the results obtained.

3.6.4 Computation Time

The scaling factor methodology requires an optimization run for every wrench direction. Optimization routines involve heavy computation, and the analysis for one pose approximately takes 15 seconds on a P4 3.2 GHz computer. This becomes an issue when the analysis is performed throughout the whole workspace of the manipulator, and limits the usefulness of the optimization solution as a design tool.

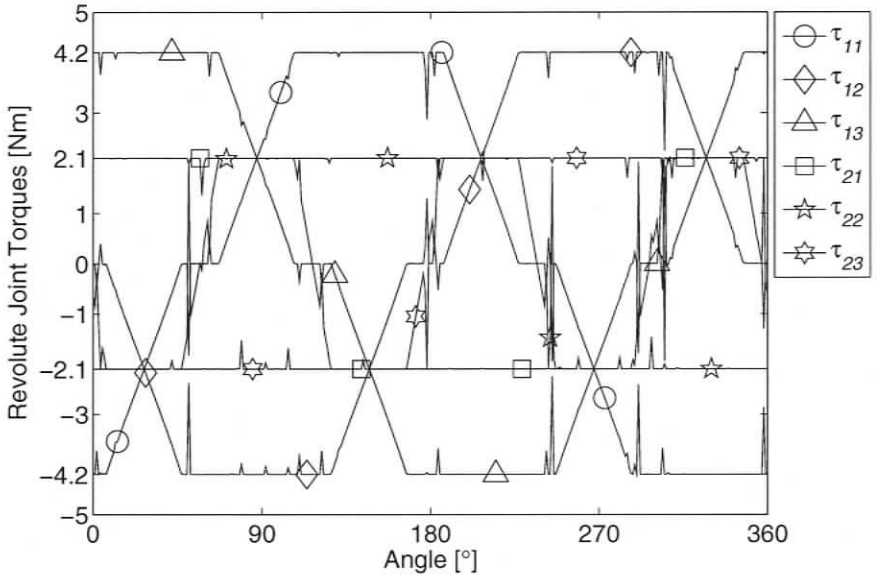

Figure 3.6: Actuator Torques, with p-norm=10^6

Chapter 4

Wrench Capability Analysis with an Explicit Methodology

4.1 Overview

In the optimization of the scaling factor methodology, it has been observed that, greater output wrenches are obtained when the individual actuators are close to their maximum capabilities. A solution is developed in [32] and [33] to explicitly set the largest number of actuators to their maximum capabilities while satisfying various constraints which will be introduced for different types of analyses.

This chapter will describe an explicit methodology to find the F_{app}, and F_{iso}, and compare it with the optimization solution of the scaling factor methodology. Following this, a more efficient way of constructing the force polygon will be presented. Then, the wrench polyhedrons will be introduced. Finally, five different analysis types are proposed which implement the explicit methodology.

4.2 Explicit Methodology

Assuming that the manipulator has k actuated joints, the forward force solution yields:

$$[\$'\mathbf{W}]_{3\times k}\boldsymbol{\tau}_{k\times 1} = \boldsymbol{F}_{3\times 1} \tag{4.1}$$

where $\boldsymbol{F}$ can be expressed as $\{f\cos(\alpha), f\sin(\alpha); m\}^{\mathrm{T}}$; with f being the wrench intensity, α being the direction and m being the moment of the output wrench. All the elements of $[\$'\mathbf{W}]$ are known through the geometry and the pose of the manipulator. All the elements of $\boldsymbol{\tau}$ and $\boldsymbol{F}$ are unknown, i.e., there are $k+3$ unknowns. Vector equation (4.1) contains 3 scalar equations to be satisfied, thus, k unknowns can be set arbitrarily.

The selection of which k unknowns to set arbitrarily depends on the type of analysis. In order to compare this methodology to the optimization solution, the same constraints will be employed: the moment of the wrench will be a prescribed constant value, and the force polygon will be constructed by varying the direction of the force through 360°, finding the maximum force for each direction, and finally extracting F_{app} and F_{iso} among those maximum forces. Therefore, m and α should be specified and considered as known variables. This leaves $k-2$ unknowns to be chosen arbitrarily. Hence, $k-2$ actuator torques can be set to their maximum capabilities, i.e., torques at their maximums (τ_{m}). The force magnitude f and the remaining two unknown torques, which will have a value between their limits, i.e., torques in

transition (τ_{t}), can be solved for by properly arranging equation (4.1) as follows:

$$\underbrace{\begin{bmatrix} -\$'\mathrm{w}_{1,\mathrm{t}_1} & -\$'\mathrm{w}_{1,\mathrm{t}_2} & \cos(\alpha) \\ -\$'\mathrm{w}_{2,\mathrm{t}_1} & -\$'\mathrm{w}_{2,\mathrm{t}_2} & \sin(\alpha) \\ -\$'\mathrm{w}_{3,\mathrm{t}_1} & -\$'\mathrm{w}_{3,\mathrm{t}_2} & 0 \end{bmatrix}}_{\mathbf{A}} \underbrace{\begin{Bmatrix} \tau_{\mathrm{t}_1} \\ \tau_{\mathrm{t}_2} \\ f \end{Bmatrix}}_{\mathbf{x}} = \underbrace{\begin{bmatrix} \$'\mathrm{w}_{1,\mathrm{m}_1} & \$'\mathrm{w}_{1,\mathrm{m}_2} & \cdots & \$'\mathrm{w}_{1,\mathrm{m}_{k\text{-}2}} \\ \$'\mathrm{w}_{2,\mathrm{m}_1} & \$'\mathrm{w}_{2,\mathrm{m}_2} & \cdots & \$'\mathrm{w}_{2,\mathrm{m}_{k\text{-}2}} \\ \$'\mathrm{w}_{3,\mathrm{m}_1} & \$'\mathrm{w}_{3,\mathrm{m}_2} & \cdots & \$'\mathrm{w}_{3,\mathrm{m}_{k\text{-}2}} \end{bmatrix} \begin{Bmatrix} \pm\tau_{\mathrm{m}_1} \\ \pm\tau_{\mathrm{m}_2} \\ \vdots \\ \pm\tau_{\mathrm{m}_{k\text{-}2}} \end{Bmatrix} - \begin{Bmatrix} 0 \\ 0 \\ m \end{Bmatrix}}_{\mathbf{b}} \tag{4.2}$$

where $\boldsymbol{\tau}_{\mathrm{t}_j}$ are the unknown torques that are in transition, $\$'\mathrm{w}_{i,\mathrm{t}_j}$ are the elements of the $[\$'\mathbf{W}]$ matrix that are associated with $\boldsymbol{\tau}_{\mathrm{t}_j}$, $\boldsymbol{\tau}_{\mathrm{m}_j}$ are the maximum capabilities of the actuators that are at their maximums, and $\$'\mathrm{w}_{i,\mathrm{m}_j}$ are the elements of the $[\$'\mathbf{W}]$ matrix that are associated with $\boldsymbol{\tau}_{\mathrm{m}_j}$. The linear equation $[\mathbf{A}]\mathbf{x}=\mathbf{b}$ can be solved to obtain the wrench intensity f and the two unknown torques in transition τ_{t_1} and τ_{t_2}.

In order to find the maximum wrench intensity from equation (4.2) one must know which of the k actuators are at their maximum and if they are at their positive maximum or negative maximum. For the first wrench direction α_1, this is accomplished by trying all possible actuators that are at their maximums and their sign combinations. If $k-2$ actuators are chosen out of k actuators at a time, and all of them can be either positive or negative, then there is a total of $n_{C_{(k-2)}}$ combinations:

$$n_{C_{(k-2)}} = n_A \cdot n_S = \underbrace{\frac{k!}{(k-(k-2))! \cdot (k-2)!}}_{n_A} \cdot \underbrace{2^{k-2}}_{n_S} = k \cdot (k-1) \cdot 2^{k-3} \tag{4.3}$$

where n_A is the number of actuator combinations and n_S is the number of sign combinations. Equation (4.2) is solved with all of the possible combinations, i.e., $n_{C_{(k-2)}}$ times. The solutions in which the torques in transition exceed their maximum

capabilities are filtered out. Among the remaining solutions, the solution that yields the highest wrench magnitude is selected as the correct solution for this first direction.

The next direction of the wrench is solved again through equation (4.2) by assuming the same τ_{m} combination as the previous one, i.e., the torques that are at their maximums with their corresponding signs are preserved. The same combination is used for subsequent directions until one of the torques in transition exceeds its maximum value. When this occurs, the exceeded torque is set to its maximum and one of the torques that is at its maximum becomes a torque in transition. To determine the new torque in transition, equation (4.2) is solved for $n_{C_{(k-2)}}$ combinations. Note that solving for $n_{C_{(k-2)}}$ combinations is necessary since both torques may exceed their maximums at the same direction (ensured by n_A combinations), and a torque that is at its maximum may switch from its positive maximum to its negative maximum at the next direction (ensured by n_S combinations).

4.3 Comparison of the Scaling Factor and the Explicit Methodologies

In order to compare the two methodologies, the same manipulator system in Section 3.6.2 has been analyzed with the explicit methodology outlined above. Thus, m is set to zero and the force capabilities are found for every degree. Figure 4.1 shows the actuator torques solved with the explicit methodology. Four of the actuators are at their respective maximum at any given wrench direction, and as a result of the explicit solution, there are no spikes in the graph. The maximum applicable force of all directions is 68.26 N, i.e., the manipulator can sustain at most 68.26 N in one

specific direction. Note that there is no improvement in the maximum applicable force compared to the optimization-based p-norm solution when $p = 10^6$. This shows

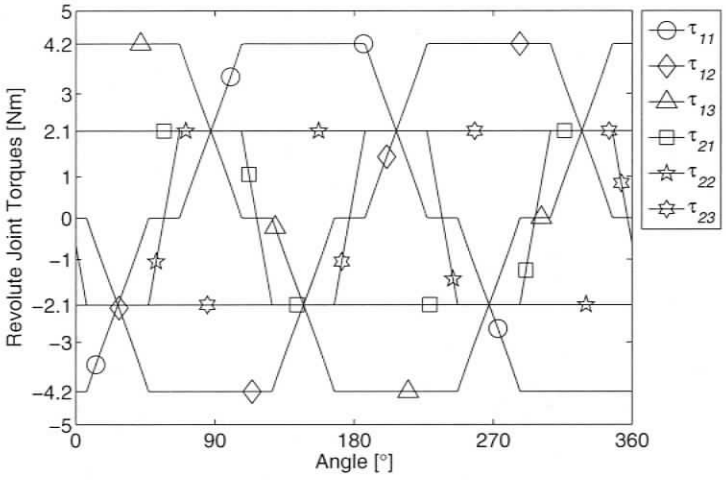

Figure 4.1: Actuator Torques with the Explicit Methodology

that, a higher p-norm may result in good force capabilities, but the reliability of the optimization solution decreases due to the complexity of a higher p-norm function, which may lead to incorrect results if local minimums are encountered. With the explicit methodology, however, it is guaranteed that the maximum number of actuators will perform at their limits, and the elimination of the spikes ensures that the maximum force is achieved for every direction of the force.

Another advantage of the explicit methodology is that one can explicitly introduce a moment value to the resulting wrench and carry out the analysis. This allows the determination of the force capability polygon under any specified moment load, which was not possible with the scaling factor methodology.

Lastly, since no optimization routine is used in the explicit methodology, the

computation time is substantially improved. The force capability analysis for one pose is completed in 15 seconds with the scaling factor methodology when running on a P4 3.2 GHz computer. In the explicit methodology this time drops to 0.1 second. This improvement extends the scope of the analysis that can be made on the force capabilities of PPMs.

4.4 Construction of the Force Polygon

In Figure 4.1, it can be noted that when a torque in transition reaches its limit, another actuator becomes a torque in transition. At that particular direction, there are $k-1$ torques that are at their maximums as opposed to $k-2$. This wrench direction corresponds to a vertex of the force polygon, as can be seen in Figure 3.4. Investigating this observation led to a method for fast and accurate computation of the force polygon. The following is a proof of concept for this observation and a trivial example.

Let $\mathbf{A}$ be a linear transformation from $\mathbb{R}^m$ to $\mathbb{R}^n$. A unit *hypercube*[1] centred at the origin in $\mathbb{R}^m$, has 2^m vertices (v_i, $i = 1, \ldots, 2^m$) with all m coordinates being plus or minus 1. Applying the linear transformation $\mathbf{A}$ to the hypercube will result in a centrosymmetric convex polytope in $\mathbb{R}^n$, with vertices being the convex hull[2] of $\mathbf{A}v_i$ [48].

According to the above statement, assuming $[\$'\mathbf{W}]$ is a linear mapping from the actuator space to the task space, the vertex forces of the force polygon will be produced when the actuator torques are at their maximums. Consider a simple 2-DOF

[1] A hypercube is a convex polytope in n-dimension which is the analogue of a square in 2-dimensions and or a cube in 3-dimensions [12].

[2] Convex hull is the minimum convex set that contains a set of points in n-dimension [47].

2-RPR manipulator as shown in Figure 4.2. Let the actuator capabilities of the

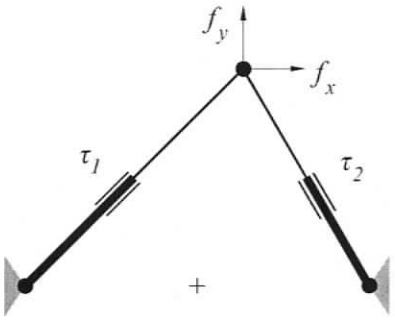

Figure 4.2: 2-DOF, 2-RPR Manipulator

prismatic joints τ_1 and τ_2 be ± 1 N. These constraints define a hypercube in the actuator space ($\mathbb{R}^2$), i.e., a square, and can be expressed as:

$$\max(|\boldsymbol{\tau}|) \leq 1 \tag{4.4}$$

The vertices of this square are:

$$\mathbf{v}_\tau = \begin{Bmatrix} 1 & -1 & -1 & 1 \\ 1 & 1 & -1 & -1 \end{Bmatrix} \tag{4.5}$$

where the columns of $\mathbf{v}_\tau$ are the vertex coordinates. For the configuration shown in Figure 4.2, with the linear mapping matrix being:

$$[\$'\mathbf{W}] = \begin{bmatrix} \cos(45°) & \cos(120°) \\ \sin(45°) & \sin(120°) \end{bmatrix} \tag{4.6}$$

the resulting domain is a centrosymmetric polytope in the task space ($\mathbb{R}^2$), i.e., a

parallelogram, with the vertices being:

$$\mathbf{v}_F = \mathbf{A}\mathbf{v}_\tau = \begin{Bmatrix} 0.21 & -1.21 & -0.21 & 1.21 \\ 1.57 & 0.16 & -1.57 & -0.16 \end{Bmatrix} \tag{4.7}$$

Figure 4.3 shows this mapping process of the vertices as well as some intermediate points along the constraints.

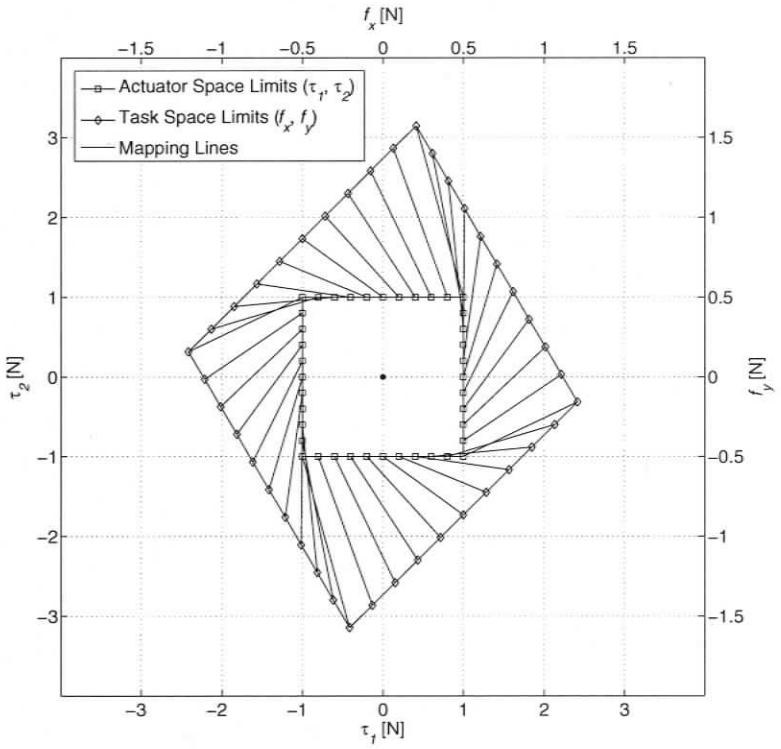

Figure 4.3: Linear Mapping of Actuator Limits Into the Task Space

Note that when mapping from $\mathbb{R}^m$ to $\mathbb{R}^n$, if $m = n$, all the vertices from $\mathbb{R}^m$ will correspond to a vertex in $\mathbb{R}^n$, and therefore, there is no need to take the convex hull of the mapped vertices. However, when $n < m$, some of the vertices in $\mathbb{R}^m$ will no longer be a vertex in $\mathbb{R}^n$, but an inner point within the polytope. This corresponds

to the redundant case in manipulators where there are more actuators than the DOF of the task space.

Going back to the original problem, in order to construct the force polygon, it is sufficient to locate only the vertices rather than searching through all the wrench directions. F_{app} and F_{iso} can then be found through the force polygon (see Figure 1.4).

Eliminating the search of all wrench directions removes the constraint α from equation (4.2). Assuming the angle α as an unknown, yields $k-1$ actuators being at their maximums[3]. This also complies with the fact that $k-1$ actuators are at their maximums at the vertices of the polygon in Figure 3.4. With α as an unknown, equation (4.1) yields:

$$\begin{bmatrix} -\$'w_{1,t} & 1 & 0 \\ -\$'w_{2,t} & 0 & 1 \\ -\$'w_{3,t} & 0 & 0 \end{bmatrix} \begin{Bmatrix} \tau_t \\ f\cos(\alpha) \\ f\sin(\alpha) \end{Bmatrix} = \begin{bmatrix} \$'w_{1,m_1} & \$'w_{1,m_2} & \cdots & \$'w_{1,m_{k-1}} \\ \$'w_{2,m_1} & \$'w_{2,m_2} & \cdots & \$'w_{2,m_{k-1}} \\ \$'w_{3,m_1} & \$'w_{3,m_2} & \cdots & \$'w_{3,m_{k-1}} \end{bmatrix} \begin{Bmatrix} \pm\tau_{m_1} \\ \pm\tau_{m_2} \\ \vdots \\ \pm\tau_{m_{k-1}} \end{Bmatrix} - \begin{Bmatrix} 0 \\ 0 \\ m \end{Bmatrix} \tag{4.8}$$

where τ_t is the only unknown torque that is in transition, and $\$'w_{i,t}$ are the elements of the $[\$'\mathbf{W}]$ matrix that are associated with τ_t. This linear equation can be solved to obtain the wrench intensity f, the wrench direction α, and the unknown torque in transition τ_t.

In order to find the vertices of the force polygon through equation (4.8), all possible actuators that are at their maximums and their sign combinations have to be tried.

[3]Note that unlike the trivial example given before, not all actuators can be maxed out in this case, since an additional constraint exists in the system, i.e., m. Therefore $k-1$ actuators can be maxed out.

If $k-1$ actuators are chosen out of k actuators at a time, and all of them can be either positive or negative, then there is a total of:

$$n_{C_{(k-1)}} = n_A \cdot n_S = \underbrace{\frac{k!}{(k-(k-1))! \cdot (k-1)!}}_{n_A} \cdot \underbrace{2^{k-1}}_{n_S} = k \cdot 2^{k-1} \tag{4.9}$$

combinations. Equation (4.8) is solved $n_{C_{(k-1)}}$ times and the solutions where the torque in transition exceeds its maximum capability are filtered out. The remaining solutions constitute a set of wrenches which are the vertices of the force polygon, and for the redundant case some wrenches that are within the force polygon. The maximum applicable force F_{app} can be found by selecting the wrench that has the highest force magnitude among the solution set. Figure 4.4 shows a set of such wrenches as dots on the x-y plane, and the force polygon formed by them. The

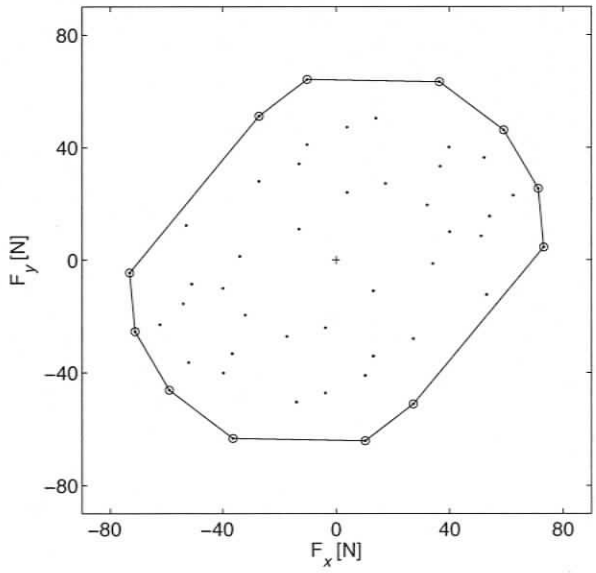

Figure 4.4: Force Polygon Formed by a Set of Wrenches

maximum isotropic force F_{iso}, however, lies on one of the edges, and the force polygon has to be constructed in order to determine it.

The problem of determining the vertices of the force polygon, given the set of wrenches found in equation (4.8) is a 2-dimensional convex hull problem. This is a widely investigated problem and there are numerous algorithms in the literature [49]. The *Javis' March Method* [50] is used in this work to solve this convex hull problem. This method is also known as the *gift wrapping* algorithm and is analogous to wrapping a taut string around a set of nails sticking out of a board. Computation begins with a point A that is known to be a vertex, e.g., the wrench that has the highest force magnitude. The next vertex is found by selecting the point B such that all other points fall to the right of the line $\overline{AB}$. The solution is complete when point A is reached as the last vertex.

The magnitude of the minimum isotropic force F_{iso} is the minimum of the distances between each edge and the centre of the polygon as shown in Figure 4.5. Once the force polygon is identified by its vertices, these distances can be found as follows:

$$d_i = \frac{|-F_{y_i} + s_i \cdot F_{x_i}|}{\sqrt{1 + s_i^2}} \tag{4.10}$$

where d_i is the distance between the centre of the polygon and the edge between vertex i and vertex $i+1$, s_i is the slope of the edge between vertex i and vertex $i+1$, and F_{x_i} and F_{y_i} are the x and y components of the wrench of the vertex i, respectively. The direction of F_{iso} can be found as:

$$\alpha_{iso} = \arctan(-\frac{1}{s_i}) \tag{4.11}$$

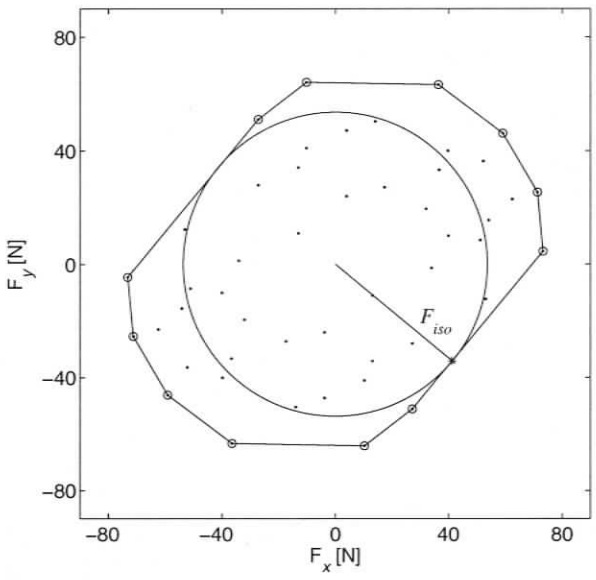

Figure 4.5: F_{iso} of a Force Polygon

since it is perpendicular to the slope of the edge where F_{iso} resides. Note that the resulting α_{iso} may lead to the wrong quadrant due to the arctan operator. This can be verified by checking whether F_{iso} falls between the correct vertices or not. According to this, α_{iso} can be replaced with $\alpha_{iso} + \pi$.

Constructing the force polygon through the vertices method is significantly more efficient than computing the maximum force along every direction. Another advantage of the vertices method is that F_{app} and F_{iso} are exact in terms of their magnitudes and directions, whereas, when computed for discrete directions, their precision is limited by the number of the directions considered within a full 360° revolution.

4.5 Construction of the Wrench Polyhedrons

So far, the force capabilities were presented as a polygon in a 2-dimensional space since planar manipulators are of interest and the force has two components. In order to have a better and visual understanding of the force and moment capabilities, a third dimension depicting the moment of the applied wrench will be introduced. In this 3-dimensional task space, the linear mapping of the actuators will be a polyhedron.

In order to construct the wrench polyhedron of a manipulator for a given pose, one has to identify all the vertices of the actuator space hypercube defined by the actuator capabilities, map these vertices into the task space, and finally take the convex hull of the mapped vertices if the manipulator is redundant. Note that the actuators may have different maximum capabilities than each other and have a value other than 1. Therefore, the unit hypercube mentioned in the previous section may not be unitary and may not be a hypercube but rather an n-dimensional rectangular prism called a *hypercuboid*.

As an example, wrench polyhedrons of the two manipulators presented in Section 3.5 will be generated. Figure 4.6 shows the wrench polyhedron of the 3-$\underline{\text{R}}$RR manipulator for its centre pose. Note that since this manipulator has three actuators, and therefore is non-redundant, it has $2^3 = 8$ vertices in both actuator and task spaces. It is also worth to mention that each parallel face corresponds to the positive and negative limits of one of the actuators. This is because the number of remaining actuators that can be varied is two, and therefore, they form a 2-dimensional space, i.e., a surface. The intersection of any two faces form an edge of the polyhedron, where two actuators are at their maximums. The intersection of three planes forms a vertex, and as established before, is produced when three actuators are at their

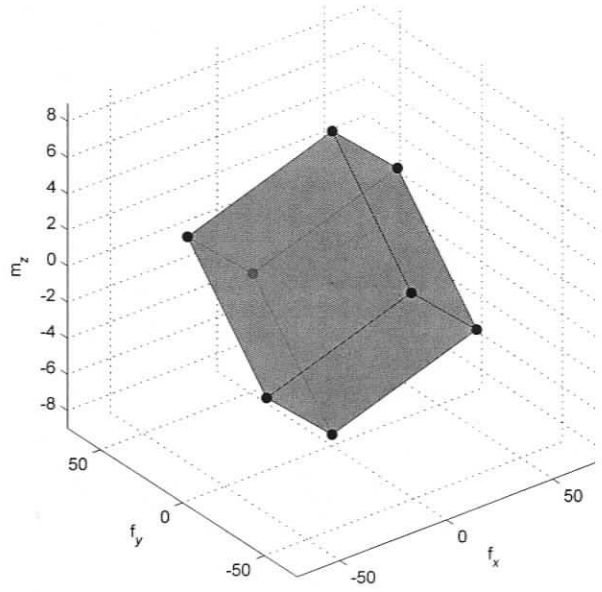

Figure 4.6: Wrench Polyhedron of the 3-RRR for Its Center pose

maximums.

Figure 4.7 shows the wrench polyhedron of the 3-RRR manipulator for its centre pose. Since this manipulator has six actuators, there are $2^6 = 64$ vertices of the hypercuboid in the actuator space. When these 64 vertices are mapped to the task space, only 30 of them form a convex hull[4] (shown as large dots in Figure 4.7), and the remaining 34 become inner points (shown as small dots in Figure 4.7). In a redundant manipulator's wrench polyhedron, actuators do not limit the polyhedron simply by surfaces as in the non-redundant case. For the 3-RRR manipulator, for instance, if one actuator is set to its positive limit, there are five other actuators which form a 5-dimensional cuboid in the actuator space. In the task space, this 5-dimensional cuboid is transformed into a sub-polyhedron which is within the original polyhedron.

[4]For this particular example, the convex hull of the three dimensional points was computed by the n-dimensional convex hull function (convhulln) of MATLAB®. This function is based on the Quickhull algorithm [51].

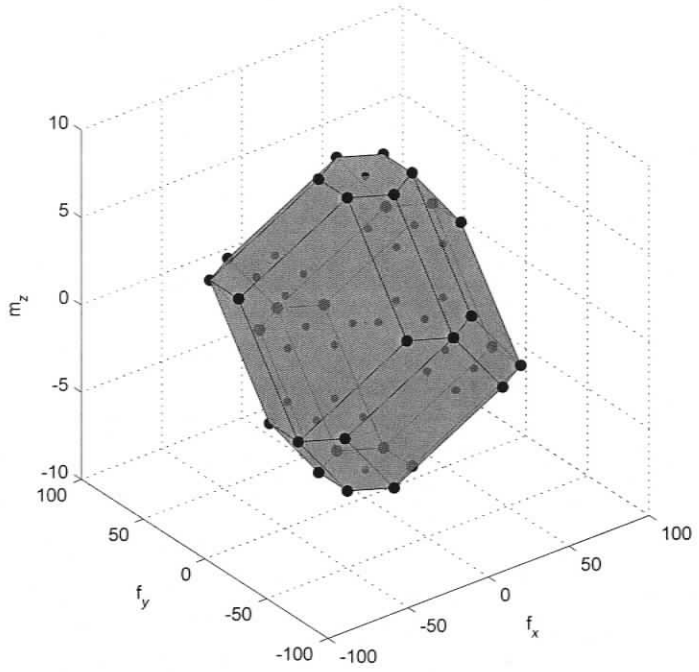

Figure 4.7: Wrench Polyhedron of the 3-RRR for Its Center Pose

Thus, in the task space, an actuator limit represents the image of an $n-1$ dimensional cuboid. Figure 4.8 shows the limiting sub-polyhedrons for all individual actuators for this manipulator (lighter volumes depict positive, and darker volumes negative limits). Note that all the inner points of the polyhedron are contained within the limiting sub-polyhedrons.

4.6 Analysis Types

4.6.1 Types of Analyses and Variables

The explicit methodology presented above is used to implement five different types of analysis based on the selection of the unknown variables in equation (4.1):

1) Maximum force with a prescribed moment,

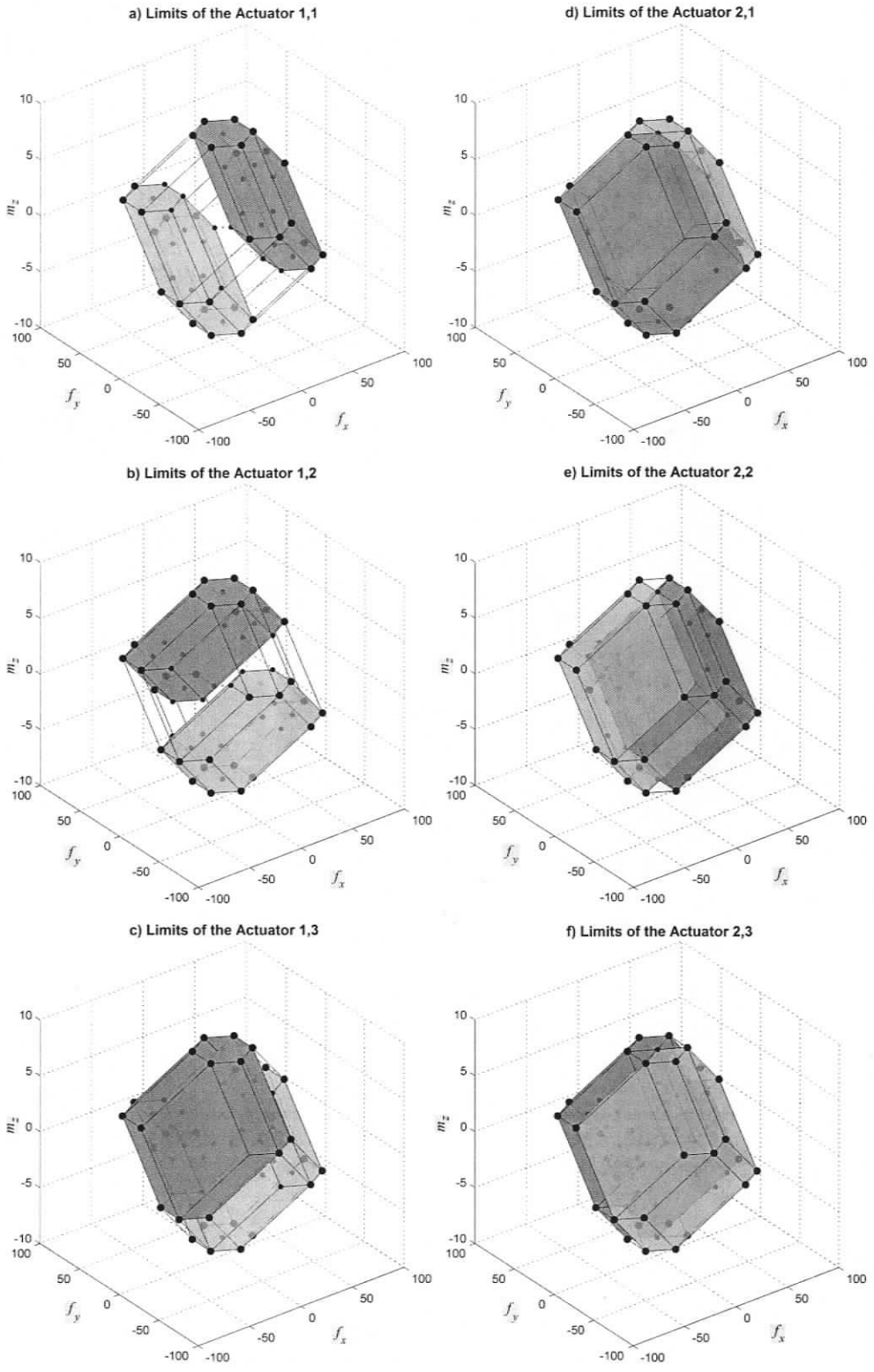

Figure 4.8: Individual Actuator Limits of the 3-RRR

2) Maximum force with an associated moment,

3) Maximum moment with a prescribed force,

4) Maximum moment with a prescribed force magnitude (no specified direction),

5) Maximum moment with an associated force.

Table 4.1 shows known and unknown variables, number of torques in transition, and number of torques that are at their maximums for the analysis types. The

Table 4.1: Variables of the Analysis Types

Analysis Type	Knowns	Unknowns	Number of τ_t	Number of τ_m
1	m	f, α	1	$k-1$
2	-	f, α, m	0	k
3	f, α	m	2	$k-2$
4	f	α, m	1	$k-1$
5	-	f, α, m	0	k

following subsections will present the above analysis types in detail.

4.6.2 Maximum Force with a Prescribed Moment

This analysis has essentially the same goal and constraints as the one implemented with the scaling factor methodology. The goal is to find the force polygon of maximum forces while having a prescribed moment value in the wrench applied by the end-effector. Prescribing the moment to zero will result in pure force capabilities of the manipulator.

Since the moment is prescribed, and the maximum force is to be found, m is a known, and f and α are unknown variables. With three scalar equations to be satisfied in equation (4.1), one τ can be in transition and $k-1$ τ can be at

their maximums. This is the case that has been examined in Section 4.4, hence equation (4.8) can be evaluated $n_{C_{(k-1)}}$ times to generate the candidate wrenches of the force polygon vertices. Once the force polygon is constructed with the Javis' March Method, the maximum applicable force F_{app} and the maximum isotropic force F_{iso} can be found as explained in Section 4.4.

In terms of the geometrical interpretation, this analysis is equivalent to slicing the wrench polyhedron with a plane that is parallel to the x-y plane and crosses the z axis at the prescribed moment value. The resulting cross section is the force polygon in question. Figure 4.9a shows the wrench polyhedron and the cross section force polygon of the 3-$\underline{\text{R}}$RR at the centre pose with a zero prescribed moment.

4.6.3 Maximum Force with an Associated Moment

In this analysis, the constraint on the moment has been removed and the maximum force has been studied. As a result, the maximum wrench contains an associated moment along with the maximum force. Since there is no constraint on the system, this maximum wrench corresponds to the absolute maximum force that can be applied by the manipulator.

Geometrically, this corresponds to taking the projection of the wrench polyhedron onto the x-y plane, i.e., the force plane, and finding the F_{app} and F_{iso} from the projected polygon. Figure 4.9b shows this projected polygon and the polyhedron of the 3-$\underline{\text{R}}$RR at its centre pose.

Since there are no constraints on the system, f, α, and m are unknown variables. With three scalar equations to be satisfied, there are no torques in transition at the vertices of the polygon, and all torques are at their maximums. Hence, equation (4.1)

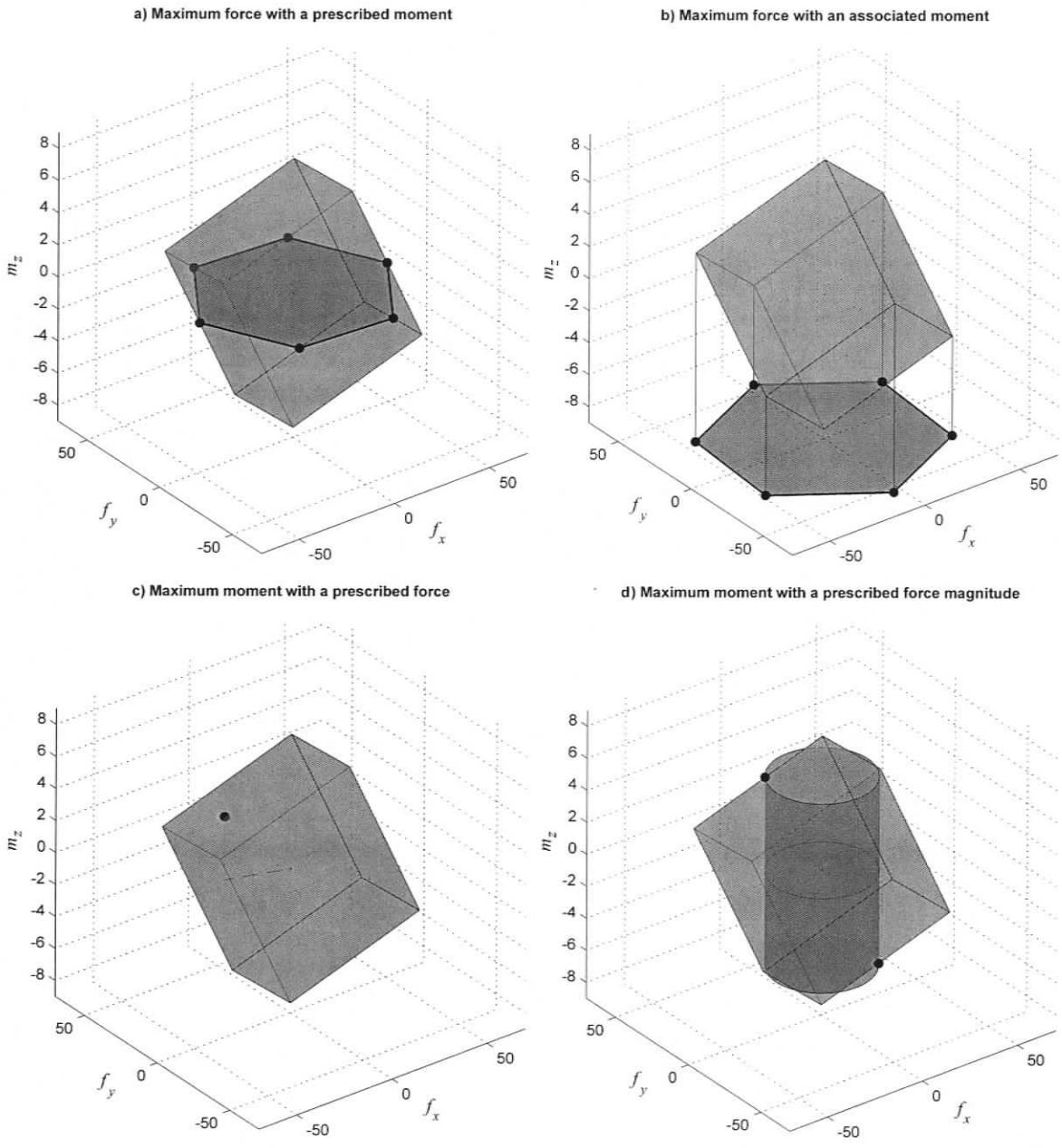

Figure 4.9: Wrench Polyhedrons and Analysis Types

can be evaluated directly to find the candidate wrenches of the force polygon vertices without any arrangement. The evaluation has to be done for all sign combinations of k maximum actuators:

$$n_{C_{(k)}} = n_S = 2^k \tag{4.12}$$

Once the force polygon is constructed, F_{app} and the F_{iso} can be found.

The associated moment of F_{app} is revealed from the maximum output wrench. The associated moment of F_{iso}, however, requires further computation on the force polygon.

F_{iso} was found through the geometry of the force polygon as shown in Figure 4.5. The vertices of the force polygon for this analysis have k actuators at their maximums, whereas the edges have $k-1$ actuators at their maximums. Therefore, along the edges, one actuator torque is in transition between its positive and negative maximum. By comparing the change in the signs of the actuator torques at the vertices between which F_{iso} resides, the index of the actuator in transition can be determined. Once the actuator in transition is known, one of the first two scalar equations of equation (4.1) can be solved for this actuator:

$$\$'\mathrm{w}_{1,\mathrm{t}} \cdot \tau_{\mathrm{t}} = f_{iso}\cos(\alpha_{iso}) - \begin{bmatrix} \$'\mathrm{w}_{1,\mathrm{m}_1} & \$'\mathrm{w}_{1,\mathrm{m}_2} & \cdots & \$'\mathrm{w}_{1,\mathrm{m}_{k\text{-}1}} \end{bmatrix} \begin{Bmatrix} \pm\tau_{\mathrm{m}_1} \\ \pm\tau_{\mathrm{m}_2} \\ \vdots \\ \pm\tau_{\mathrm{m}_{k\text{-}1}} \end{Bmatrix} \tag{4.13}$$

Once τ_{t} is determined, the last scalar equation of equation (4.1) that is related to

the moment can be solved to find the moment associated with the force F_{iso}:

$$m = \begin{bmatrix} \$'w_{3,m_1} & \$'w_{3,m_2} & \cdots & \$'w_{3,m_k} \end{bmatrix} \begin{Bmatrix} \pm\tau_{m_1} \\ \pm\tau_{m_2} \\ \vdots \\ \pm\tau_{m_k} \end{Bmatrix} \tag{4.14}$$

4.6.4 Maximum Moment with a Prescribed Force

In addition to the force capabilities, the moment capabilities of the manipulator can be studied with the explicit methodology. In this analysis the goal is to find the maximum moment while having a prescribed force value in the wrench applied by the end-effector. Geometrically, this is equivalent to setting a point on the x-y plane, and vertically moving from that point to find the intersection with the wrench polyhedron (see Figure 4.9c). Prescribing the force to zero will result in the pure moment capability of the manipulator.

When the prescribed force is known (f, α) and the moment m is to be found, there are $k-2$ torques that can be at their maximums. Properly arranging equation (4.1) yields:

$$\begin{bmatrix} -\$'w_{1,t_1} & -\$'w_{1,t_2} & 0 \\ -\$'w_{2,t_1} & -\$'w_{2,t_2} & 0 \\ -\$'w_{3,t_1} & -\$'w_{3,t_2} & 1 \end{bmatrix} \begin{Bmatrix} \tau_{t_1} \\ \tau_{t_2} \\ m \end{Bmatrix} = \begin{bmatrix} \$'w_{1,m_1} & \$'w_{1,m_2} & \cdots & \$'w_{1,m_{k-2}} \\ \$'w_{2,m_1} & \$'w_{2,m_2} & \cdots & \$'w_{2,m_{k-2}} \\ \$'w_{3,m_1} & \$'w_{3,m_2} & \cdots & \$'w_{3,m_{k-2}} \end{bmatrix} \begin{Bmatrix} \pm\tau_{m_1} \\ \pm\tau_{m_2} \\ \vdots \\ \pm\tau_{m_{k-2}} \end{Bmatrix} - \begin{Bmatrix} f\cos(\alpha) \\ f\sin(\alpha) \\ 0 \end{Bmatrix} \tag{4.15}$$

The moment and the two unknown torques are solved by evaluating equation (4.15) $n_{C_{(k-2)}}$ times. After excluding the solutions in which the torques in transi-

tion exceed their maximum values, the maximum moment can be found among the remaining solutions.

4.6.5 Maximum Moment with a Prescribed Force Magnitude

This analysis is similar to the previous one. The difference is that, instead of prescribing the force vector, which includes magnitude and direction information, only the magnitude is prescribed. Therefore, the resulting wrench will have an arbitrary direction that will make the moment maximum. Geometrically, this can be interpreted as the intersection of one of the edges of the wrench polyhedron and a fixed radius cylinder, where the radius is the prescribed force magnitude (see Figure 4.9d). Note that prescribing the force magnitude to zero, will yield the same results as prescribing the force to zero in the previous analysis.

In this analysis, the force magnitude f is known, and force direction α and moment m are unknown. Therefore, $k-1$ actuators can be at their maximums. Equation (4.1) can be arranged in the following form:

$$f\cos(\alpha) = \underbrace{\$'\mathrm{w}_{1,\mathrm{m}_1}\tau_{\mathrm{m}_1} + \cdots + \$'\mathrm{w}_{1,\mathrm{m}_{k\text{-}1}}\tau_{\mathrm{m}_{k\text{-}1}}}_{a_1} + \underbrace{\$'\mathrm{w}_{1,\mathrm{t}}\tau_{\mathrm{t}}}_{b_1} \tag{4.16a}$$

$$f\sin(\alpha) = \underbrace{\$'\mathrm{w}_{2,\mathrm{m}_1}\tau_{\mathrm{m}_1} + \cdots + \$'\mathrm{w}_{2,\mathrm{m}_{k\text{-}1}}\tau_{\mathrm{m}_{k\text{-}1}}}_{a_2} + \underbrace{\$'\mathrm{w}_{2,\mathrm{t}}\tau_{\mathrm{t}}}_{b_2} \tag{4.16b}$$

$$m = \underbrace{\$'\mathrm{w}_{3,\mathrm{m}_1}\tau_{\mathrm{m}_1} + \cdots + \$'\mathrm{w}_{3,\mathrm{m}_{k\text{-}1}}\tau_{\mathrm{m}_{k\text{-}1}}}_{a_3} + \underbrace{\$'\mathrm{w}_{3,\mathrm{t}}\tau_{\mathrm{t}}}_{b_3} \tag{4.16c}$$

In order to eliminate α, equations (4.16a) and (4.16b) are squared and summed together, yielding the quadratic equation:

$$f^2 = (a_1 + b_1\tau_{\mathrm{t}})^2 + (a_2 + b_2\tau_{\mathrm{t}})^2 \tag{4.17}$$

where, the only unknown τ_t can be solved. The found τ_t, is back substituted into equations (4.16a) and (4.16c) to find α and m, respectively. Out of the two solution sets of the quadratic equation (4.17), the one that yields the maximum moment and does not exceed the limit of the τ is selected. This solution is repeated $n_{C_{(k-1)}}$ times for all combinations and the maximum moment can be selected among the results.

4.6.6 Maximum Moment with an Associated Force

If the constraint of the prescribed force is removed from the previous analyses, the absolute maximum moment that can be applied by the manipulator can be obtained. Given the absence of the force constraint, the absolute maximum moment presents an associated force. Geometrically, this is the highest vertex of the wrench polyhedron.

With no constraints on the system, f, α, and m are all unknown variables, and all torques are at their maximum values. For this analysis, there is no need to evaluate the equation n_S times (for the sign combination of the torques that are at their maximums) to find the maximum moment. The moment m, is bound to equation (4.14) which only contains elements of $[\$'\mathbf{W}]$ and the values of the torques that are at their maximums. Hence, selecting the torque signs the same as their corresponding $[\$'\mathbf{W}]$ elements will always result in the maximum possible moment m.

It is worth to mention that the above five analyses do not require the creation of the whole wrench polyhedrons, which involves the computationally expensive 3-dimensional convex hull operation. In essence, each analysis, extracts the relevant information from the wrench polyhedron through proper arrangement of the linear mapping equation, and without computing the whole polyhedron. Wrench polyhedron examples are solely given for a better and visual understanding of the analyses.

Chapter 5

Wrench Capability Analysis Results

5.1 Overview

This chapter will present the results of the five wrench capability analyses for nine different PPM architectures.

First, the selection procedure of the architectures and details about the presentation scheme of the results is explained. Following this, results for each family of architectures are presented. For each architecture, a schematic diagram of the manipulator and its geometric properties are provided. The wrench capabilities of each manipulator are presented in a single figure comprised of nine plots, as well as a table that shows various results derived from the plots. A short discussion of the results is given at the end of each section.

5.2 Analyzed Architectures and Presentation of the Results

The architectures analyzed in this work were selected in order to cover a wide range of symmetric PPMs[1]. According to their redundancy types, three groups were chosen to be analyzed: non-redundant, in-branch-redundant, and branch-redundant, all of which require only three joints per branch.

There are two typical joint types that can be used in a parallel manipulator branch: prismatic joints and revolute joints. The type of a branch is defined with a sequence of at least three joints chosen among the two typical joint types[2]. For a three jointed branch, the possible branch types are: RRR, RRP, RPR, RPP, PRR, PRP, PPR, and PPP. A PPP branch is fundamentally degenerate for a PPM, since it cannot provide three DOF. The bulkiness of prismatic joints compared to revolute joints, makes it hard to implement branches containing more than one prismatic joint. This eliminates RPP, PRP, and PPR from the list. RRP and PRR are architecturally the same if the end-effector is considered as the base, and vice versa. Out of the two, PRR is more preferable, since the prismatic joint is fixed to the base and does not add extra inertia into the system. This leaves three common branch types for PPMs: RRR, RPR, and PRR.

For the non-redundant architectures group, only the first joints of each branch are actuated: 3-RRR, 3-RPR, and 3-PRR. For the in-branch-redundant architectures group, the first two joints of each branch are actuated: 3-RRR, 3-RPR, 3-PRR which yields three DOR. For the branch-redundant architectures an additional branch is

[1] A PPM that has identical architectures in all its branches.

[2] In a PPM, at least three joints per branch are required in order to allow three DOF motion of the end-effector.

introduced, and only the first joints are actuated: 4-RRR, 4-RPR, 4-PRR, which yield one DOR.

Considering the variety and the large amount of data resulting from the analyses, presentation of the results of one architecture was condensed into one figure. The figure for each PPM architecture is comprised of nine plots that show various force and moment capability results which were found through the five analysis types presented in Section 4.6. For each manipulator, the analyses have been carried out throughout a range of end-effector locations with an interval of 0.001 m along x and y, while the orientation has been kept constant at 0°. The x and y coordinates of each plot are the x and y positions of the end-effector, with $(0, 0)$ being the centre of the base polygon of the manipulator (an equilateral triangle in three-branch cases, or a square in four-branch cases). The greyscale axis bar shows the corresponding force or moment capability of each plot.

The plots in Figures 5.2 to 5.12 are placed in the following order:

Table 5.1: Plot Position Matrix of the Analysis Result Figures

1-a) Pure F_{iso} [N]	1-b) Pure F_{app} [N]	3,4) Maximum Pure Moments [Nm]
2-a) Absolute F_{iso} [N]	2-c) Absolute F_{app} [N]	5-a) Maximum Applicable Moments with an Associated Force [Nm]
2-b) Associated Moments of the Absolute F_{iso} [Nm]	2-d) Associated Moments of the Absolute F_{app} [Nm]	5-b) Associated Forces of the Maximum Applicable Moments [N]

Plots 1-a and 1-b are the results of the first analysis type, i.e., maximum force with a prescribed moment, where 1-a is the maximum isotropic force of the force polygon, and 1-b is the maximum applicable force of the force polygon. The prescribed moment has been set to zero, hence the results are pure forces that do not contain any moment.

Plots 2-a, 2-b, 2-c, and 2-d are the results of the second analysis type, i.e., maximum force with an associated moment, where 2-a is the maximum isotropic force of the force polygon, 2-b is the associated moments to the forces of plot 2-a. The plot 2-c is the maximum applicable force of the force polygon, and 2-d is the associated moments to the forces of plot 2-c. The results on 2-a and 2-c are the absolute maximum forces that can be applied by the manipulator.

Plot 3 and 4 are the result of the third and fourth analysis type, i.e., maximum moment with a prescribed force and maximum moment with a prescribed force magnitude, respectively. The prescribed force has been set to zero, hence the results for analysis three and four are the same, and yield pure moments that do not contain any force.

Plots 5-a and 5-b are the results of the fifth analysis type, i.e., maximum moment with an associated force, where 5-a is the absolute maximum moment that can be applied by the manipulator, and 5-b is the associated forces of the moments of plot 5-a.

Due to the singular poses of the manipulators, some values on the plots reach infinity, and destroy the readability of the greyscale graph. In those cases, the graphs were *capped*, i.e., results higher than a specific value were plotted in the lightest shade of the greyscale. This specific value changes in every plot, and it can be read from the greyscale axis bar. Whether a plot is capped or not, is indicated in its title.

Finally, a table for each architecture is provided in order to give an insight view on the plots. These tables include the *minimum*, and the *median*[3] values of all locations on their corresponding plots. The minimum indicates the maximum force value

[3]The median of a finite list of numbers is the middle value when the list is arranged from the lowest to the highest. If there are an even number of values, the median is the mean of the two middle values [52].

(whether F_{app} or F_{iso}, depending on the plot) that can be applied/sustained at any location in the workspace. The median value is given as an indication of the overall workspace performance of the manipulator. The median function is preferred over the *mean* function because the plots contain a small number of very large values, i.e., the singular values, that are known to affect the reliability of the mean function. The maximum value of all locations was excluded from these tables for two reasons. For those plots that are capped at a value, it has no useful meaning since the maximum value reaches infinity at the singular poses. For the rest of the plots, i.e., plots that are not capped, since the maximum will only give a F_{app} or F_{iso} value of a single location on the workspace, it cannot be used as an indicator for the whole workspace of the manipulator.

The minimum and median values shown in the tables are not given for the plots that show the associated forces or moments, i.e., plots 2-b, 2-d and 5-b. This is because, in these studies, the goal was to maximize the main force or the moment (force for study two, and moment for study five) and not their associated moments or forces. Associated moments or forces are just accompanying values so that the main forces and moments are maximum. Therefore, the minimum or the median value of these quantities have no useful meaning.

5.3 Non-Redundant Architectures

5.3.1 Architecture Properties

This group of architectures are non-redundantly-actuated, i.e., only one joint in each branch is actuated. As a common practice, the joints to be actuated are selected to be

the first joints since this prevents the unnecessary displacement of the actuator inertia during the end-effector motion. Hence, the layouts 3-RRR, 3-RPR, and 3-PRR were analyzed. Figure 5.1 shows the schematic diagrams for these three architectures.

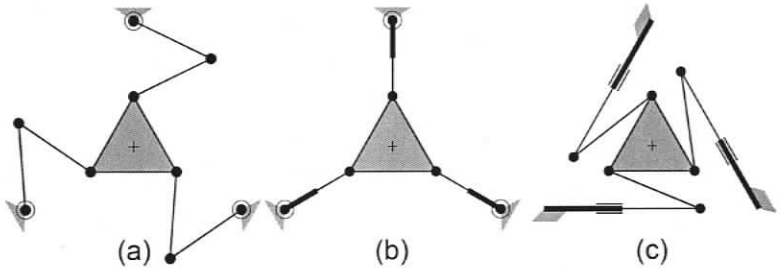

Figure 5.1: Schematic Diagrams of a) 3-RRR, b) 3-RPR, and c) 3-PRR

For all three architectures, the base triangle edge length was 0.5 m and the end-effector triangle edge length was 0.2 m. The length of the passive link was 0.2 m in the RRR and 0.23 m in the PRR branch. The orientations of the prismatic joints were 0°, 120°, and 240° for the PRR branches. The extension limits for the prismatic joints in the RPR branches were between 0-0.4 m. For the PRR branches this limit was extended to 0-1.0 m in order to achieve a workspace comparable in size to the other manipulators. The actuator capabilities of the base revolute joints were ± 4.2 Nm for the RRR and RPR branches, and ± 10 N for the prismatic joint of the PRR branch. The assembly modes of the RRR and PRR branches were assumed to be as shown in Figure 5.1.

5.3.2 Wrench Capability Results

Figures 5.2, 5.3, and 5.4 show the wrench capabilities, and Tables 5.2, 5.3, and 5.4 show the minimums and the medians for the 3-RRR, 3-RPR, and 3-PRR architectures, respectively.

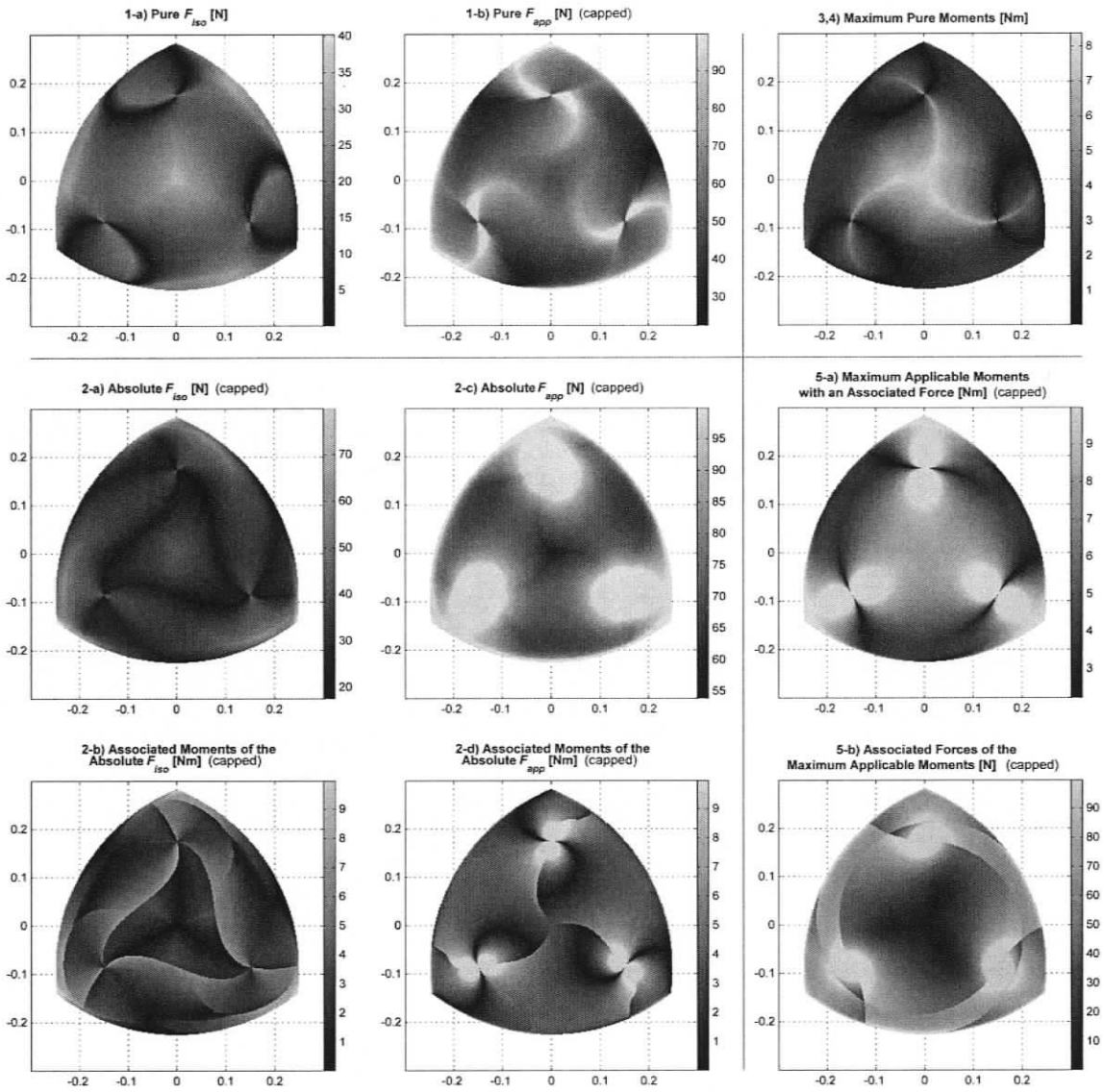

Figure 5.2: Wrench Capabilities of the 3-RRR Architecture

Table 5.2: Mimimum and Median Values of the 3-RRR Architecture

1-a)	min:	0.00 N	1-b)	min:	22.33 N	3,4)	min:	0.00 Nm
	med:	17.13 N		med:	57.11 N		med:	2.00 Nm
2-a)	min:	17.41 N	2-c)	min:	53.80 N	5-a)	min:	2.21 Nm
	med:	31.22 N		med:	79.76 N		med:	6.87 Nm

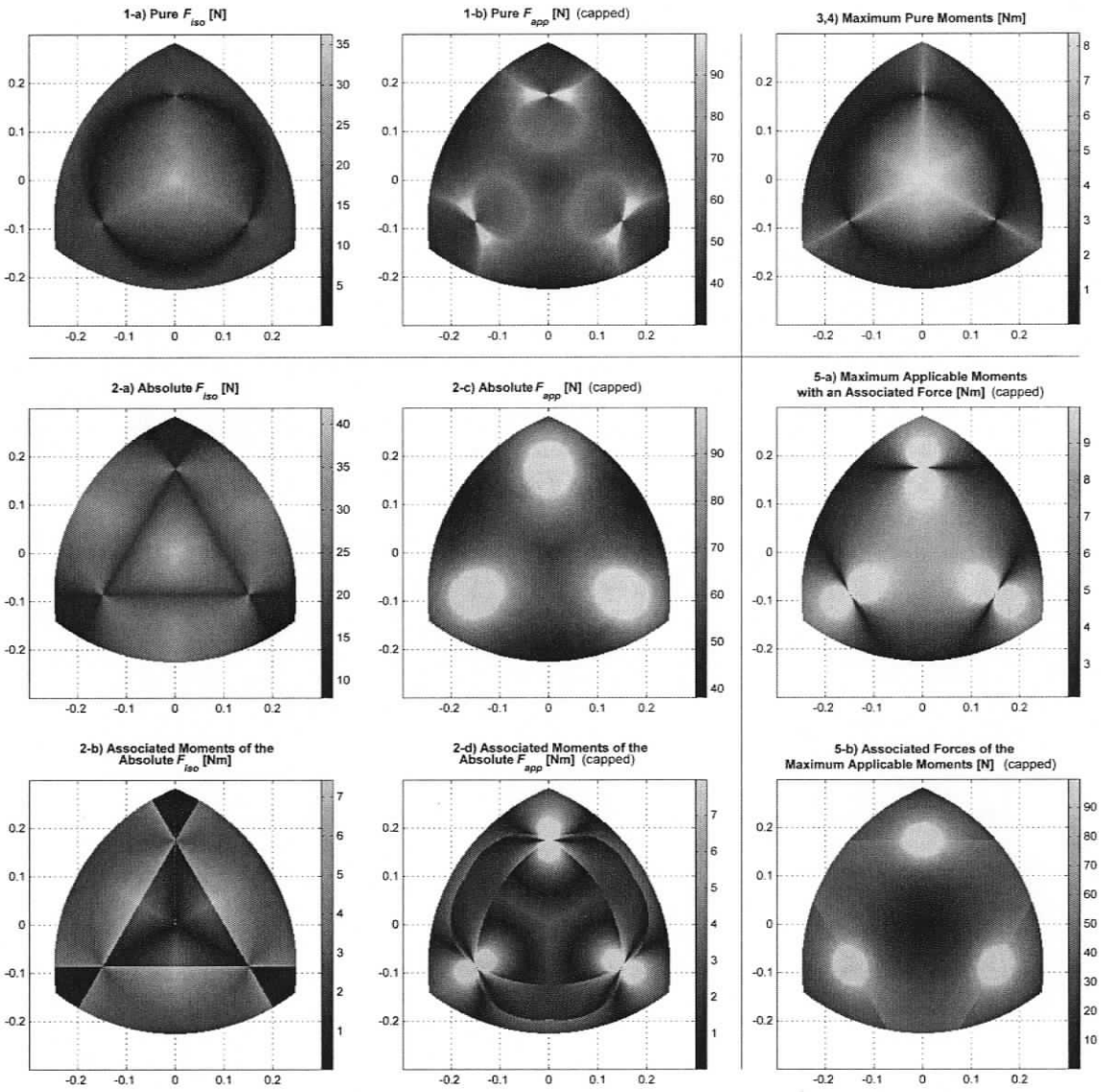

Figure 5.3: Wrench Capabilities of the 3-RPR Architecture

Table 5.3: Mimimum and Median Values of the 3-RPR Architecture

1-a)	min:	0.00 N	1-b)	min:	29.90 N	3,4)	min:	0.00 Nm
	med:	9.57 N		med:	53.42 N		med:	1.62 Nm
2-a)	min:	7.88 N	2-c)	min:	38.08 N	5-a)	min:	2.10 Nm
	med:	22.98 N		med:	63.23 N		med:	6.43 Nm

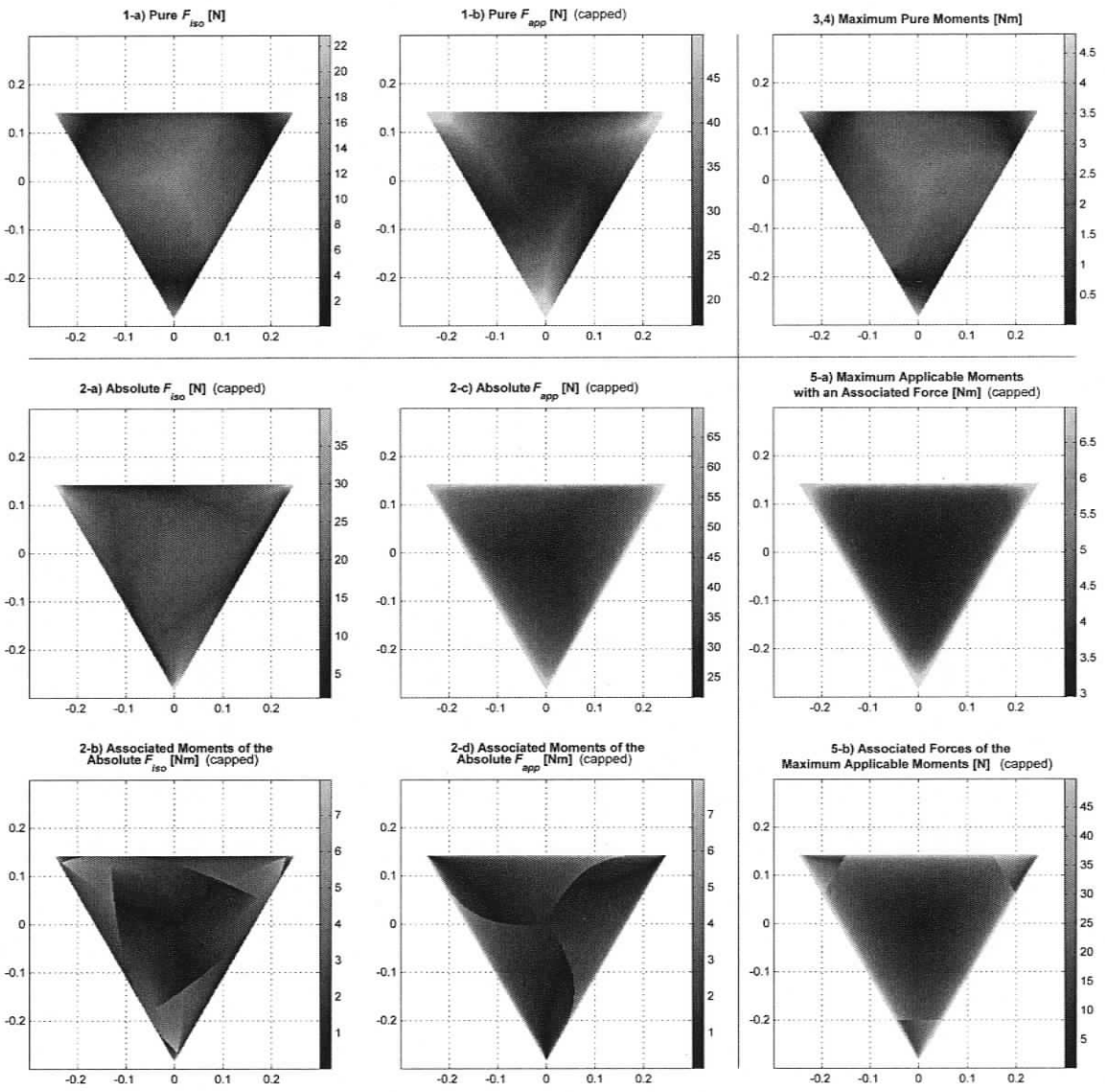

Figure 5.4: Wrench Capabilities of the 3-PRR Architecture

Table 5.4: Mimimum and Median Values of the 3-PRR Architecture

1-a)	min:	0.00 N	1-b)	min:	17.06 N	3,4)	min:	0.00 Nm
	med:	8.57 N		med:	25.06 N		med:	1.90 Nm
2-a)	min:	1.83 N	2-c)	min:	21.59 N	5-a)	min:	2.95 Nm
	med:	13.95 N		med:	34.37 N		med:	3.58 Nm

The differences in the shapes of the workspaces of the three architectures are due to their designs. The workspace of the 3-RRR and the 3-RPR are equal since RRR and RPR branches are kinematically equivalent. The 3-PRR architecture, on the other hand, has a different workspace shape.

As mentioned before, due to singular configurations, some results have infinite values. For the 3-RRR architecture, these occur on the edge of the workspace and on three singular poses within the workspace. On the edge of the workspace, at least one branch is fully extended to its maximum length. Along this extended branch direction, the manipulator can theoretically sustain an infinite amount of force, and therefore, pure F_{app} and absolute F_{app} reach infinity. At the vertices of the workspace, pure F_{iso} reaches infinity as well. This is due to two branches being fully extended at the same time. On the singular poses within the workspaces, one branch is folded back on to itself, making two revolute joints coaxial. This makes pure F_{app} and absolute F_{app} forces infinite magnitude. Note that on all the poses where there is an infinite force, theoretically, the manipulator can sustain an infinite amount of moment as well. However, this holds true only for the maximum applicable moment analysis, since in maximum pure moment analysis there is a prescribed force to be sustained.

For the 3-RPR architecture, there are no singular configurations on the edge of the workspace since it is only constrained by the extension limit of the prismatic joint. Within the workspace, however, the same singular poses where two revolute joints are coaxial exist. Those poses occur when the length of the prismatic joint is zero. This leads to infinite sustainable forces, as well as infinite sustainable moments. The 3-RPR architecture also has a set of force unconstrained poses. The location of these poses form a circle that is centred at the origin of the workspace and passes through the singular poses where two revolute joints are coaxial. Force unconstrained poses

make the minimum pure forces, and maximum pure moments, zero. This circle can be seen in the subplots 1-a, 3, and 4 of Figure 5.3.

For the 3-PRR architecture, in the singular configurations which occur at the vertices of the workspace triangle, the second links of two branches are perpendicular to their prismatic joints. This allows an infinite amount of pure F_{app} to be sustained along a direction that is the bisector of the two second links, and an infinite amount of absolute F_{app} to be sustained along all directions. On the edge of the workspace, only one branch's second link is perpendicular to its prismatic joint, which allows an infinite amount of force to be sustained in the direction of the second link. For all the poses where an infinite force can theoretically be sustained, theoretically an infinite amount of moment can be sustained as well.

Comparing the results of the 3-RRR and 3-RPR, it can be seen that they have a similar pattern of force and moment capabilities. The difference is that the 3-RRR results are swirled about the aforementioned singular poses where two revolute joints are coaxial compared to the 3-RPR results. This is due to the difference in the force applied by the first revolute joints to the end-effector. In RRR branches, this force changes sinusoidally according to the second joint angle, whereas, in RPR branches it changes linearly according to the prismatic joint length.

For all three architectures it can be seen that forces with associated moments are always larger than pure forces, as expected. This is true for pure moments and moments with associated forces as well. On the other hand, comparing the force and moment capabilities of these three architectures with each other is not very meaningful since their branch structures are different, and different actuator types, i.e., revolute and prismatic, use different units for their capabilities.

5.4 In-Branch-Redundant Architectures

5.4.1 Architecture Properties

This group of architectures have in-branch redundancy, i.e., more than one joint is actuated in each branch. The joints to be actuated are selected to be the first two joints. This provides the minimum amount of displacement of the actuator inertia during the end-effector motion. Hence, the layouts 3-RRR, 3-RPR, and 3-PRR were analyzed. Figure 5.5 shows the schematic diagrams for these three architectures.

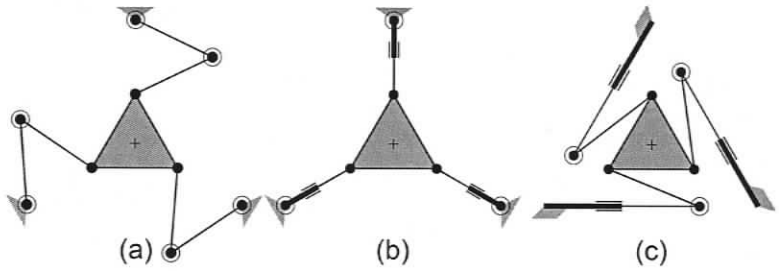

Figure 5.5: Schematic Diagrams of a) 3-RRR, b) 3-RPR, and c) 3-PRR

All architectural properties are the same as the non-redundant architectures. The actuator capabilities of the elbow revolute joints were ± 2.1 Nm for the RRR and PRR branches, and ± 10 N for the prismatic joint of the PRR branch. The assembly modes of the RRR and PRR branches were assumed to be as shown in Figure 5.5.

5.4.2 Wrench Capability Results

Figures 5.6, 5.7, and 5.8 show the wrench capabilities and Tables 5.5, 5.6, and 5.7 show the minimums and the medians of the 3-RRR, 3-RPR, and 3-PRR architectures, respectively.

Comparing to the non-redundant architectures, there are no differences in the

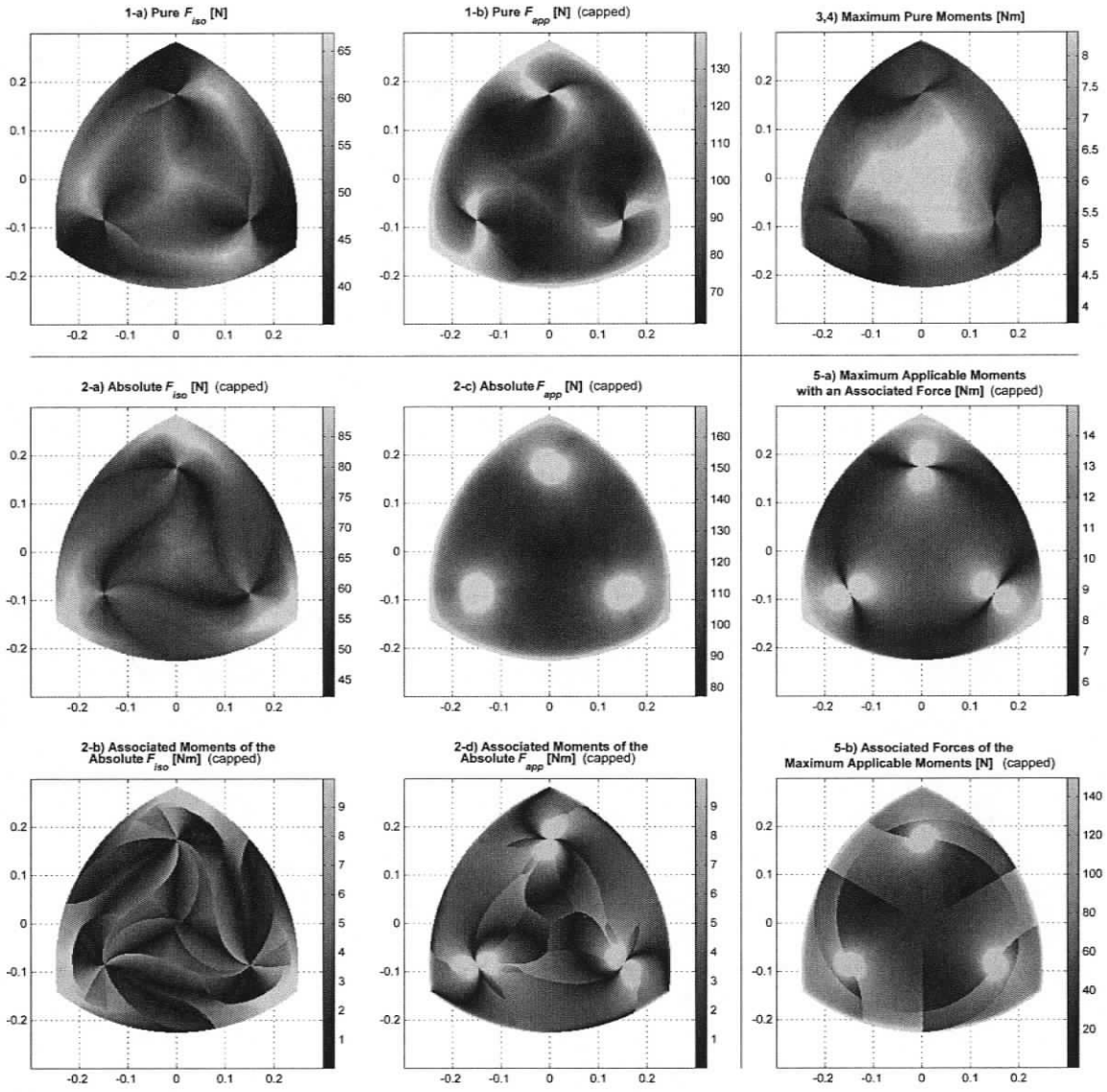

Figure 5.6: Wrench Capabilities of the 3-RRR Architecture

Table 5.5: Mimimum and Median Values of the 3-RRR Architecture

1-a)	min:	35.92 N	1-b)	min:	61.40 N	3,4)	min:	3.73 Nm
	med:	46.92 N		med:	87.25 N		med:	5.51 Nm
2-a)	min:	42.17 N	2-c)	min:	77.05 N	5-a)	min:	5.55 Nm
	med:	56.29 N		med:	114.06 N		med:	8.98 Nm

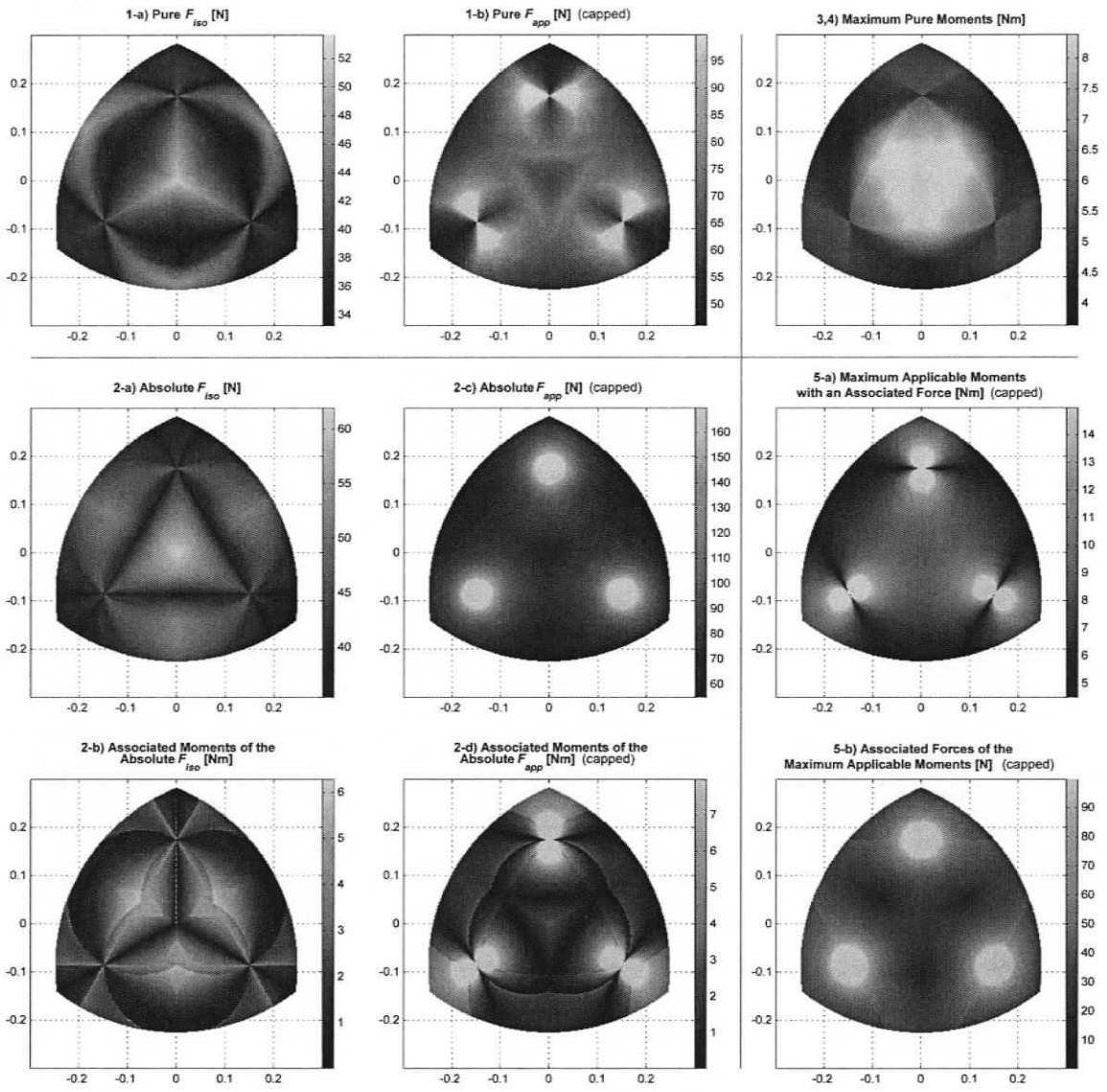

Figure 5.7: Wrench Capabilities of the 3-RPR Architecture

Table 5.6: Mimimum and Median Values of the 3-RPR Architecture

1-a)	min:	33.19 N	1-b)	min:	45.97 N	3,4)	min:	3.63 Nm
	med:	37.22 N		med:	70.25 N		med:	5.03 Nm
2-a)	min:	35.34 N	2-c)	min:	54.59 N	5-a)	min:	4.47 Nm
	med:	43.05 N		med:	77.43 N		med:	8.27 Nm

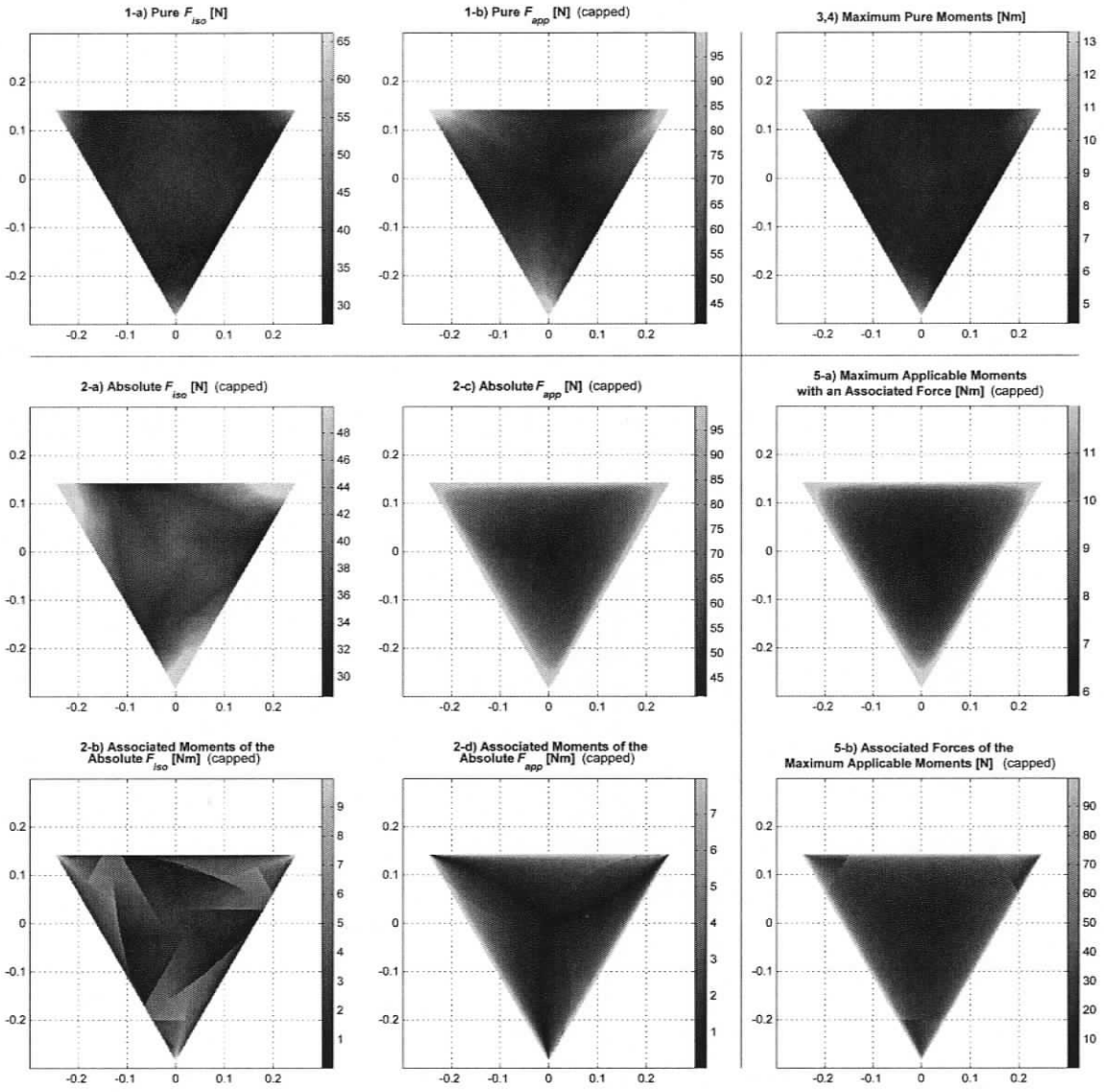

Figure 5.8: Wrench Capabilities of the 3-PRR Architecture

Table 5.7: Mimimum and Median Values of the 3-PRR Architecture

1-a)	min:	27.48 N	1-b)	min:	40.86 N	3,4)	min:	4.40 Nm
	med:	31.66 N		med:	49.18 N		med:	5.07 Nm
2-a)	min:	28.49 N	2-c)	min:	41.20 N	5-a)	min:	5.91 Nm
	med:	34.05 N		med:	59.75 N		med:	7.19 Nm

workspaces since the geometry of the architectures are kept identical. This also results in the same singular configurations as the non-redundant architectures. As in the non-redundant architectures, the 3-RRR and 3-RPR layouts show a similarity except the swirling distortion about the singular poses where two revolute joints are coaxial.

Table 5.5, 5.6, and 5.7 show that for all architectures, the addition of extra actuation resulted in improvement of force and moment capabilities. It is worthy to notice that the minimum values on the pure maximum isotropic force and maximum pure moment plots of all three non-redundant architectures were zero (See Tables 5.2, 5.3, and 5.4). This means that there are one or more poses within the workspace, where the manipulator cannot apply a force along a particular direction, and cannot apply a moment. Adding extra actuation solved this shortcoming as can be seen in Tables 5.5, 5.6, and 5.7.

5.5 Branch-Redundant Architectures

5.5.1 Architecture Properties

This group of architectures have an extra redundant branch. The joints to be actuated are selected to be the first joints as the non-redundant architectures. Hence, the layouts 4-RRR, 4-RPR, and 4-PRR were analyzed. Figure 5.9 shows the schematic diagrams for these three architectures.

The base square edge length was 0.5 m and the end-effector square edge length was 0.2 m. All other architectural properties are the same as the non-redundant architectures. The assembly modes of the RRR and PRR branches were assumed to

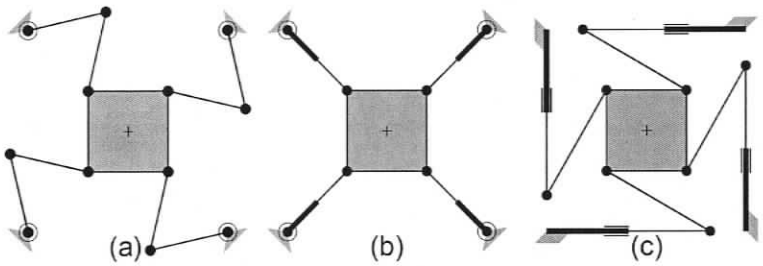

Figure 5.9: Schematic Diagrams of a) 4-RRR, b) 4-RPR, and c) 4-PRR

be as shown in Figure 5.9.

5.5.2 Wrench Capability Results

Figures 5.10, 5.11, and 5.12 show the wrench capabilities and Tables 5.8, 5.9, and 5.10 show the minimums and the medians of 4-RRR, 4-RPR, and 4-PRR architectures, respectively.

The workspaces of the branch-redundant architectures are different than the non-redundant and in-branch-redundant architectures due to the additional branch. However they still show a correlation. Four-branch architecture workspaces are somewhat a four vertex version of their three-branch architecture counterpart workspaces. Also, note that the workspace surface areas are decreased compared to the three-branch architectures due to the geometric constraints that were introduced by the additional branch.

The correlation between the three and four branch architectures can be observed in terms of the singular poses and the plot pattern as well. All results show similarities between their non-redundant architecture counterparts. There are four singular poses with coaxial revolute joints that shape the plots instead of three. The plot patterns are four-fold versions of the three-fold patterns of the three-branch architectures,

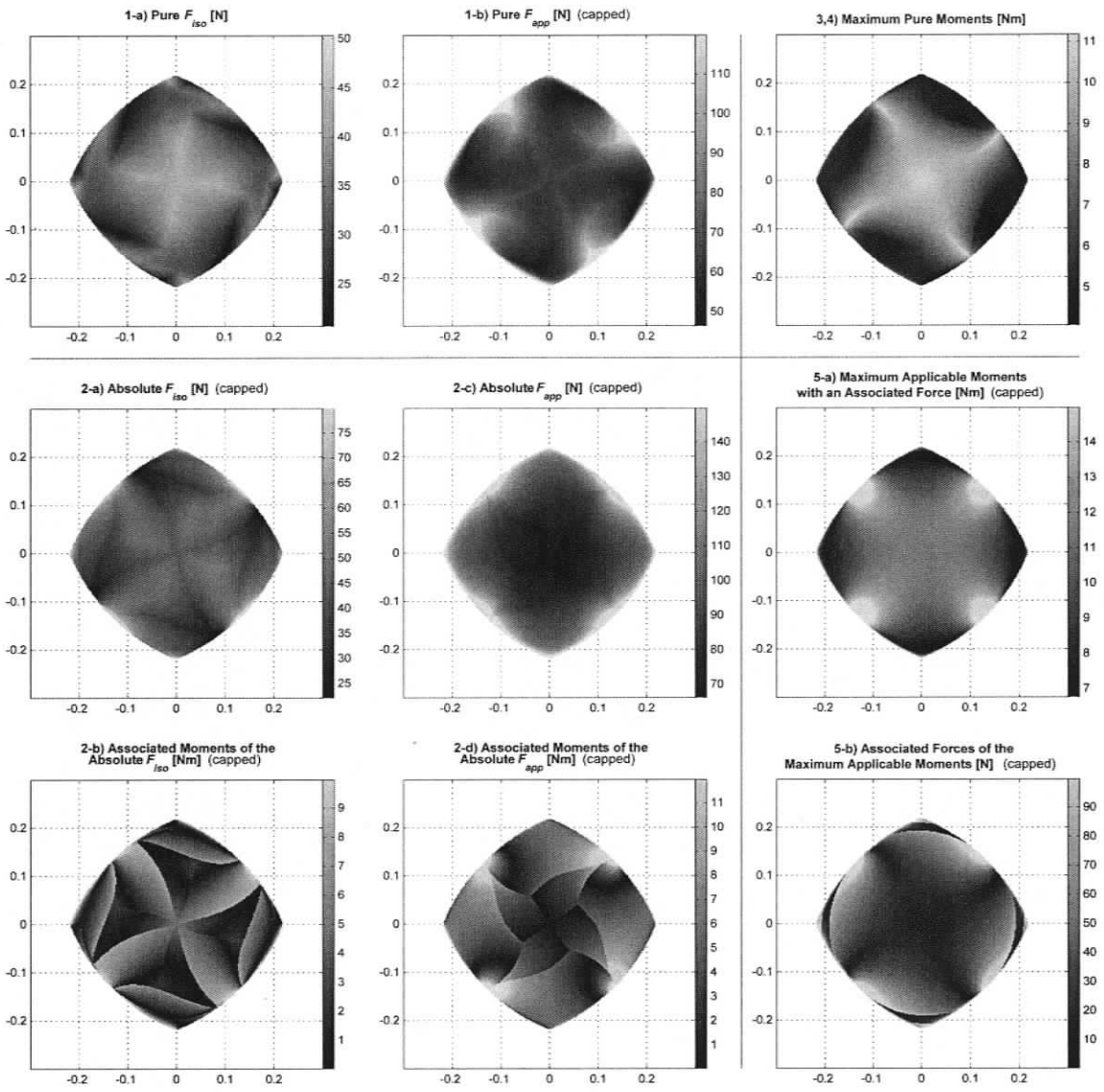

Figure 5.10: Wrench Capabilities of the 4-RRR Architecture

Table 5.8: Mimimum and Median Values of the 4-RRR Architecture

1-a)	min:	20.61 N	1-b)	min:	46.30 N	3,4)	min:	4.06 Nm
	med:	34.47 N		med:	66.24 N		med:	7.01 Nm
2-a)	min:	22.02 N	2-c)	min:	66.05 N	5-a)	min:	6.75 Nm
	med:	46.14 N		med:	92.14 N		med:	11.06 Nm

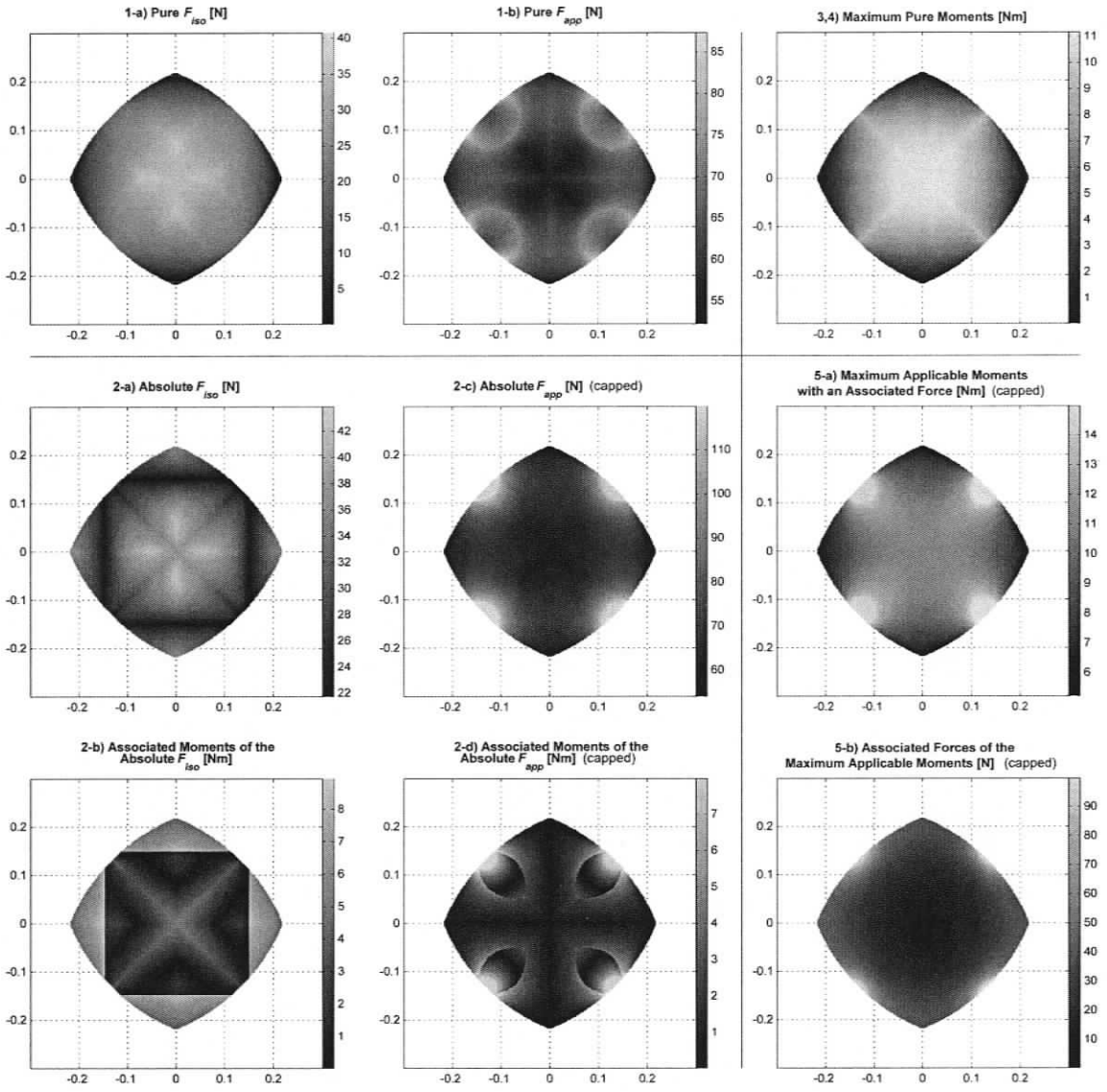

Figure 5.11: Wrench Capabilities of the 4-RPR Architecture

Table 5.9: Mimimum and Median Values of the 4-RPR Architecture

1-a)	min:	0.01 N	1-b)	min:	52.17 N	3,4)	min:	0.00 Nm
	med:	26.81 N		med:	65.58 N		med:	7.71 Nm
2-a)	min:	21.69 N	2-c)	min:	53.89 N	5-a)	min:	5.19 Nm
	med:	30.92 N		med:	67.76 N		med:	11.03 Nm

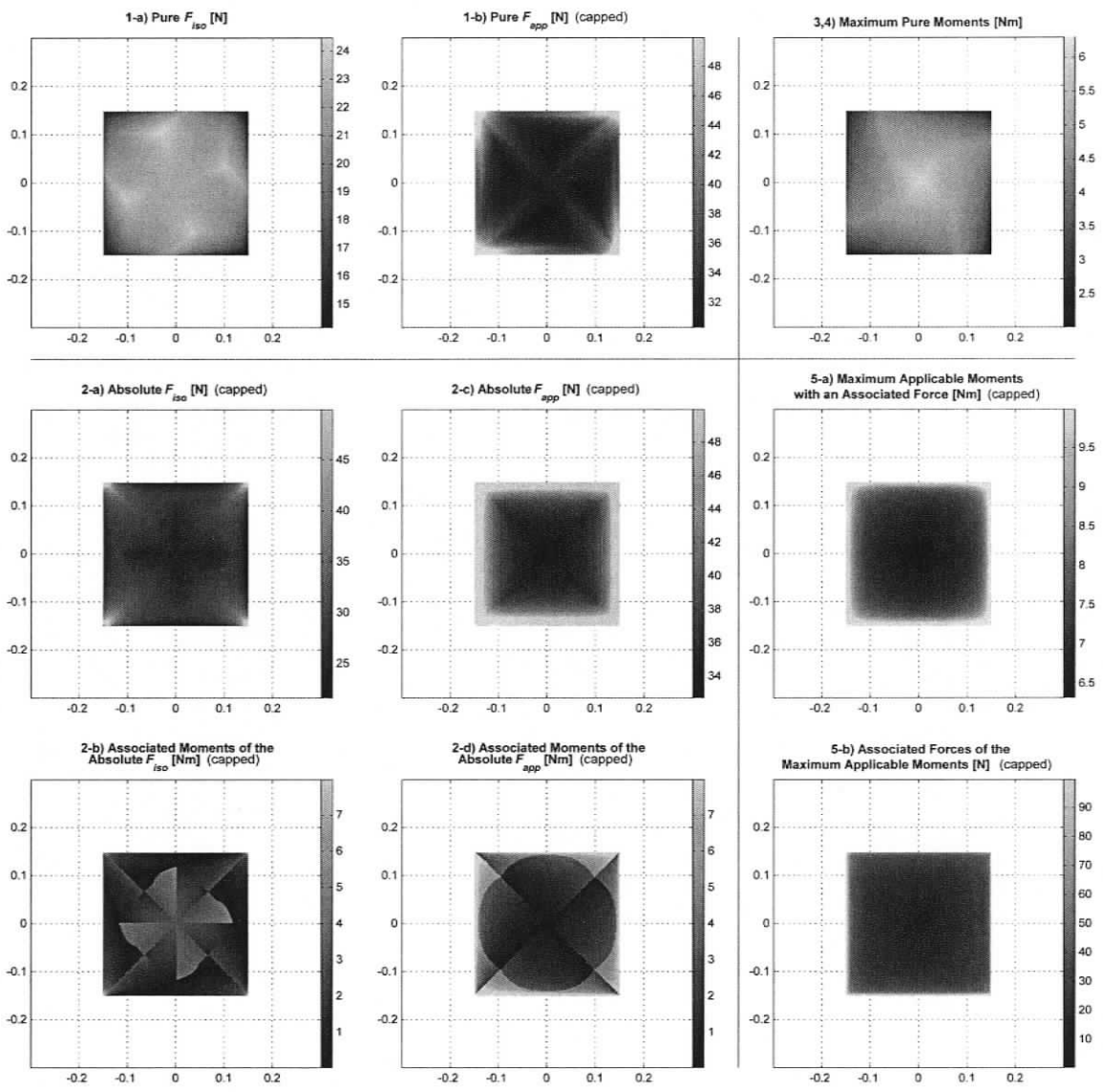

Figure 5.12: Wrench Capabilities of the 4-PRR Architecture

Table 5.10: Mimimum and Median Values of the 4-PRR Architecture

1-a)	min:	14.14 N	1-b)	min:	30.27 N	3,4)	min:	2.00 Nm
	med:	22.32 N		med:	33.29 N		med:	4.56 Nm
2-a)	min:	21.55 N	2-c)	min:	32.66 N	5-a)	min:	6.31 Nm
	med:	27.84 N		med:	38.63 N		med:	7.10 Nm

although, they are cropped due to the extra branch's constraints.

This set of architectures share the same singular configuration poses, except that the 4-RPR has no infinite forces in maximum pure force analysis, because the singular poses where two revolute joints are coaxial fall outside of the workspace areas.

As in the in-branch-redundant architectures, addition of redundancy improved most of the results compared to the non-redundant architectures. The only exception to this occurs in the 4-RPR architecture. The minimum value of the pure maximum isotropic forces and the maximum pure moments are still near zero as they were in the 3-RPR architecture. This is due to a set of force unconstrained poses that form a circle centred at the origin, and passes through the singular poses where two revolute joints are coaxial as in the 3-RPR architecture. The majority of these poses fall outside of the workspace, but the rest exist near the four vertices and makes the pure F_{iso} and the maximum pure moments zero.

Comparing the improvements of the in-branch redundancy and branch redundancy over the non-redundant architectures, it can be seen that for all force analyses in-branch redundancy provides better improvement. However, directly comparing the improvements is not fair since in-branch-redundant architectures have three additional actuators, whereas branch-redundant architectures have only one additional actuator.

An interesting result is that, in contrast to the previous paragraph, the improvements in both maximum pure and maximum applicable moment capabilities of the RRR and RPR architectures are better with the branch-redundant architectures, compared to the in-branch-redundant architectures. This shows that the addition of one extra branch has more effect on the applied moment than the addition of three elbow actuators. Note that the exception to this observation occurs in the RPR architecture's pure moment results where there were a set of force unconstrained poses.

However, despite the zero pure moments occurring at those poses, the median values of all workspace results are still higher than the 3-RPR architecture.

Chapter 6

Conclusion

6.1 Overview

In this chapter, a summary and conclusions about each chapter of the thesis will presented. In addition, recommendations about possible future research areas will be made.

6.2 Conclusions

Chapter 2 - Screw Theory

Fundamentals of screw theory were presented. Basic concepts such as twists and wrenches were defined and properties of screw quantities were given. Modelling of manipulators with screws was explained. Finally, velocity and force solutions of both serial and parallel manipulators were derived through screw theory. Screw coordinates and ARS coordinates of RRR, RPR, and PRR branch types were derived using screw theory in Appendix A.

Chapter 3 - Scaling Factor Methodology

A previously developed scaling factor methodology for determining force capabilities of PMs was presented in detail. For redundantly-actuated manipulators two methods were presented: pseudo-inverse and optimization. The two methods were compared with an example study, and the distinctions between them were pointed out. It was shown that the optimization method results were superior to the ones of the pseudo-inverse method. The problems associated with the optimization method and the limitations of the scaling factor methodology were identified.

Chapter 4 - Explicit Methodology

Through the observation on the tendency of the optimization method's results to converge to actuator output limits, a new methodology for determining the force capabilities of PPMs was developed. An example case was studied in order to compare the new explicit methodology with the optimization method, and it was shown that the explicit methodology was computationally approximately 150 times more efficient and yielded more accurate results. The observation made on the optimization method results was then geometrically proved through the mapping of the vertices in the actuator space to the vertices in the wrench space. Using the new methodology, an efficient way of generating force polygons was presented. Wrench polyhedrons were introduced in order to give a better visual understanding of the wrench capabilities. After establishing the explicit methodology, five studies that introduce new indices for the wrench capabilities of PPMs were presented. These indices provide a good insight into the wrench capabilities of PPMs.

Chapter 5 - Wrench Capability Analyses Results

The explicit methodology developed, was used to generate the wrench capability indices of nine PPM architectures. Nine architectures were selected to be in three redundancy groups: non-redundant, in-branch-redundant, and branch-redundant. All wrench capability indices of these architectures were generated for their whole workspace and the results were compiled in one figure for each architecture. A short discussion on the results was presented for each architecture. In general, it was shown that, while the addition of in-branch-redundant actuation showed more improvement in the force capabilities, branch-redundant actuation showed more improvement in the moment capabilities.

6.3 Recommendations for Future Work

The indices proposed in this work, provide an insight of the manipulator capabilities and thus, are useful for the designer. However, due to the differences in the actuation schemes, these indices are not suitable for direct comparisons between different architectures. A possible avenue to explore would be generating different indices that take the actuation scheme into account, and give a better performance indicator that depends solely on the design of the manipulator. One such index would be normalizing the proposed indices by the number of actuators used in the manipulator. Such an index would reveal how well a manipulator makes use of its actuators, and would provide more insight about the design of the manipulator rather than simply the capabilities of the manipulator.

The wrench capabilities of the presented manipulators were found by assuming

a constant zero orientation throughout their workspaces. Different end-effector orientations could be considered and orientations that yield the best results could be explored.

PPMs were considered in this work. A new avenue would be implementing the new explicit methodology and proposed capability indices to spatial PMs. 6-DOF wrench space can be partitioned into 3-DOF force and moment spaces. This will allow separate force and moment capability polyhedrons to be generated and would aid in visualization of the performance of a spatial PM.

References

[1] J. J. Craig, *Introduction to Robotics, Mechanism and Control, second edition.* Addison-Wesley Publishing Company: Don Mills, ON, Canada, 1987.

[2] J. P. Merlet, *Parallel Robots.* Kluwer Academic Publishers: The Netherlands, 2000.

[3] V. Gough, "Contribution to discussion of papers on research in automobile stability, control and tyre performance," in *Proceedings of the Automotive Division of the Institution of Mechanical Engineers*, pp. 392–395, 1956.

[4] D. Stewart, "A platform with six degrees of freedom," in *Proceedings of the Institution of Mechanical Engineers*, pp. 371–386, 1965.

[5] J. P. Merlet, "Singular configurations of parallel manipulators and Grassmann geometry," *The International Journal of Robotics Research*, vol. 8, no. 5, pp. 45–56, 1989.

[6] R. Fisher, R. P. Podhorodeski, and S. B. Nokleby, "Design of a reconfigurable planar parallel manipulator," *Journal of Robotic Systems*, vol. 21, no. 12, pp. 665–675, 2004.

[7] J. Merlet, "Redundant parallel manipulators," *Journal of Laboratory Robotics and Automation*, vol. 8, pp. 17–24, 1996.

[8] I. Ebrahimi, J. A. Carratero, and R. Boudreau, "3-PRRR redundant planar parallel manipulator: Inverse displacement, workspace and singularity analyses," *In press: Mechanism and Machine Theory*, 2007.

[9] F. Firmani and R. P. Podhorodeski, "Force-unconstrained poses for a redundantly-actuated planar parallel manipulator," *Mechanism and Machine Theory*, vol. 39, no. 5, pp. 459–476, 2004.

[10] F. Firmani and R. P. Podhorodeski, "Force-unconstrained poses of the 3-PRR and 4-PRR planar parallel manipulators," in *Proceedings of the 2005 CCToMM Symposium on Mechanisms, Machines, and Mechatronics*, (Saint-Hubert, QC, Canada), 12 pages, May 2005.

[11] R. S. Ball, *A Treatise of the Theory of Screws.* Cambridge University Press: New York, NY, USA, 1900.

[12] H. S. M. Coxeter, *Regular polytopes.* Dover Publications: New York, NY, USA, 1973.

[13] T. Yoshikawa, "Analysis and control of robot manipulators with redundancy," in *Robotics Research: The First International Symposium, M. Brady and R. Paul, Eds.*, (Cambridge, MA, USA), pp. 735–747, 1984.

[14] T. Yoshikawa, "Manipulability of Robotic Mechanisms," *The International Journal of Robotics Research*, vol. 4, no. 2, pp. 3–9, 1985.

[15] S. L. Chiu, "Task compatibility of manipulator postures," *The International Journal of Robotics Research*, vol. 7, pp. 13–21, 1988.

[16] P. Chiacchio, S. Chiaverini, L. Sciavicco, and S. B., "Global task space manipulability ellipsoids for multiple-arm systems," *IEEE Transactions on Robotics and Automation*, vol. 7, no. 5, pp. 678–685, 1991.

[17] C. Melchiorri, "Comments on "Global task space manipulability ellipsoids for multiple-arm systems" and further consideration," *IEEE Transactions on Robotics and Automation*, vol. 9, no. 2, pp. 232–236, 1993.

[18] K. L. Doty, C. Melchiorri, E. M. Schwartz, and C. Bonivento, "Robot manipulability," *IEEE Transactions on Robotics and Automation*, vol. 11, no. 3, pp. 462–468, 1995.

[19] Y. F. Zheng and J. Y. S. Luh, "Optimal load distribution for two industrial robots handling a single object," in *Proceedings of the 1988 IEEE International Conference on Robotics and Automation*, (Philadelphia, PA, USA), pp. 344–349, April 24-29 1988.

[20] V. Kumar and K. J. Waldron, "Force distribution in closed kinematic chains," *IEEE Journal of Robotics and Automation*, vol. 4, no. 6, pp. 657–664, 1988.

[21] J. M. Tao and J. Y. S. Luh, "Coordination of two redundant manipulators," in *Proceedings of the 1989 IEEE International Conference on Robotics and Automation*, (Scottsdale, AZ, USA), pp. 425–430, May 14-19 1989.

[22] P. Buttolo and B. Hannaford, "Advantages of actuation redundancy for the design of haptic displays," in *Proceedings of the 1995 ASME International Mechanical Engineering Congress and Exposition Part 2*, (San Francisco, CA, USA), pp. 578–599, November 12-17 1995.

[23] L. Beiner, "Redundant actuation of a closed-chain device," *Advanced Robotics*, vol. 11, no. 3, pp. 233–245, 1997.

[24] S. B. Nokleby, R. Fisher, R. P. Podhorodeski, and F. Firmani, "Force capabilities of redundantly-actuated parallel manipulators," *Mechanism and Machine Theory*, vol. 40, no. 5, pp. 578–599, 2005.

[25] S. B. Nokleby, "Force-moment capabilities of parallel manipulators using different redundant-actuation configurations," in *Proceeding of the 2005 CCToMM Symposium*, (St.-Hubert, QC, Canada), 13 pages, May 26-27 2005.

[26] T. Kokkinis and B. Paden, "Kinetostatic performance limits of cooperating robots using force-velocity polytopes," in *ASME Winter Annual Meeting - Robotics Research*, (San Francisco, CA, USA), pp. 151–155, 1989.

[27] A. Bicchi, C. Melchiorri, and D. Balluchi, "On the mobility and manipulability of general multiple limb robots," *IEEE Transactions on Robotics and Automation*, vol. 11, no. 2, pp. 215–228, 1995.

[28] J. Lee, "A study on the manipulability measures for robot manipulators," in *IEEE International Conference on Intelligent Robots and Sytems*, vol. 3, (Grenoble, France), pp. 1458–1465, September 7-11 1997.

[29] R. Finotello, T. Grasso, G. Rossi, and A. Terribile, "Computation of kinetostatic performances of robot manipulators with polytopes," in *IEEE International Conference on Robotics and Automation*, (Leuven, Belgium), pp. 3241–3246, May 1998.

[30] Y. S. Hwang, L. Jihong, and T. C. Hsia, "A recursive dimension-growing method for computing robotic manipulability polytope," in *IEEE International Conference on Robotics and Automation*, (San Francisco, CA, USA), pp. 2569–2574, April 2000.

[31] S. Krut, O. Company, and F. Pierrot, "Force performance indexes for parallel mechanisms with actuation redundancy, especially for parallel wire-driven manipulators," in *IEEE International Conference on Intelligent Robots and Sytems*, (Sendai Japan), pp. 3936–3941, September 23 - October 2 2004.

[32] A. Zibil, F. T. Firmani, S. B. Nokleby, and R. P. Podhorodeski, "An analytic method for determining the force moment capabilities of redundantly actuated planar parallel manipulators," in *Proceeding of the 2006 CCToMM Symposium*, (Calgary, AB, Canada), 13 pages, May 22-24 2006.

[33] A. Zibil, F. T. Firmani, S. B. Nokleby, and R. P. Podhorodeski, "An explicit method for determining the force moment capabilities of redundantly actuated planar parallel manipulators," *In Press: Transactions of the ASME, Journal of Mechanical Design*, 2007.

[34] S. B. Nokleby, F. T. Firmani, A. Zibil, and R. P. Podhorodeski, "Force-moment capabilities of redundantly-actuated planar-parallel architectures," in *Proceedings of the IFToMM 2007 World Congress*, (Besançon, France), 6 pages, June 17-21 2007.

[35] F. T. Firmani, A. Zibil, S. B. Nokleby, and R. P. Podhorodeski, "Force-moment capabilities of revolute-jointed planar parallel manipulators with additional actuated branches," in *Proceedings of the 2007 CCToMM Symposium on Mechanisms, Machines, and Mechatronics*, (Montreal, QC, Canada), May 31 - June 1 2007.

[36] S. B. Nokleby, F. T. Firmani, A. Zibil, and R. P. Podhorodeski, "An analysis of the force-moment capabilities of branch-redundant planar-parallel manipulators," in *Proceedings of the ASME 2007 International Design Engineering Technical Conferences & Computers and Information in Engineering Conference*, (Las Vegas, NV, USA), 8 pages, September 4-7 2007.

[37] G. Garg, S. B. Nokleby, and J. A. Carretero, "Force-moment capabilities of redundantly-actuated spatial parallel manipulators using two novel methods," in *Proceedings of the 2007 CCToMM Symposium on Mechanisms, Machines, and Mechatronics*, (Montreal, QC, Canada), 6 pages, May 31 - June 1 2007.

[38] G. Mozzi, "Discorso matematico sopra il rotamento momentaneo dei corpi," in *Stamperia di Donato Campo*, Naples, 1763.

[39] L. Poinsot, *La théorie générale de l'équilibre et du mouvement des systèmes.* l'Université de Paris: Paris, France, 1975 (reprint, first edition in 1806).

[40] M. Chasles, "Note sur les proprietes generales du systeme de deux corps semblables entr'eux," in *Bullettin de Sciences Mathematiques, Astronomiques Physiques et Chimiques*, vol. 14, (Baron de Ferussac, Paris), pp. 321–326, 1830.

[41] R. S. Ball, *Theory of Screws: A Study in the Dynamics of a Rigid Body.* Hodges, Foster, and Co.: Dublin, Ireland, 1876.

[42] K. H. Hunt, *Kinematic Geometry of Mechanisms.* Oxford University Press: Toronto, ON, Canada, 1978.

[43] R. Penrose, "On best approximate solution of linear matrix equations," *Proceedings of the Cambridge Philosophical Society*, vol. 52, pp. 17–19, 1956.

[44] H. G. Golub and C. F. Van Loan, *Matrix Computations.* The Johns Hopkins University Press: Baltimore, Maryland, 1983.

[45] G. Strang, *Linear Algebra and its Applications.* Harcourt Brace: Orlando, FL, USA, 1988, Second Edition.

[46] MathWorks, *Optimization Toolbox User's Guide, Version 2.* MathWorks Inc.: Natick, MA, USA, 2001.

[47] R. T. Rockafellar, *Convex Analysis.* Princeton University Press: Princeton, NJ, USA, 1973.

[48] V. Visvanathan and L. S. Milor, "An efficient algorithm to determine the image of a parallelepiped under a linear transformation," in *Proceedings of the Second Annual Symposium on Computational Geometry*, (Yorktown Heights, NY, USA), pp. 207–215, June 2-4 1986.

[49] T. H. Cormen, C. E. Leiserson, R. L. Rivest, and C. Stein, *Introduction to Algorithms.* MIT Press and McGraw-Hill: Cambridge, MA, USA, 2001, Second Edition.

[50] R. A. Jarvis, "On the identification of the convex hull of a finite set of points in the plane," *Information Processing Letters*, vol. 2, no. 1, pp. 18–21, 1973.

[51] C. B. Barber, D. P. Dobkin, and H. Huhdanpaa, "The quickhull algorithm for convex hulls," *ACM Transactions on Mathematical Software*, vol. 22, no. 4, pp. 469–483, 1996.

[52] D. C. Montgomery and G. C. Runger, *Applied Statistics and Probability for Engineers.* John Wiley & Sons, Inc.: New York, NY, USA, 1994.

Appendix A

Screw Coordinates of RRR, RPR, and PRR Branch Types

A.1 Overview

The inverse displacement solutions[1] (IDS), screw coordinates, and ARS coordinates of a parallel manipulator are required to be found in order to analyze the wrench capabilities of the manipulator.

The parallel manipulators analyzed in this work are constructed from three types of branches: RRR, RPR and PRR. In this section, IDSs, screw coordinates, and ARS coordinates of those branch types are presented.

[1] Finding the joint values for a given end-effector position and orientation.

A.2 Inverse Displacement Solutions

The IDS solution is required to calculate the screw and the ARS coordinates of the joints. In a symmetric PPM, the base and the end-effector of the manipulator are equilateral polygons, based on the number of the branches (See Figure A.1 for a three-branch example). Therefore, regardless of the branch type, the wrist joint positions of each branch can be found from:

$$x_{3_i} = l_p \cos\left(\frac{\pi(3b+4i-6)}{2n} + \phi\right) + x_p, \tag{A.1a}$$

$$y_{3_i} = l_p \sin\left(\frac{\pi(3b+4i-6)}{2b} + \phi\right) + y_p \tag{A.1b}$$

and the base joint positions of each branch can be found from:

$$x_{1_i} = l_b \cos\left(\frac{\pi(3b+4i-6)}{2n}\right) + x_b \tag{A.2a}$$

$$y_{1_i} = l_b \sin\left(\frac{\pi(3b+4i-6)}{2b}\right) + y_b \tag{A.2b}$$

where b is the number of the branches, i is the branch index with $i = 1 \ldots b$, and x_{3_i} & y_{3_i} are the coordinates of the wrist joints. The quantities x_{1_i} & y_{1_i} are the coordinates of the base joints, l_p is the distance between the centre of the platform and the wrists joint, l_b is the distance between the centre of the base and the base joints, x_p & y_p are the coordinates of the centre of the platform, ϕ is the orientation of the platform, and x_b & y_b are the coordinates of the centre of the base. Note that every coordinate has been defined with respect to the *Base Reference Frame* ($\{B.\}$), a frame located at the first joint of the first branch and oriented such that its x axis points to the first joint of the second branch as shown in Figure A.1. The rest of

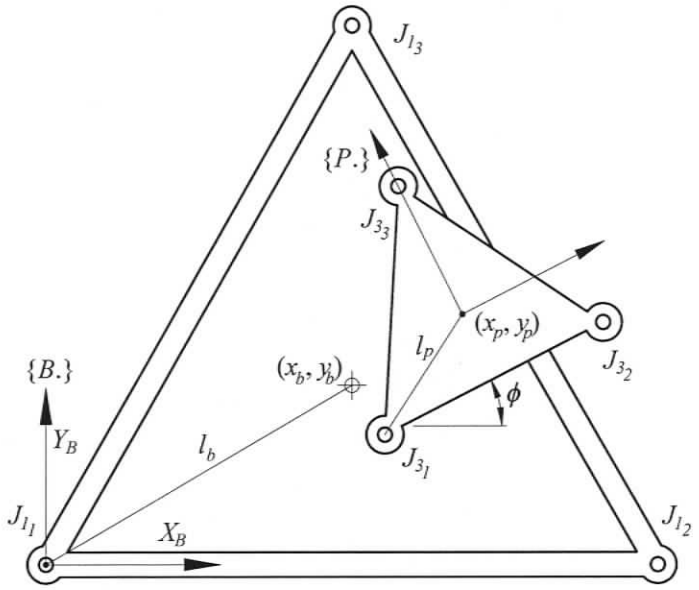

Figure A.1: Base and Platform Geometry of a Three-Branch PPM

the IDS problem is specific to each branch type and will be presented in the next sections.

A.2.1 IDS of an RRR Branch

An RRR type branch is shown in Figure A.2. Forward displacement equations of an RRR type branch can be written as:

$$x_{3_i} = x_{1_i} + l_{1_i}\cos(q_{1_i}) + l_{2_i}\cos(q_{1_i} + q_{2_i}) \quad \text{(A.3a)}$$

$$y_{3_i} = y_{1_i} + l_{1_i}\sin(q_{1_i}) + l_{2_i}\sin(q_{1_i} + q_{2_i}) \quad \text{(A.3b)}$$

where l_{1_i} and l_{2_i} are the link lengths of the first and second links, respectively, q_{1_i} and q_{2_i} are the joint values of the first and second joints, respectively. Squaring and adding equations (A.3a) and (A.3b) yields:

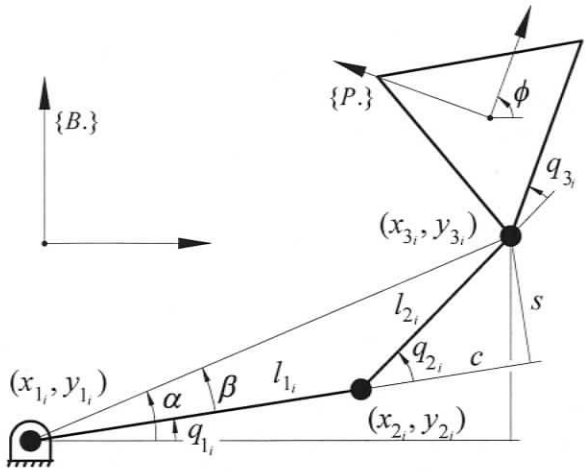

Figure A.2: A RRR Type Branch and Its Parameters

$$(x_{3_i} - x_{1_i})^2 + (y_{3_i} - y_{1_i})^2 = l_{1_i}^2 + l_{2_i}^2 + 2l_{1_i}l_{2_i}\cos(q_{2_i}) \tag{A.4}$$

Hence,

$$\cos(q_{2_i}) = \frac{(x_{3_i} - x_{1_i})^2 + (y_{3_i} - y_{1_i})^2 - l_{1_i}^2 - l_{2_i}^2}{2l_{1_i}l_{2_i}} \tag{A.5}$$

Therefore, the two solutions of q_{2_i} are:

$$q_{2_i} = \arctan2\left(\pm\sqrt{1 - \cos^2(q_{2_i})}, \cos(q_{2_i})\right) \tag{A.6}$$

where the two solutions correspond to elbow up and elbow down assembly modes. Note that arctan2 is a two-argument arc tangent operator that takes into account the signs of the inputs and returns the angle in the correct quadrant.

The base joint angle q_{1_i} can be expressed as $\alpha - \beta$:

$$q_{1_i} = \arctan2(y_{3_i} - y_{1_i}, x_{3_i} - x_{1_i}) - \arctan2(s, c + l_{1_i}) \tag{A.7}$$

where α, β, $s = l_{2_i}\sin(q_{2_i})$, and $c = l_{2_i}\cos(q_{2_i})$ are shown in Figure A.2.

Lastly, wrist joint angle q_{3_i} can be found as:

$$q_{3_i} = \phi + \frac{2\pi(i-1)}{b} - q_{1_i} - q_{2_i} \tag{A.8}$$

A.2.2 IDS of an RPR Branch

An RPR type branch is shown in Figure A.3. Forward displacement equations of an

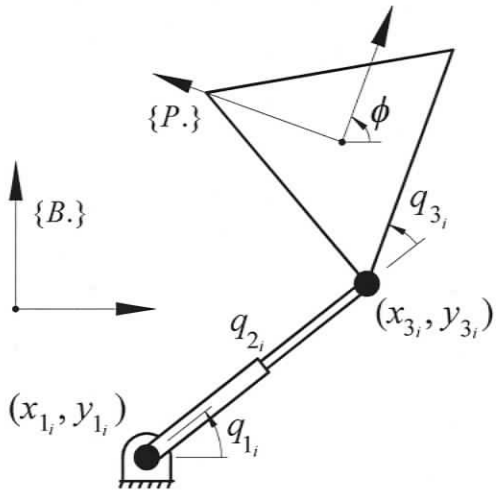

Figure A.3: An RPR Type Branch and Its Parameters

RPR type branch can be written as:

$$x_{3_i} = x_{1_i} + q_{2_i}\cos(q_{1_i}) \tag{A.9a}$$

$$y_{3_i} = y_{1_i} + q_{2_i}\sin(q_{1_i}) \tag{A.9b}$$

where q_{1_i} is the value of the first joint, i.e., base joint angle and q_{2_i} is the value of the second joint, i.e., the length of the prismatic joint. Squaring and adding equations

(A.9a) and (A.9b) yields:

$$q_{2_i} = \pm\sqrt{(x_{3_i} - x_{1_i})^2 + (y_{3_i} - y_{1_i})^2} \tag{A.10}$$

where a negative solution of the joint value may not be feasible.

Base joint angle q_{1_i} can be found as:

$$q_{1_i} = \arctan2(y_{3_i} - y_{1_i}, x_{3_i} - x_{1_i}) \tag{A.11}$$

and the wrist joint angle q_{3_i} can be found as:

$$q_{3_i} = \phi + \frac{2\pi(i-1)}{b} - q_{1_i} \tag{A.12}$$

A.2.3 IDS of a PRR Branch

A PRR type branch is shown in Figure A.4. Forward displacement equations of a PRR type branch can be written as:

$$x_{3_i} = x_{1_i} + q_{1_i}\cos(\gamma_i) + l_{2_i}\cos(\gamma_i + q_{2_i}) \tag{A.13a}$$

$$y_{3_i} = y_{1_i} + q_{1_i}\sin(\gamma_i) + l_{2_i}\sin(\gamma_i + q_{2_i}) \tag{A.13b}$$

where γ_i is the orientation of the prismatic joint, l_{2_i} is the length of the second link, q_{1_i} is the value of the first joint, i.e., the length of the prismatic joint, and q_{2_i} is the value of the second joint. Squaring and adding equations (A.13a) and (A.13b) yields

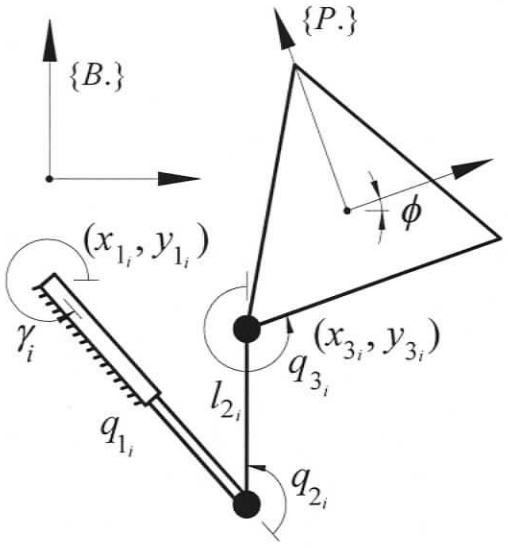

Figure A.4: A PRR Type Branch and Its Parameters

the following second order equation:

$$q_{1_i}^2 + \underbrace{2\left((x_{1_i} - x_{3_i})\cos(\gamma_i) + (y_{1_i} - y_{3_i})\sin(\gamma_i)\right)}_{b} q_{1_i} + \underbrace{(x_{3_i} - x_{1_i})^2 + (y_{3_i} - y_{1_i})^2 - l_{2_i}^2}_{c} = 0 \tag{A.14}$$

where q_{1_i} can be solved as:

$$q_{1_i} = -\frac{b}{2} \pm \frac{\sqrt{b^2 - 4c}}{2} \tag{A.15}$$

The two solutions of q_{1_i} correspond to elbow up and elbow down assembly modes. q_{2_i} can then be found as:

$$q_{2_i} = \arctan2(y_{3_i} - y_{1_i} - q_{1_i}\sin(\gamma_i), x_{3_i} - x_{1_i} - q_{1_i}\cos(\gamma_i)) - \gamma_i \tag{A.16}$$

and the wrist joint angle q_{3_i} can be found as:

$$q_{3_i} = \phi + \frac{2\pi(i-1)}{b} - \gamma_i - q_{2_i} \tag{A.17}$$

A.3 Screw Coordinates

Screw coordinates of the joints can be determined regardless of the branch type. In the form presented in Section 2.3.1, the screw coordinates of a revolute joint are:

$$\$_{revolute} = \{1; y_{j_i}, -x_{j_i}\} \tag{A.18}$$

and the screw coordinates of a prismatic joint are:

$$\$_{prismatic} = \{0; \cos(\phi_{j_i}), \sin(\phi_{j_i})\} \tag{A.19}$$

where x_{j_i}, and y_{j_i} are the coordinates of the j^{th} joint of the i^{th} branch, and ϕ_{j_i} is the orientation of the joint, all assumed to be determined in the IDS.

A.4 Associated Reciprocal Screw Coordinates

Geometrically, the ARS coordinates of a joint in a planar manipulator can be denoted as $\$' = \{\hat{x}, \hat{y}; d\}$, where $\hat{x}$ and $\hat{y}$ specifies the unit direction of the force that is caused by the joint, and d is the magnitude of the moment of this unit direction about the origin of the reference frame (i.e., the perpendicular distance between the origin of the reference frame and the force vector). ARS coordinates of the joints are dependent on the branch type and will be presented in the next sections.

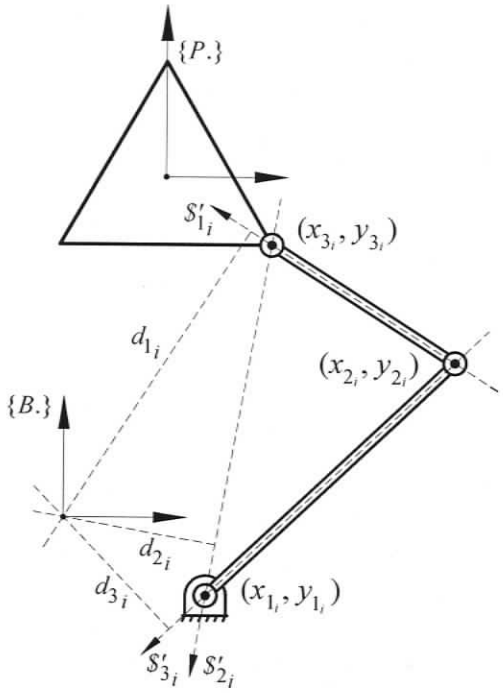

Figure A.5: ARS Coordinates of an RRR Type Branch

A.4.1 ARS Coordinates of an RRR Branch

ARS coordinates of an RRR type branch can be geometrically defined from Figure A.5 as follows:

$$\$'_{1_i} = \{\cos(q_{1_i} + q_{2_i}), \sin(q_{1_i} + q_{2_i}); d_{1_i}\} \quad \text{(A.20a)}$$

$$\$'_{2_i} = \left\{\frac{x_{1_i} - x_{3_i}}{norm}, \frac{y_{1_i} - y_{3_i}}{norm}; d_{2_i}\right\} \quad \text{(A.20b)}$$

$$\$'_{3_i} = \{\cos(q_{1_i} + \pi), \sin(q_{1_i} + \pi); d_{3_i}\} \quad \text{(A.20c)}$$

where $norm = \sqrt{(x_{3_i} - x_{1_i})^2 + (y_{3_i} - y_{1_i})^2}$. d_{j_i} are the perpendicular distances between the origin of the base frame and the screw vector (see Figure A.5), and can be

found as:

$$d_{1_i} = x_{2_i}\sin(q_{1_i}+q_{2_i}) - y_{2_i}\cos(q_{1_i}+q_{2_i}) \quad \text{(A.21a)}$$

$$d_{2_i} = x_{1_i}\frac{y_{1_i}-y_{3_i}}{norm} - y_{1_i}\frac{x_{1_i}-x_{3_i}}{norm} \quad \text{(A.21b)}$$

$$d_{3_i} = x_{2_i}\sin(q_{1_i}+\pi) - y_{2_i}\cos(q_{1_i}+\pi) \quad \text{(A.21c)}$$

A.4.2 ARS Coordinates of an RPR Branch

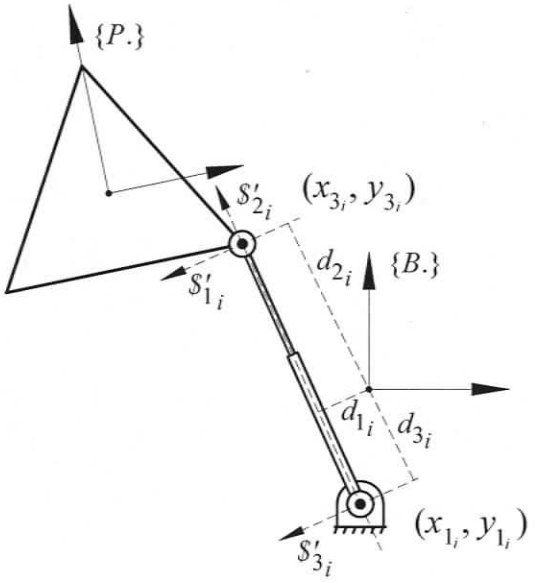

Figure A.6: ARS Coordinates of an RPR Type Branch

ARS coordinates of an RPR type branch can be geometrically defined from Figure A.6 as follows:

$$\$'_{1_i} = \left\{\cos(q_{1_i}+\frac{\pi}{2}), \sin(q_{1_i}+\frac{\pi}{2}); d_{1_i}\right\} \quad \text{(A.22a)}$$

$$\$'_{2_i} = \{\cos(q_{1_i}), \sin(q_{1_i}); d_{2_i}\} \quad \text{(A.22b)}$$

$$\$'_{3_i} = \left\{\cos(q_{1_i}+\frac{\pi}{2}), \sin(q_{1_i}+\frac{\pi}{2}); d_{3_i}\right\} \quad \text{(A.22c)}$$

where d_{j_i} are the perpendicular distances between the origin of the base frame and the screw vector (see Figure A.6), and can be found as:

$$d_{1_i} = x_{3_i}\sin(q_{1_i} + \frac{\pi}{2}) - y_{3_i}\cos(q_{1_i} + \frac{\pi}{2}) \quad \text{(A.23a)}$$

$$d_{2_i} = x_{1_i}\sin(q_{1_i}) - y_{1_i}\cos(q_{1_i}) \quad \text{(A.23b)}$$

$$d_{3_i} = x_{1_i}\sin(q_{1_i} + \frac{\pi}{2}) - y_{1_i}\sin(q_{1_i} + \frac{\pi}{2}) \quad \text{(A.23c)}$$

A.4.3 ARS Coordinates of a PRR Branch

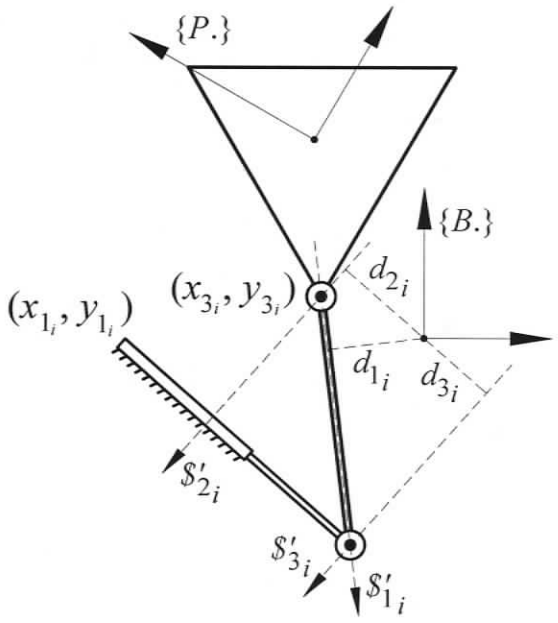

Figure A.7: ARS Coordinates of an PRR Type Branch

ARS coordinates of an RPR type branch can be geometrically defined from Figure A.7 as follows:

$$\$'_{1_i} = \left\{ \frac{x_{2_i} - x_{3_i}}{norm}, \frac{y_{2_i} - y_{3_i}}{norm}; d_{1_i} \right\} \tag{A.24a}$$

$$\$'_{2_i} = \left\{ \cos(q_{1_i} - \frac{\pi}{2}), \sin(q_{1_i} - \frac{\pi}{2}); d_{2_i} \right\} \tag{A.24b}$$

$$\$'_{3_i} = \left\{ \cos(q_{1_i} - \frac{\pi}{2}), \sin(q_{1_i} - \frac{\pi}{2}); d_{3_i} \right\} \tag{A.24c}$$

where $norm = \sqrt{(x_{2_i} - x_{3_i})^2 + (y_{2_i} - y_{3_i})^2}$. d_{j_i} are the perpendicular distances between the origin of the base frame and the screw vector (see Figure A.7), and can be found as:

$$d_{1_i} = x_{2_i} \frac{y_{2_i} - y_{3_i}}{norm} - y_{2_i} \frac{x_{2_i} - x_{3_i}}{norm} \tag{A.25a}$$

$$d_{2_i} = x_{3_i} \sin(q_{1_i} - \frac{\pi}{2}) - y_{3_i} \cos(q_{1_i} - \frac{\pi}{2}) \tag{A.25b}$$

$$d_{3_i} = x_{2_i} \sin(q_{1_i} - \frac{\pi}{2}) - y_{2_i} \cos(q_{1_i} - \frac{\pi}{2}) \tag{A.25c}$$